

Synthesis, Detection, and Hepatotoxic
Evaluation of Novel Cathinones Recently
Identified in the Night-Time Economy.

Emily Jane Dawber

A thesis submitted in fulfilment for the
requirements of Manchester Metropolitan
University for the degree of Masters by
Research.

Department of Natural Science
Manchester Metropolitan University

2024

Abstract

The rapid emergence of novel synthetic cathinones, commonly found in night-time economy settings, presents significant challenges for public health and forensic science. This research focuses on the synthesis of derivatised 3,4-methylenedioxycathinones, detection of the synthesised products, and hepatotoxic evaluation of several newly synthesised synthetic cathinones. Five cathinones; pentylone, dimethylpentylone, *N*-ethylpentylone (NEP), butylone and putylone, were successfully synthesized with varying yields of 9-65%, using established organic chemistry methods. The synthesised products were fully characterized through ^1H -NMR, $^{13}\text{C}\{^1\text{H}\}$ -NMR, ^1H - ^1H COSY NMR, HMBC, HSQC, DEPT-135, ATR-FTIR and GC-MS to confirm their structures and purity.

A robust GC-MS method was developed and validated for the simultaneous detection of these compounds, demonstrating high sensitivity and specificity. The hepatotoxic potential of the synthesized cathinones was assessed using *in vitro* cytotoxicity assays on LX2 and HepG2 cell lines. Results indicated varying degrees of cytotoxicity among the compounds. In LX-2 cell lines, MDPV induced a concentration-dependent increase in cytotoxicity, with a significant elevation observed at 1.8 μM . Initial HepG2 assays recorded at 24hrs after dosing, indicated minimal to no cytotoxicity for all compounds at lower concentrations, reflected by minimal cytotoxicity percentage in respects to the maximum cytotoxicity (Obtained by Promega Lysis Buffer). All synthetic cathinones showed similar toxicity profiles between 0.01 and 1 mM, followed by a reduction in cytotoxicity at 2 mM, possibly indicative of cellular adaptation, compound degradation, or assay saturation effects at higher concentrations. MDPHP and putylone exhibited a dose-dependent increase in cytotoxicity, showing a higher cytotoxicity than the other cathinones tested, yet remained below the positive control. These findings suggest that the consumption of these substances may pose possible health risks to users who continuously abuse them or from single high dose usage.

This study not only provides critical insights into the toxicological profiles of these emerging synthetic cathinones but also contributes to the development of reliable analytical methods for their detection in forensic contexts. The outcomes underscore the need for ongoing monitoring and regulation of these substances to safeguard public health.

Acknowledgements

First and foremost, I would like to express my deepest gratitude to my supervisors, Dr Oliver Sutcliffe, Dr Ryan Mewis and Dr James Pritchett for their invaluable guidance, support, and encouragement throughout the course of this research. Their expertise and insights have been instrumental in shaping this thesis, and I am truly grateful for their mentorship.

I would also like to extend my thanks to the faculty and staff of the Department of Natural Science and Department of Life Science at Manchester Metropolitan University for providing a stimulating academic environment and access to the resources necessary for my research.

Special thanks to the 7th floor postgraduates and MChems for their assistance and for creating a collaborative and supportive atmosphere that made this journey both productive and enjoyable. They not only offered their knowledge and assistance but also their friendship. The discussions, feedback and encouragement I received from them have greatly contributed to the completion of this thesis.

To my parents, thank you for your endless encouragement, love, and guidance, which have been the foundation of my achievements. To my partner Jay, your patience, understanding, and constant belief in me have been my greatest source of strength. Your support has made this accomplishment possible, and I am forever grateful.

I would like to express my heartfelt gratitude to my friends, especially to Abbie, Arianna and Michael for their unwavering support and encouragement throughout this journey. Your constant belief in me, along with your understanding and patience, has been invaluable. Thank you for always being there to lift my spirits and for making this challenging process more manageable and enjoyable. Your friendship has been a true source of strength.

And finally, to everyone who has been a part of this journey, I extend my sincerest thanks. This accomplishment would not have been possible without your help and support.

Contents

Abstract	1
Acknowledgements	3
Contents	4
List of Figures	7
List of Tables	9
1 Introduction.....	10
2 Aims.....	17
3 Research Premise	18
4 Experimental	19
4.1 Methods & Materials (Chemistry).....	19
4.1.1 Nuclear Magnetic Resonance (NMR) Spectroscopy.....	19
4.1.2 Attenuated Total Reflectance Fourier-Transform Infra Red (ATR-FTIR) spectroscopy.....	20
4.1.3 Gas Chromatography-Mass spectrometry (GC-MS).....	20
4.2 Synthesis of methylenedioxy-cathinone derivatives.....	21
4.2.1 General procedure for synthesis of methylenedioxycathinones	21
4.2.2 Synthesis of 1-(1,3-benzodioxol-5-yl) penta-1-one (2).....	21
4.2.3 Preparation of the intermediate (\pm)- α -bromoketones (5-7)	22
4.2.4 Preparation of (\pm)-cathinones hydrochlorides (8a,b, 9a-c, 10a).....	22
4.3 Methylenedioxy cathinone derivatives 8a-10a	23
4.3.1 Pentylone hydrochloride (1-(3,4-methylenedioxyphenyl)-2-(methylamino)pentan-1-one, 8a).....	23
4.3.2 Dimethylpentylone hydrochloride (1-(1,3-benzodioxol-5-yl)-2-(dimethylamino)pentan-1-one, 8b)	23
4.3.3 <i>N</i> -ethylpentylone hydrochloride (1-(benzo[d][1,3]dioxol-5-yl)-2-(ethylamino)pentan-1-one, 8c)	23

4.3.4	Butylone hydrochloride (1-(1,3-Benzodioxol-5-yl)-2-(methylamino)butan-1-one, 9a)	24
4.3.5	Putylone hydrochloride (1-(1,3-benzodioxol-5-yl)-2-(propylamino)butan-1-one, 9b)	24
4.3.6	MDPHP hydrochloride (1-(benzo[d][1,3]dioxol-5-yl)-2-(pyrrolidin-1-yl)hexan-1-one, 10a)	25
4.4	Method & Materials (Cytotox)	25
4.4.1	Mycoplasma	26
4.4.2	LX-2 Cell Culture	26
4.4.3	HepG2 Cell Culture	26
4.4.4	Compound Preparation and cell treatments	26
4.4.5	CellTox™ Green	27
4.4.6	Statistical Analysis	27
5	Results & Discussion	29
5.1	Nuclear Magnetic Resonance (NMR) Spectroscopy	31
5.1.1	Pentylone hydrochloride (8a)	31
5.1.2	Dimethylpentylone hydrochloride (8b)	41
5.1.3	<i>N</i> -ethylpentylone hydrochloride (8c)	46
5.1.4	Butylone hydrochloride (9a)	51
5.1.5	Putylone hydrochloride (9b)	56
5.1.6	MDPHP hydrochloride (10a)	61
5.2	Attenuated Total Reflectance-Fourier Transform Infra Red (FT-IR) Spectroscopy	67
5.3	Gas Chromatography-Mass Spectrometry (GC-MS)	70
5.4	Cytotox Evaluation	75
5.4.1	Assay 1: Four Compounds, 0 - 1.8 μM in LX-2 Cell lines	75
5.4.2	Assay 2: Four Compounds, 0 - 7.3 μM in HepG2 Cell lines	77
5.4.3	Assay 3 Four Compounds, 0 - 2000 mM in HepG2 Cell lines	78

5.4.4	Assay 4: 2 Compounds, 0 - 2000 mM in HepG2 cell lines.....	81
6	Conclusion	83
7	Future Work	84
	References.....	85
	Supplementary	88

List of Figures

Figure 1. Picture of bath salts containing cathinones labelled “not for human consumption”. ⁶	10
Figure 2. Clustered column graph showing the different NPS substances identified over the years. ⁸	10
Figure 3. Picture of prescribed Diazepam® and its chemical structure.....	11
Figure 4. Chemically structures of pentylone (8a), <i>N</i> -ethylpentylone (8c), 3,4-methylenedioxy pyrovalerone (MDPV) and putylone (9b).....	12
Figure 5. Chemical structure of the 3,4-methylenedioxy group within the cathinone core.....	14
Figure 6. ¹ H NMR spectrum of 8a acquired in DMSO-d ₆	32
Figure 7. ¹³ C{ ¹ H} NMR spectrum of 8a acquired in DMSO-d ₆	33
Figure 8. ¹ H- ¹ H COSY NMR spectrum of 8a in DMSO-d ₆	34
Figure 9. ¹ H- ¹³ C{ ¹ H} HSQC NMR spectrum of 8a in DMSO-d ₆	35
Figure 10. ¹ H- ¹³ C{ ¹ H} HMBC NMR spectrum of 8a in DMSO-d ₆	36
Figure 11. DEPT-135 NMR spectrum of 8a in DMSO-d ₆	37
Figure 12. Chemical Structure of 8a with positions numbered.....	38
Figure 13. ¹ H NMR spectrum of 8b acquired in DMSO-d ₆	42
Figure 14. ¹³ C{ ¹ H} NMR spectrum of 8b acquired in DMSO-d ₆	43
Figure 15. Chemical Structure of 8b with positions numbered.....	44
Figure 16. ¹ H NMR spectrum of 8c acquired in DMSO-d ₆	47
Figure 17. ¹³ C{ ¹ H} NMR spectrum of 8c acquired in DMSO-d ₆	48
Figure 18. Chemical Structure of 8c with positions numbered.....	49
Figure 19. ¹ H NMR spectrum of 9a acquired in DMSO-d ₆	52
Figure 20. ¹³ C{ ¹ H} NMR spectrum of 9a acquired in DMSO-d ₆	53
Figure 21. Chemical Structure of 9a with positions numbered.....	54
Figure 22. ¹ H NMR spectrum of 9b acquired in DMSO-d ₆	57
Figure 23. ¹³ C{ ¹ H} NMR spectrum of 9b acquired in DMSO-d ₆	58
Figure 24. Chemical Structure of 9b with positions numbered.....	59
Figure 25. ¹ H NMR spectrum of 10a acquired in DMSO-d ₆	62
Figure 26. ¹³ C{ ¹ H} NMR spectrum of 10a acquired in DMSO-d ₆	63
Figure 27. Chemical Structure of 10a with positions numbered.....	64
Figure 28. ATR-FTIR spectrum of 8a	68

Figure 29. Gas chromatograph of compounds 8a-c,9a and 10a	70
Figure 30. Gas chromatograph of compounds 8b and 8c	70
Figure 31. Mass spectrum of 8a	71
Figure 32. Cytotoxic effects of synthetic methylenedioxcathinones (MDPV, pentylone, dimethylpentylone and NEP) 24hrs after dosing at concentrations of 0.00–1.8 μ M on LX-2 hepatic stellate cell lines.....	75
Figure 33: Cytotoxic effects of synthetic methylenedioxcathinones (MDPV, pentylone, dimethylpentylone and NEP) 24 hrs after dosing at concentrations of 0.00–1.8 μ M on LX-2 hepatic stellate cell lines. An expanded view of Figure 32, highlighting the minor peaks within the cytotoxic profile).....	76
Figure 34: Cytotoxicity of four methylenedioxcathinones (MDPV, pentylone, dimethylpentylone, NEP) in invitro HepG2 cells, readings 24hrs after dosage (1-2000 μ M).....	79
Figure 35: Cytotoxic effects of MDPHP and Putylone at concentration between 0 to 2 mM on HepG2 cell lines.....	81

List of Tables

Table 1. Chemical shifts for signals in the ^1H and $^{13}\text{C}\{^1\text{H}\}$ NMR spectra of 8a	38
Table 2. Chemical shifts for signals in the ^1H and $^{13}\text{C}\{^1\text{H}\}$ NMR spectra of 8b	44
Table 3. Chemical shifts for signals in the ^1H and $^{13}\text{C}\{^1\text{H}\}$ NMR spectra of 8c	49
Table 4. Chemical shifts for signals in the ^1H and $^{13}\text{C}\{^1\text{H}\}$ NMR spectra of 9a	54
Table 5. Chemical shifts for signals in the ^1H and $^{13}\text{C}\{^1\text{H}\}$ NMR spectra of 9b	59
Table 6. Chemical shifts for signals in the ^1H and $^{13}\text{C}\{^1\text{H}\}$ NMR spectra of 10a	64
Table 7. Functionalities in the FT-IR spectra for compounds 8a-10a	69
Table 8. GC-EI-MS validation data for the quantification of 8a-10a	73

1 Introduction

New Psychoactive Substances (NPS), which constitutes a multifaceted and varied array of compounds, are commonly referred to as designer or synthetic drugs, or sometimes inaccurately labelled as 'legal highs'.^{1,2} These substances typically fall into two categories; either derivatives of regulated drugs and pharmaceuticals or novel synthetic compounds engineered to emulate the effects and psychoactive properties of authorised medications and other controlled substance.^{3,4} NPS are often medically defined as narcotic and psychotropic drugs which are commonly found in various forms such as powders, pills liquids and even herbal mixtures, often labelled as "not for human consumption" to bypass drug regulations that can be seen in **Figure 1**.⁵



Figure 1: Picture taken of bath salts containing cathinones labelled "Not for human consumption".⁶

Across Europe, the Early EU Warning system for NPS currently monitors over 670 different substances, with over 150 substances only recently being discovered from the early 2010s as seen in **Figure 2**, proving the significant increase in detection.⁷

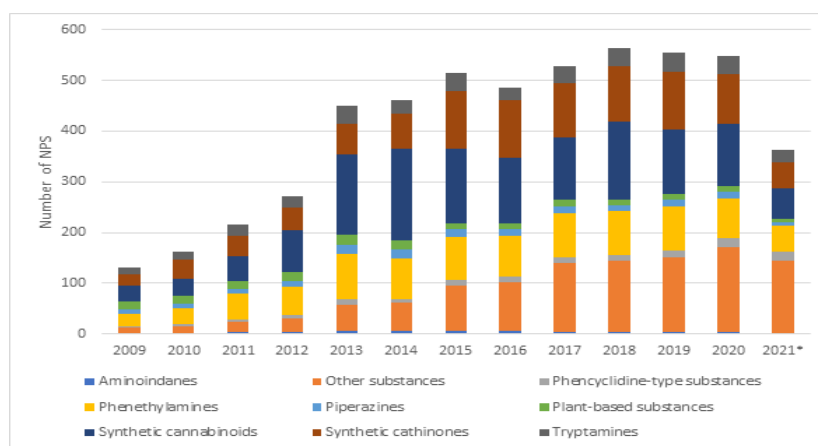


Figure 2: Clustered column graph showing the different New Psychoactive Substances identified over the years.⁸

Globally, over 892 NPS are being monitored by the United Nations Office on Drugs and Crime (UNODC).⁹ With legislations on existing illicit substances increasing, frequent identification of new substances will increase due to drug markets attempting to bypass laws with unidentified and unknown substances causing global concern due to the minimal information published about them and their effects.¹⁰

NPS are often considered by users as a safer alternative to illicit substances and have previously been used in the medical workplace. An important example of medical NPS would be phencyclidine, also referred to as PCP and classified as an arylcycloalkylamines under NPS. PCP was sold as an injectable anaesthetic in the United states up until 1967 under the trade names Sernyl[®] and Sernylan[®], before being used as a recreational drug.¹¹ An example of a current NPS, widely known to medical industries and been available since 1963 is 'diazepam', also referred to by its trade names as; Valium[®], Ducene[®], Antenex[®], Valpam[®]. Diazepam[®] belongs to a sub-group of NPS known as Benzodiazepines and is widely prescribed as a sedative for conditions such as anxiety and insomnia.¹²



Figure 3: Picture of prescribed diazepam (Left) and its chemical structure (Right).¹³

Although NPS have some positive uses, they still possess similar psychoactive effects. Structural modifications to the parent NPS can lead to the enhancement of hallucinogenic and psychostimulant effects. Furthermore, their legal status, the use of these substances brings significant health risk and can lead to detrimental consequences.^{10,15}

Despite all the legislations and warnings, these compounds have attracted considerable interest since the 2000s due to their potent psychoactive effects.⁷ Among primary constituents of NPS are cathinones, originally derived from naturally occurring khat plant leaves. Recently, the demand for the synthesised replica of these naturally occurring substances has increased as seen in **Figure 2**.

Synthetic cathinones are characterised by distinct variations in chemical structure that result in differences in potency, duration and potential effects. They are recognised by users for their neurological impacts; including heightened attention, euphoria, and increased sociability.^{14,15} These attributes have drawn significant attention in social and nighttime economies (NTEs), as well as among recreational drug users, often marketed under the name 'bath salts'.¹⁶ Their rising popularity and potential for misuse in recent years has prompted medical professional, law enforcement agencies, and policy makers to intensify efforts in public awareness regarding the associated risks of their consumption.

In the UK, law enforcement regularly conducts drug testing in off-site locations, revealing a growing prevalence of synthetic cathinones (SCs) within the NTE and broader circulation in recent years. The latest data indicates that synthetic cathinones, sharing similar chemical structures as seen in **Figure 4**, such as pentylone (**8a**), *N*-ethylpentylone (NEP, **8c**), 3,4-methylenedioxy pyrovalerone (MDPV) and putylone (**9b**) are being increasingly utilised, as evidence by their heightened detection rates during seizures, often recorded via similarity scores and spectra in ATR-FTIR, EI-MS (mass spectra) comparisons via GC-MS, LC-MS and even ICP tests which replicate techniques used in this thesis.¹⁷

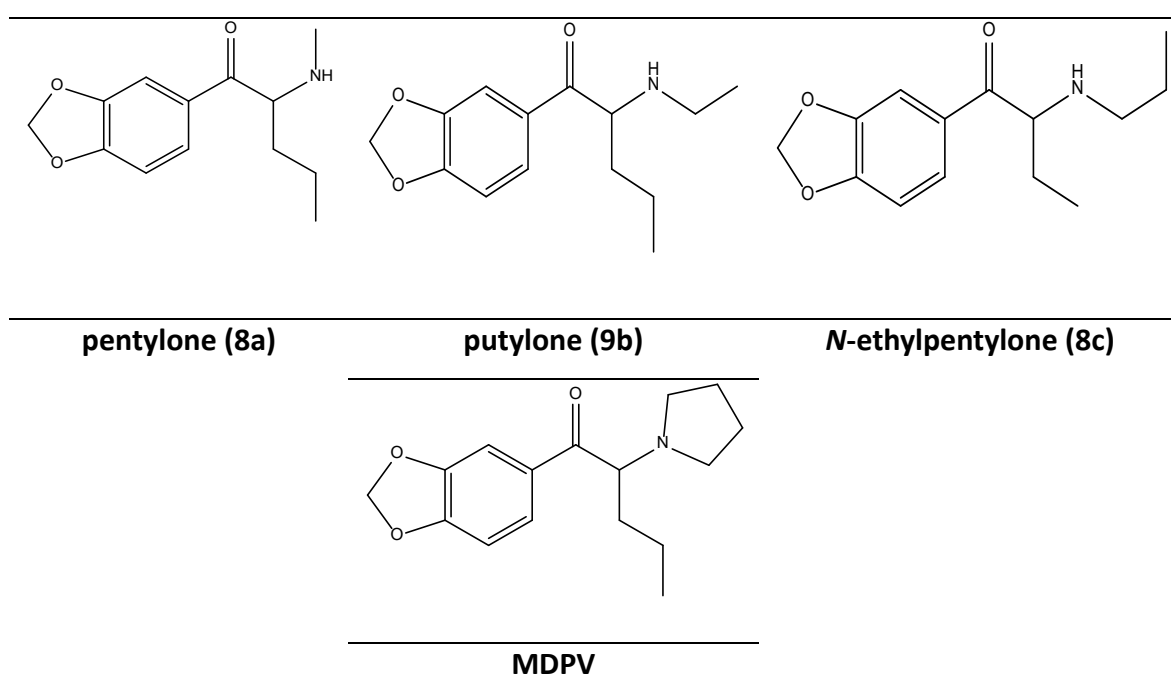


Figure 4: Chemical structures of pentylone (**8a**), *N*-ethylpentylone (**8c**), 3,4-methylenedioxy pyrovalerone (MDPV) and putylone (**9b**).

Substances at this thesis' focal point include NEP (**8c**), also referred to as ephylone or BK-EDBP is known for its similarities to the well-known psychoactive substance 3,4-

methylenedioxyamphetamine (MDMA, also referred to as ecstasy).^{18,19} It emerged in the early 2010s as a popular recreational drug and gained notoriety for its potent effects and risks. In 2016, NEP was identified by the European Monitoring Centre for Drugs and Drug Addiction (EMCDDA) by Slovenia and equated to 0.5% of all phenylamine reports for that year. Investigation into NEP usage showed that synthesis dated back to 1969 along with pentylone and butylone. NEP popularity comes from its two main effects, enhanced sensory and euphoria, but it is important to note that the substance has substantial health risks as well. Of pentylone, dimethylpentylone and NEP, NEP is associated with the most adverse effects, including but not limited to, severe agitation, paranoia and even death. These adverse effects stem from the original methylenedioxy cathinones (MDC), discovered before the identification of pentylone, dimethylpentylone and NEP.^{18,20}

A primary substitute for NEP and eutylone is dimethylpentylone (**8b**) (1-(1,3-benzodioxol-5-yl)-2-(dimethylamino) pentan-1-one). Due to existing restrictions on most known illicit substances, users are forced to resort to similar drugs which has caused a high increase in the identification and seizure of cathinones, especially dimethylpentylone, in recreational party drugs. Most often the substance is seized in the form of a crystalline powder or tablet but has been reported to have the potential to be smoked too.²¹

Dimethylpentylone was initially identified in 2014, both in Kansas USA and Sweden. Despite the elevated use between October -December 2021, it was not controlled under the 1961, 1971 or 1988 UN Convention and so it still has the potential to be sold globally. Usage of this cathinone has increased over the years as in April 2022, the Centre for Forensic Science Research and Education (CFSRE) had to issue a public alert regarding the high increase in the frequency of dimethylpentylone intoxication. Recent papers also prove the increase in usage with 32 toxicology cases in the USA all being linked to dimethylpentylone, with concentrations in postmortem blood ranging from 33 to 970 ng/mL.²² Most countries are unfamiliar with the drug due to there being minimal information; however, some countries have introduced legislations to reduce the use and minimise danger to the public.

Dimethylpentylone is described as a low potency substance; although, with recent research there are suspicions that it acts as a prodrug of the mono-*N*-methyl analogue, pentylone. Pentylone (**8a**) is one of the major metabolites of dimethylpentylone, as one of the main mechanisms of cathinone metabolism is *N*-dealkylation.²³ 2-methylamino-1-(3,4-

methylenedioxyphenyl)-pentan-1-one (pentylone) is the most common drug detected out of these synthetic cathinones and often compared to substances such as methyldone and butylone which are often sold as “bath salts”.²⁴ Research shows that these chemicals are often sold in the forms of powder or crystals to recreational drug users because of their short-term sensational effects in the recreational drug market. The most common routes the drug is administered is orally, inhaled or injected directly into the bloodstream.²⁵

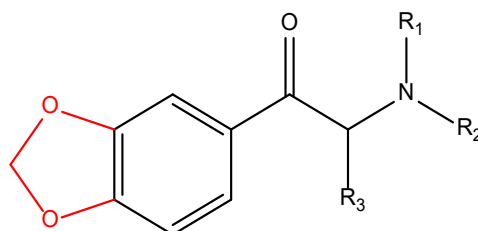


Figure 5: Chemical structure of the 3,4-methylenedioxy group (red) within the cathinone core.

Pentylone, dimethylpentylone, NEP and putylone are all structural modifications of synthetic cathinones often characterised by the presence of the methylenedioxy group (-O-CH₂-O-) attached to the methylenedioxy ring as seen in **Figure 5**. MDCs represent a class of synthetic compounds known for their diverse pharmacological effects, including stimulant, empathogenic, and hallucinogenic properties. These substances, which include popular drugs like MDMA (3,4-methylenedioxy-*N*-methylamphetamine), have drawn significant attention due to their widespread recreational use and potential therapeutic applications. Given MDCs hydrophobic nature and ability to cross the blood-brain-barrier, they primarily act as a substrate-type releasers of serotonin, dopamine and norepinephrine, leading to heightened synaptic levels of these neurotransmitters. In 2013, research into cathinones demonstrated their preferential release of serotonin by MDMA compared to dopamine and norepinephrine in *in-vitro* assays, highlighting its distinctive pharmacological profile.²⁶ Drugs targeting serotonin receptors, may influence the mood and emotional state of a person such as improved mood, reduced anxiety, and increased feelings of well-being.²⁷ Although, an increased release of serotonin can positively alter a person’s mood; excessive serotonin release/ prolonged activation of the receptor, can cause adverse effects. One of the primary pathways in which MDC's induce neurotoxicity is the inhibition of the monoamine reuptake transporters. Interfering with the reuptake of neurotransmitters of dopamine, serotonin and norepinephrine can interrupt neural

signalling and lead to adverse effects on the brain such as serotonin syndrome, manifested as agitation, confusion, rapid heart rate, high blood pressure, dilated pupils, loss of muscle function and even fever.^{14,28} MDCs can also induce oxidative stress, occurring when an imbalance between reactive oxygen species (ROS) and antioxidants is present, leading to damage to biological materials including DNA, proteins and lipids, resulting in cytotoxicity.²⁹ In such severe instances, failure to intervene could lead to fatal outcomes.

Acute and chronic toxicity of methylenedioxy cathinone derivatives have been researched, providing valuable insights into their pharmacokinetics and organ-specific effects. Studies by Luethi *et al.* highlighted the cardiotoxic effects of methylenedioxy cathinones, including arrhythmias and myocardial damage, suggesting a heightened risk of cardiovascular complications associated with their use.¹ Additionally, neurotoxicological assessments have revealed alterations in neurotransmitter systems and neuronal morphology following chronic exposure to these compounds, as documented by Baumann *et al.*¹⁴

Within this thesis hepatotoxic evaluation was another main focal point. Previous research by Simmler *et al.* highlighted the hepatotoxic potential of certain MDC derivatives.²⁶ Hepatotoxicity refers to a compound's ability to damage liver cells, and studies such as Vanlente *et al.* has demonstrated that exposure to MDCs can lead to elevated liver enzymes in animal models, indicating possible liver injury. These substances could potentially contribute to multiple liver-related complications. Once ingested, MDCs are metabolised in the liver, where they can form reactive or toxic metabolites that are not easily eliminated from the body.¹

One of the more popular compounds, MDPV, has shown a notable potential for hepatotoxicity.³⁰ Upon entering the body, MDPV undergoes extensive hepatic metabolism. *In vitro* studies using liver microsomes, alongside *in vivo* investigations in both humans and rats, have identified that MDPV is initially metabolized via O-demethylation of its 3,4-methylenedioxy ring, forming 3,4-dihydroxypropylone (3,4-catechol-PV), followed by O-methylation to produce 4-hydroxy-3-methoxy-propylone (4-OH-3-MeO-PV). These metabolic steps are primarily facilitated by cytochrome P450 enzymes- more specifically CYP1A2, CYP2D6 and CYP2C19- with catechol-O-methyltransferase (COMT) responsible for the methylation. Both phase I metabolites are further processed through phase II conjugation pathways. In human and rat urine, glucuronide conjugates are predominant,

while sulphate conjugates are also observed in human liver microsomes.³¹ These metabolic by-products may contribute to compounds hepatotoxic effects. Research has identified that chronic use of MDPV has been linked to significant liver damage, including inflammation, cellular injury, fibrosis, and in severe cases, liver failure.³² These findings underline the importance of understanding MDC metabolism as a key factor of assessing their toxicological risk.

Recognising the signs of liver toxicity is crucial as early intervention will potentially prevent further damage. Common symptoms of liver damage include jaundice (skin visible looking yellow), abdominal pain, nausea, vomiting dark urine and fatigue.³³ To reduce the risks of liver toxicity, it is advisable to avoid the use of methylenedioxy methcathinones altogether. Education and public awareness campaigns about the potential risks of these substances are essential in preventing their use and promoting safer alternatives for recreational activities.

With MDCs it is difficult to pinpoint the result of cytotoxic effect. Synthetic cathinones have been found to be more cytotoxic than others due to their concentration and exposure times influencing the severity of cytotoxicity.¹ Cytotoxic studies are typically conducted in lab-based environments using cell cultures and the results may not directly translate to the effects observed in a person.

By examining existing literature, this study aims to contribute to the current understanding of MDC's and their toxicity in preestablished liver cell lines, shedding light on the potential dangers they pose to users and the importance of effective prevention and harm reduction strategies.

2 Aims

The primary objective of this research was to replicate the synthesis of methylenedioxypropylamphetamine (MDPV) and investigating the feasibility of synthesising seven structurally related methylenedioxy cathinone derivatives. The compounds were intended for use as reference standards in forensic drug testing, specifically within the MANDRAKE (**MAN**chester **D**rug **A**nd **K**nowledge **E**xchange) initiative, which aims to identify and distinguish seized substances based on their chemical profiles.

Each compound was fully characterised using ^1H and ^{13}C nuclear magnetic resonance (NMR), attenuated total reflectance Fourier-transform infrared spectroscopy (ATR-FTIR), and gas chromatography-mass spectrometry (GC-MS) to confirm structural identity. Novel analogues, including putylone (**9b**) and MDPHP (**10a**), were prioritised for full characterisation due to the lack of existing reference data and will be reported for future comparative use.

A GC-MS method was developed and validated for the detection and separation of the target cathinones, alongside caffeine (a common adulterant) and methyl stearate (internal standard). This method was designed to support high-throughput screening and to be incorporated into the MANDRAKE analytical library.

In conjunction with the synthesis and characterisation work, the hepatotoxic potential of the synthesised compounds was assessed using *in vitro* liver cell lines (LX-2 and HepG2). Cytotoxicity assays were performed at concentrations reflecting both postmortem toxicological data and higher theoretical exposures to evaluate potential liver toxicity under acute and chronic conditions.^{34, 35}

3 Research Premise

It is proposed that all methylenedioxy-substituted cathinone derivatives—specifically MDPV, pentylone, dipentylone, N-ethylpentylone, putylone and MDPHP— can be successfully synthesised using a generalised synthetic route adapted for each individual compound, yielding sufficient quantities for complete chemical and cytotoxic analysis. Each derivative is expected to be structurally confirmed through comprehensive ^1H and ^{13}C NMR characterisation, with key spectral similarities identified to support the future recognition of related novel derivatives.

Due to shared core structure of the methylenedioxy cathinone class, ATR-FTIR spectra are anticipated to be highly similar across all compounds. In parallel, a validated GC-MS method will be developed to ensure complete chromatographic separation of all derivatives from a single mixture, thereby enabling rapid and accurate identification. This method will also be optimised to prevent compound degradation during analysis, enhancing its suitability for integration into MANDRAKE drug testing framework.

In terms of toxicological evaluation, it is expected that all derivatives will exhibit measurable cytotoxicity in LX-2 cell lines, which will enable the progression of HepG2 cell line testing. The cytotoxic effects in HepG2 cell lines are predicted to be observable at both postmortem-reported concentrations and at higher theoretical doses, suggesting a significant potential for hepatotoxicity upon ingestion. The resulting toxicological data will complement existing literature for known methylenedioxy cathinone derivatives and will provide a complete characterisation profile—both chemical and cytotoxic—for the novel compounds putylone and MDPHP, addressing a current gap in the scientific record.

4 Experimental

4.1 Methods & Materials (Chemistry)

Commercially available reagents, purchased from Sigma Aldrich (Sigma-Aldrich, Gillingham, UK), Apollo Scientific (Apollo Scientific, Stockport, UK), Key Organics (Key Organics Ltd, Cornwall, UK), Thermo-scientific (Thermo Fisher Scientific, Altrincham, UK) or Fisher Chemical (Fisher Scientific, Leicestershire, UK), were all used throughout, without further purification. Solvents were dried, where necessary, using standard procedure. Melting points were determined using Stuart Melting point instrument (Barloworld Scientific, Staffordshire, UK). Thin layer chromatography (TLC) was performed on aluminium-backed, silica gel 60 plates (Merck, Darmstadt, Germany) and spots visualised using ultraviolet light from the UVP Chromato-Vue Instrument. (Thistle Scientific, Warwickshire, UK).

4.1.1 Nuclear Magnetic Resonance (NMR) Spectroscopy

High-field ^1H NMR and $^{13}\text{C}\{^1\text{H}\}$ NMR spectra (20 mg/mL in DMSO-d_6) were acquired on a JOEL ECZR-500 FT (JOEL, Tokyo, Japan) 11.7 Tesla Nuclear Magnetic Resonance spectrometer operating at a proton resonance frequency of 500.17 MHz and a carbon Resonance of frequency of 125.77 MHz, referenced to the residual solvent peak (DMSO-d_6 : ^1H NMR $\delta = 2.50$ ppm. $^{13}\text{C}\{^1\text{H}\}$ NMR $\delta = 39.52$ ppm, respectively).³⁶ A micro spatula of the material (5 – 10 mg ca) were dissolved in DMSO-d_6 (0.7 mL). All samples were filtered through 0.45 μm polyvinylidene difluoride syringe filters into a small ampule, which was then transferred using a glass pipette into an NMR tube. After the sample has been inserted, an automated procedure began whereby the instrument would lock on to the deuterated signature of DMSO (thus used as a chemical shift reference) before acquiring 16 scans. Following acquisition, the data was processed in MNova (Mestrelab Research, Santiago de Compostela, Spain) using an automated script file.

4.1.2 Attenuated Total Reflectance Fourier-Transform Infra Red (ATR-FTIR) spectroscopy.

Infrared spectra were obtained in the range 4000 – 650 cm^{-1} using a Thermo Scientific Nicolet iS10ATR-FTIR instrument (Thermo Scientific, Rochester, USA) equipped with diamond attenuated total reflectance (ATIR) accessories. Samples were ground using a pestle and motor prior to analysis to ensure good sample homogeneity. Sixteen scans were acquired of each sample (ca 2-5 mg) with a resolution of 4 cm^{-1} . Qualitative identification of the components present in a sample were performed using OMNIC (Thermo Scientific, Rochester, USA) against defined libraries (Scientific database (version 10.5.3.738), SWGDRUG IR libraries (version 2.1)). Both search platforms utilised a correction search to determine the component(s) present. The highest match score was used for identification purposes.

4.1.3 Gas Chromatography-Mass spectrometry (GC-MS)

GC-MS analysis was performed using Agilent 7890B GC and MS 5977B mass selective detector (Agilent Technologies, Workington, UK) the mass spectrometer operated in the electron ionisation mode at 70 eV. Separation was achieved with a capillary column (HP5 MS, 30 m $\text{Å} \sim 0.25 \text{ mm}$.i.d 0.25 μm) using helium as the carrier gas at a constant flow rate of 1 mL min^{-1} . The initial oven temperature was set to 120 $^{\circ}\text{C}$ prior to being ramped to 300 $^{\circ}\text{C}$ in 30 $^{\circ}\text{C min}^{-1}$ intervals. A hold time of 2 min was used at 300 $^{\circ}\text{C}$ to give a total run time of 8 mins. A 0.5 μL aliquot of the sample was injected with a split ratio of 50:1. The injector was maintained at 300 $^{\circ}\text{C}$ and the GC interface temperature maintained at 300 $^{\circ}\text{C}$. The MS source and quadrupole temperatures were set at 230 $^{\circ}\text{C}$ and 150 $^{\circ}\text{C}$. Mass spectra were obtained in full scan mode (50 – 550 amu; qualitative analysis) and Selected Ion Monitoring (SIM) mode (quantitative analysis) using four specific fragment ions for each analyte. A base ion fragment was used for quantification while the two/three ions were used as qualifiers (**Table 8**). Stock solutions for quantification were prepared at 0.1 mg mL^{-1} and then diluted further to six concentrations between 0 and 70 $\mu\text{g mL}^{-1}$ containing methyl stearate (20 $\mu\text{g mL}^{-1}$). Samples were prepared in the same manner, the diluted 70 $\mu\text{g mL}^{-1}$ without the methyl stearate was used for qualitative analysis to conclude compound purity.

Validation was performed using an Agilent 7890B GC and MS 5977B mass selective detector (Agilent Technologies, Workington, UK) operating on the same parameters detailed above. Mass spectra was obtained under Selective Ion Monitoring (SIM) mode. The GC-MS method was obtained using the Selected Ion Monitoring (SIM) mode and was validated in accordance with the ICH guidelines using the following parameters: linearity, accuracy, precision, limit of detection (LOQ). *Linearity, Precision*: six replicate injections of the calibration standards were performed, and the data was analysed under the same conditions. The RSD % was calculated for each replicate test sample. *Accuracy (percentage recovery study)*: determined from the spiked samples prepared in triplicate at three levels over a range of 80 – 120 % of the target concentration ($40 \mu\text{g mL}^{-1}$). The percentage recovery and RSD % were calculated for each of the replicate samples. *Limits of Detection and quantification*: six replicate injections to the calibration standards were performed, and the data analysed under the same conditions. The limits of detection and quantification were determined on the standard deviation of the response and slope of the calibration curve, where 3.3 and 10 times the standard deviation of the response was used to calculate the LOD and LOQ, respectively.

4.2 Synthesis of methylenedioxy-cathinone derivatives

4.2.1 General procedure for synthesis of methylenedioxycathinones

The racemic compounds: pentylone hydrochloride, dimethylpentylone hydrochloride, N-ethylepentylone hydrochloride, butylone hydrochloride and Putylone hydrochloride were all synthesised from a two-step synthesis route starting from their appropriate propiophenone as seen in **Scheme 1**. All pentyl derivatives required their desired propiophenone to be synthesised as it was not commercially available. Standards of these synthetic products were provided by MANDRAKE.

4.2.2 Synthesis of 1-(1,3-benzodioxol-5-yl) penta-1-one (**2**)

To a solution of 1,3-benzodioxol (123mmol) and valeryl chloride (133 mmol) in dichloromethane (100 mL) at 3°C was added tin (IV) chloride (154 mmol) dropwise over 30 minutes. The mixture was then stirred for 15 minutes before poured into a mixture of

concentrated hydrochloric acid (75 mL) and ice (100 g) with vigorous stirring. The phases were separated, and the organic layer was washed with water (50 mL), dried over sodium sulphate, filtered and concentrated at reduced pressure. The crude product was purified via column chromatography (SiO₂) eluting with hexane/ethyl acetate (95:5) to give a yellow oil.

4.2.3 Preparation of the intermediate (\pm)- α -bromoketones (**5-7**)

To a stirring solution of ketone (**2** or **3**, 24.5 mmol) in dichloromethane (20 mL) was added one/two drops of hydrobromic acid (48% aqueous solution) and one drop of bromine. The mixture was stirred at room temperature until the bromine colour was discharged (*circa* 30 s) and additional bromine (24.5 mmol in total including the one drop) was added dropwise with stirring. The mixture was stirred for one hour and then concentrated in vacuo to reveal a dark oil. The crude product was recrystallized from diethyl ether to give a dark yellow oil and used without quantification.

4.2.4 Preparation of (\pm)-cathinones hydrochlorides (**8a,b**, **9a-c**, **10a**)

The α -bromoketone (**4** or **5**, 20 mmol) and appropriate amine hydrochloride (20 mmol) were dissolved in dichloromethane (30 mL) and triethylamine (40 mmol) was added. The mixture was stirred at room temperature for sixteen hours. The mixture was then acidified until pH~1 with 6M hydrochloric acid (50 mL). The aqueous layer was washed with dichloromethane (3 x 50 mL) and then basified until pH~10 with 5 M sodium hydroxide (*circa* 100 mL) and then re-extracted with dichloromethane (3 x 50 mL). The combined organic fraction was dried with magnesium sulphate and concentrated in vacuo to give a viscous oil. The crude free-base cathinone was redissolved in propan-2-ol (5 mL), treated with hydrochloric acid (3M in CMPE, 10 mL) and stirred to reveal a pale-yellow solid (*circa* 30 mins). The crude cathinone hydrochloride was then filtered, washed with diethyl ether and recrystallised from acetone to give **8a-10a**.³⁷

4.3 Methylenedioxy cathinone derivatives **8a-10a**

4.3.1 Pentylone hydrochloride (1-(3,4-methylenedioxyphenyl)-2-(methylamino)pentan-1-one, **8a**)

Beige Powder (61 % from 6). IR (ATR-FTIR): 3053-2526 (N-H and C-H), 1674 cm^{-1} (C=O), 1605 cm^{-1} (Aromatic C=C), 1263 cm^{-1} (C-O), 1030 cm^{-1} (C-N); ^1H NMR (500 MHz, DMSO- d_6) δ = 9.59 and 9.19 (2 x s, 2 x 1H), 7.72 (dd, 4J = 1.77, 3J = 8.24, 1H), 7.54 (d, 4J = 1.77, 1H), 7.13 (d, 3J = 8.24, 1H), 6.19 (s, 2H), 5.15 (t, 3J = 5.38, 1H), 2.53 (s, 3H), 1.75-1.93 (m, 2H), 1.22-1.34 (m, 1H), 1.0-1.15 (m, 1H), 0.79 (t, 3J = 7.3, 3H); $^{13}\text{C}\{^1\text{H}\}$ NMR (127 MHz, DMSO- d_6) δ = 194.1 (C=O, C8), 152.8 (C, C7), 148.2 (C, C2), 128.5 (C, C4), 125.8 (CH, C5), 108.5 (CH, C6), 107.8 (CH, C3), 102.5 (ArCH₂, C1), 61.6 (CH, C9), 31.9 (CH₂, C10), 31.3 (CH₃, C14), 17.1 (CH₃, C11), 13.6 (CH₃, C11); GC-EI-MS (**Fig. 31**, +ve, 70 eV): t_{R} = 4.95 min; 149 (6.5), 121.0 (7.6) and **86.0** (100.0%).

4.3.2 Dimethylpentylone hydrochloride (1-(1,3-benzodioxol-5-yl)-2-(dimethylamino)pentan-1-one, **8b**)

Beige Powder (9% from 6). IR (ATR-FTIR): 3077-2438 (N-H and C-H), 1673 cm^{-1} (C=O), 1612 cm^{-1} (Aromatic C=C), 1258 cm^{-1} (C-O), 1035 cm^{-1} (C-N); ^1H NMR (500 MHz, DMSO- d_6) δ = 10.5 (s, 1H), 7.72 (dd, 4J = 1.65, 3J = 8.25, 1H), 7.58 (d, 4J = 1.65, 1H), 7.15 (d, 3J = 8.25, 1H), 6.21 (s, 2H), 5.32 (s, 1H), 2.85 (s, 3H), 2.77 (s, 3H), 1.8-1.97 (m, 2H), 1.04-1.21 (m, 2H), 0.81 (t, 3J = 7.3, 3H); $^{13}\text{C}\{^1\text{H}\}$ NMR (127 MHz, DMSO- d_6) δ = 194.3 (C=O, C8), 153.2 (C, C7), 148.4 (C, C2), 129.6 (C, C4), 126.2 (CH, C5), 108.6 (CH, C6), 107.8 (CH, C3), 102.6 (ArCH₂, C1), 66.4 (CH, C9), 42.1 (CH₃, C14), 40.8 (CH₃, C15), 30.4 (CH₂, C10), 17.6 (CH₂, C11), 13.6 (CH₃, C12); GC-EI-MS (**Fig. S26**, +ve, 70 eV): t_{R} = 5.04 min; 148.9 (4.6), **100.0** (100.0) and 71.0 (3.9%).

4.3.3 *N*-ethylpentylone hydrochloride (1-(benzo[d][1,3]dioxol-5-yl)-2-(ethylamino)pentan-1-one, **8c**)

Colourless Powder (28% from 6). IR (ATR-FTIR): 3053-2523 (N-H and C-H), 1672 cm^{-1} (C=O), 1602 cm^{-1} (Aromatic C=C), 1253 cm^{-1} (C-O), 1035 cm^{-1} (C-N); ^1H NMR (500 MHz,

DMSO-d₆) δ = 9.17 (s, 2H), 7.71 (dd, 4J = 1.83, 3J = 8.25, 1H), 7.53 (d, 4J = 1.83, 1H), 7.08 (d, 3J = 8.25, 1H), 6.15 (s, 2H), 5.12 (t, 3J = 5.58, 1H), 2.78-2.97 (m, 2H), 1.75-1.98 (m, 2H), 1.23-1.29 (m, 1H) 1.21 (t, 3J = 7.26 3H), 0.97-1.10 (m, 1H) 0.74 (t, 3J = 7.34, 3H); $^{13}\text{C}\{^1\text{H}\}$ NMR (127 MHz, DMSO-d₆) δ = 194.2 (C=O, C8), 152.9 (C, C7), 148.2 (C, C2), 128.6 (C, C4), 125.9 (CH, C5), 108.5 (CH, C3), 107.9 (CH, C6), 102.5 (ArCH₂, C1), 60.0 (CH, C9), 41.08 (CH₂, C14), 32.1 (CH₂, C10), 17.2 (CH₂, C11), 13.68 (CH₃, C15) 11.06 (CH₃, C12); GC-EI-MS (**Fig. S27**, +ve, 70 eV): t_R = 5.09 min; 149.0 (10.9), **100.0** (100.0) and 58.0 (7.4%).

4.3.4 Butylone hydrochloride (1-(1,3-Benzodioxol-5-yl)-2-(methylamino)butan-1-one, **9a**)

Colourless powder (16 % from 5). IR (ATR-FTIR): 3006-2397 (N-H and C-H), 1664 cm⁻¹ (C=O), 1603 cm⁻¹ (Aromatic C=C), 1264 cm⁻¹ (C-O), 1034 cm⁻¹ (C-N); ^1H NMR (500 MHz, DMSO-d₆) δ = 9.44 (2 x s, 2H), 7.72 (dd, 4J = 1.83, 3J = 8.17, 1H), 7.55 (d, 4J = 1.83, 1H), 7.12 (d, 3J = 8.17, 1H), 6.19 (s, 2H), 5.16 (s, 1H), 2.52 (s, 3H), 1.84-2.07 (m, 2H), 0.76 (t, 3J = 7.57, 3H); $^{13}\text{C}\{^1\text{H}\}$ NMR (127 MHz, DMSO-d₆) δ = 193.9 (C=O, C8), 152.8 (C, C7), 148.2 (C, C2), 128.5 (C, C4), 125.8 (CH, C5), 108.5 (CH, C6), 107.8 (CH, C3), 102.5 (ArCH₂, C1), 62.4 (CH, C9), 31.2 (CH₃, C13), 23.0 (CH₂, C10), 8.18 (CH₃, C11); GC-EI-MS (**Fig. S28**, +ve, 70 eV): t_R = 4.66 min; 148.9 (5.4), 121.0 (6.1) and **72.1** (100%).

4.3.5 Putylone hydrochloride (1-(1,3-benzodioxol-5-yl)-2-(propylamino)butan-1-one, **9b**)

Colourless crystalline Powder (65 % from 5). IR (ATR-FTIR): 3116-2496 (N-H and C-H), 1668 cm⁻¹ (C=O), 1604 cm⁻¹ (Aromatic C=C), 1263 cm⁻¹ (C-O), 1034 cm⁻¹ (C-N); ^1H NMR (500 MHz, DMSO-d₆) δ = 9.64 and 9.00 (2 x s, 2 x 1H), 7.75 (dd, 4J = 1.83, 3J = 8.17, 1H), 7.57 (d, 4J = 1.83, 1H), 7.12 (d, 3J = 8.17, 1H), 6.19 (s, 2H), 5.20 (s, 1H), 2.86-2.89 (s, 1H), 2.75-2.69 (s, 1H), 1.97-2.09 (m, 1H), 1.88-1.97 (m, 1H), 1.65-1.77 (m, 2H), 0.88 (t, 3J = 7.49, 3H), 0.77 (t, 3J = 7.57, 3H); $^{13}\text{C}\{^1\text{H}\}$ NMR (127 MHz, DMSO-d₆) δ = 194.1 (C=O, C8), 152.9 (C, C7), 148.2 (C, C2), 128.6 (C, C4), 125.9 (CH, C5), 108.5 (CH, C6), 107.9 (CH, C3), 102.5 (ArCH₂, C1), 61.2 (CH, C9), 47.6 (CH₂, C13), 23.2 (CH₂, C14), 19.0 (CH₂, C10), 11.0 (CH₃, C15), 8.5

(CH₃, C11); GC-EI-MS (**Fig. S29**, +ve, 70 eV): t_R = 5.14 min; 149.0 (9.1), **100.0** (100) and 58.0 (16%).

4.3.6 MDPHP hydrochloride (1-(benzo[d][1,3]dioxol-5-yl)-2-(pyrrolidin-1-yl)hexan-1-one, **10a**)

Colourless Powder. (Standard retrieved from MANDRAKE). IR (ATR-FTIR): 3106-2368 (N-H and C-H), 1683 cm⁻¹ (C=O), 1607 cm⁻¹ (Aromatic C=C), 1257 cm⁻¹ (C-O), 1033 cm⁻¹ (C-N); ¹H NMR (500 MHz, DMSO-d₆) δ = 10.3 (s, 1H), 7.71 (dd, , ⁴J= 1.62, ³J= 8.25, 1H), 7.52 (d, ⁴J= 1.62, 1H), 7.12 (d, ³J= 8.25, 1H), 6.17 (s, 2H), 5.35 (t, ³J= 5.42, 1H), 3.5-3.62 (m, 1H), 3.33-3.43 (m, 1H), 3.09-3.2 (m, 1H), 2.88-2.99 (m, 1H), 1.8-2.05 (m, 6H), 0.9-1.23 (m, 4H), 0.72 (t, ³J= 7.09, 3H); ¹³C{¹H} NMR (127 MHz, DMSO-d₆) δ = 195.0 (C=O, C8), 153.5 (C, C7), 148.9 (C, C2), 129.5 (C, C4), 126.7 (CH, C5), 109.2 (CH, C6), 108.4 (CH, C3), 103.2 (ArCH₂, C1), 67.6 (CH, C9), 54.3 (CH₂, C18), 52.5 (CH₂, C15), 33.3 (CH₂, C16), 33.1 (CH₂, C17), 30.2 (CH₂, C10), 26.3 (CH₂, C11), 22.4 (CH₂, C12), 14.0 (CH₃, C13); GC-EI-MS (**Fig. S30**, +ve, 70 eV): t_R = 6.17 min; 149.0 (5.2), **140.0** (100) and 65.0 (2.3%).

4.4 Method & Materials (Cytotox)

For LX-2 and HepG2 culture, Dulbecco's modified Eagle's medium (DMEM: with 4.5 g/L glucose, L-glutamine and without NA-pyruvate), fetal bovine serum (FBS), penicillin/streptomycin solution (10,000 U/mL penicillin and 10,000 ug/mL streptomycin), and phosphate-buffered saline (PBS) were purchased from VWR International, LLC (Avantor, Chorley, UK). Dimethyl sulfoxide (DMSO), Gibco™ Trypan Blue Solution and Promega CellTox™ Green Cytotoxicity Assay kit were obtained from Fisher-scientific (Thermo Fisher Scientific, Rochester, USA). The 96-Well Special Optics Microplates were from Sigma Aldrich (Sigma-Aldrich, Gillingham, UK).

3,4-methylenedioxy pyrovalerone (MDPV), pentylone hydrochloride, dimethylpentylone hydrochloride, *N*-ethylpentylone hydrochloride, putylone hydrochloride and 3,4-methylenedioxy- α -pyrrolidinohexiophenone (MDPHP) standards were provided by MANDRAKE (Manchester, UK).

4.4.1 Mycoplasma

All cells used in the assays were mycoplasma free. BUF305 treatment was used to remove mycoplasma and only negative cells were used.

4.4.2 LX-2 Cell Culture

LX-2 Cells (LX-2 Human Hepatic Stellate Cell Line)³⁴, were used for the cytotoxicity studies LX-2 cells were then cultured in DMEM medium supplemented with 1% fetal bovine serum (FBS), 1% penicillin and streptomycin solution and 1% L-glutamine. Cells were cultured at 37.5°C in a 5% CO₂; complete medium was changed every 2 to 3 days. For experimental procedures, cells were seeded in 96-well plates at a concentration of 20,000 cells per well, unless otherwise specified.

4.4.3 HepG2 Cell Culture

HepG2 cells (ATCC HB-8065, a human hepatocellular carcinoma epithelial cell line)³⁵, were used for the cytotoxicity studies. HepG2 cells were cultured in DMEM medium supplemented with 10% fetal bovine serum (FBS), 1% penicillin and streptomycin solution and 1% L-glutamine. Cells were cultured at 37.5°C in a 5% CO₂; complete medium was changed every 2 to 3 days. For experimental procedures, cells were seeded in 96-well plates at a concentration of 20,000 cells per well, unless otherwise specified.

4.4.4 Compound Preparation and cell treatments

To evaluate all assays cytotoxicity, cell lysis buffer was used as a positive control. Methylenedioxy pyrovalerone (MDPV) was used as a reference in each assay as it had shown to be cytotoxic in HepG2 and HepRG cells in previous research between concentrations 0.001 to 2 mM. This data was used to validate the assays performed in this research.

LX-2 or HepG2 cells were seeded in 96-well plates and incubated for 24hrs. All compounds (5 mg) were diluted in DMSO (1 mL) and further diluted in complete medium to obtain the desired concentration (LX-2: 0.0018-0.0001 mM and HepG2: 0.001-2 mM). The medium was aspirated and a volume of 0.2 mL per well of diluted compound was added in quadruplicate (n=4). A serial dilution was performed from the starting wells, to broaden

concentrations. Cells were cultured overnight in 96-well plates. In untreated cells, half were treated with only medium to serve as a negative control. The remaining cells were treated with Lysis buffer to act as a positive control. Wells that didn't contain cells acted as a baseline for the assay. In all experiments, cells were incubated for 24 hr. After this time, the assay was performed.

4.4.5 CellTox™ Green

The use of CellTox™ Green (Promega) is based on the ability to measure changes in membrane integrity that occur because of cell death. The dye is tolerated by a wide variety of cell types and is essentially nontoxic. It can be diluted in culture medium and applied directly to the cells at the time of seeding or dosing, enabling “no-step” kinetic measurements of cytotoxicity. Alternatively, for this research, a conventional endpoint measure of 24hrs was used. The dye can be diluted in assay buffer and added to the cells after an exposure period. CellTox™ Green excludes viable cells but selectively binds to the DNA of dead cells. Upon binding to the DNA in compromised cells, the dye's fluorescence is significantly enhanced. Viable cells do not exhibit a noticeable increase in fluorescence. Thus, the fluorescent signal generated by the dye binding to dead-cell DNA is directly proportional to cytotoxicity. The fluorescence compounds can be measured by the plate reader. For cytotoxicity experiments, cells were grown in black 96-well clear view plates. The plates are designed for optimal measurement of fluorescence but that at the same time have transparent well bottoms, allowing for visual control of the cells during cell culture. After 24hrs of exposure to the different compounds, 100 µL of diluted CellTox™ Green solution (2:1000 CellTox™ Green in Buffer Solution) was added. Cells were incubated for 15 minutes at 37 °C and 5% CO₂. After this time, fluorescence was measured on a GloMax Plate reader (GloMax Explorer Multimode Microplate Reader, Promega, USA).

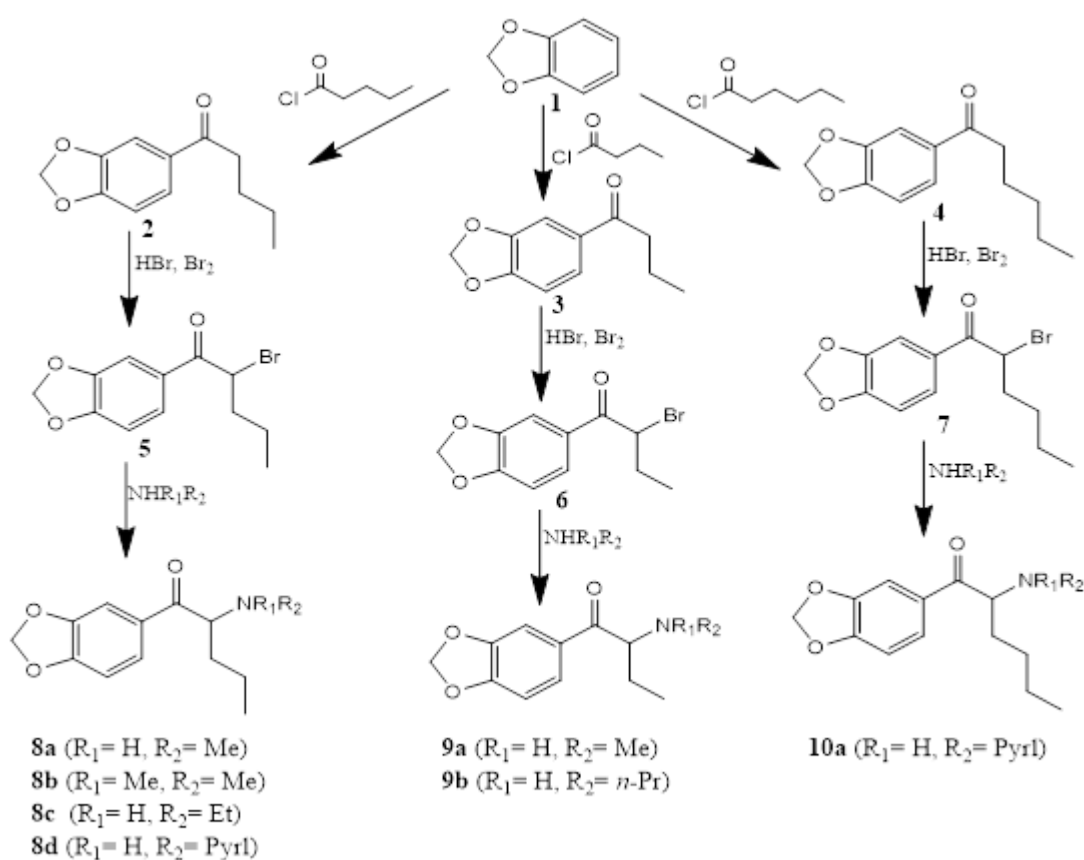
4.4.6 Statistical Analysis

Data was presented as mean ± standard error of the mean (SEM), with error bars representing SEM. Comparisons between the data sets were made using Two-Way Analysis of Variance (ANOVA) with Bonferroni's multiple comparison post hoc test. A

probability value of $p < 0.05$ was considered statistically significant. Statistical analysis and graph creation was performed using GraphPad Prism software (Version 10.2.3).

5 Results & Discussion

The methylenedioxy cathinone hydrochloride derivatised compounds, **8a-10a** were prepared as detailed in **Scheme 1**. The starting propiophenones, **2**, **3** and **4**, were protonated using hydrobromic acid to form the nucleophilic enol tautomer which were then brominated to produce **5,6** and **7** 2-bromoalkylphenones (where alkyl = propyl, butyl or pentyl respectively), which were used without purification. Nucleophilic attack on the 2-bromoalkylphenones from the lone pair on the desired amine followed by treatment with hydrochloric acid in cyclopentyl methyl ether (CMPE) and recrystallisation using acetone provided the isolation of the methylenedioxy cathinone hydrochloride salt products **8a-10a** in 8-65% yields.



Scheme 1: Synthetic route to 3,4- methylenedioxy cathinone hydrochloric derivatives **8a-10a**

Synthesis of 3,4-methylenedioxy pyrovalerone (**8d**) was deemed unsuccessful, as it remained trapped in the organic phase during acid base work-up. Despite multiple attempts at recrystallisation using various solvents such as ethanol, acetone and ether, the product failed to solidify and was persistently stuck in oil form. This result indicates that

the purification methods employed were inadequate for isolating the desired compound, potentially due to its high affinity for the organic phase or the possibility of an incomplete reaction.

Pentylone (**8a**) and dimethylpentylone (**8b**) were both synthesised twice, however, after recrystallization using 98% ethanol, it was noticed that the products yields would greatly diminish or even cause the product to dissolve and be lost after being cooled to room temperature and dried. N-ethylpentylone (**8c**) was synthesised three times and the most successful yield was recorded. Butylone (**9a**) and putylone (**9b**) were both synthesised once and isolated with enough product to allow full characterisation, which are discussed in detail below.

5.1 Nuclear Magnetic Resonance (NMR) Spectroscopy

5.1.1 Pentylone hydrochloride (**8a**)

The synthesised standard of pentylone hydrochloride (**8a**) was synthesised, purified via recrystallization using acetone, dried and obtained as a pale beige powder (**Scheme 1**, 61 % overall yield from intermediate) using an adaption of previously reported protocols in Santali *et al.*³⁷ **8a** was analysed by NMR to assist in its full characterisation. ^1H and $^{13}\text{C}\{^1\text{H}\}$ NMR spectra of compound **8a** are shown in **Figures 6** and **7**, respectively. The full assignment of ^1H and $^{13}\text{C}\{^1\text{H}\}$ NMR signals **8a** is presented in **Table 1**. The assignment relied on correlation spectroscopy (COSY, **Figure 8**) to observe ^1H - ^1H couplings, heteronuclear multiple bond correlation (HMBC, **Figure 10**) for two or three bond ^1H - ^{13}C couplings (acquired using an evolution period equivalent to $^2J_{\text{HC}} = 8\text{Hz}$), heteronuclear single quantum coherence (HSQC, **Figure 9**) for ^1H - ^{13}C single bond correlation and distortion enhancement by polarization transfer (DEPT, **Figure 11**) to determine the number of protons directly attached to the carbon atoms.

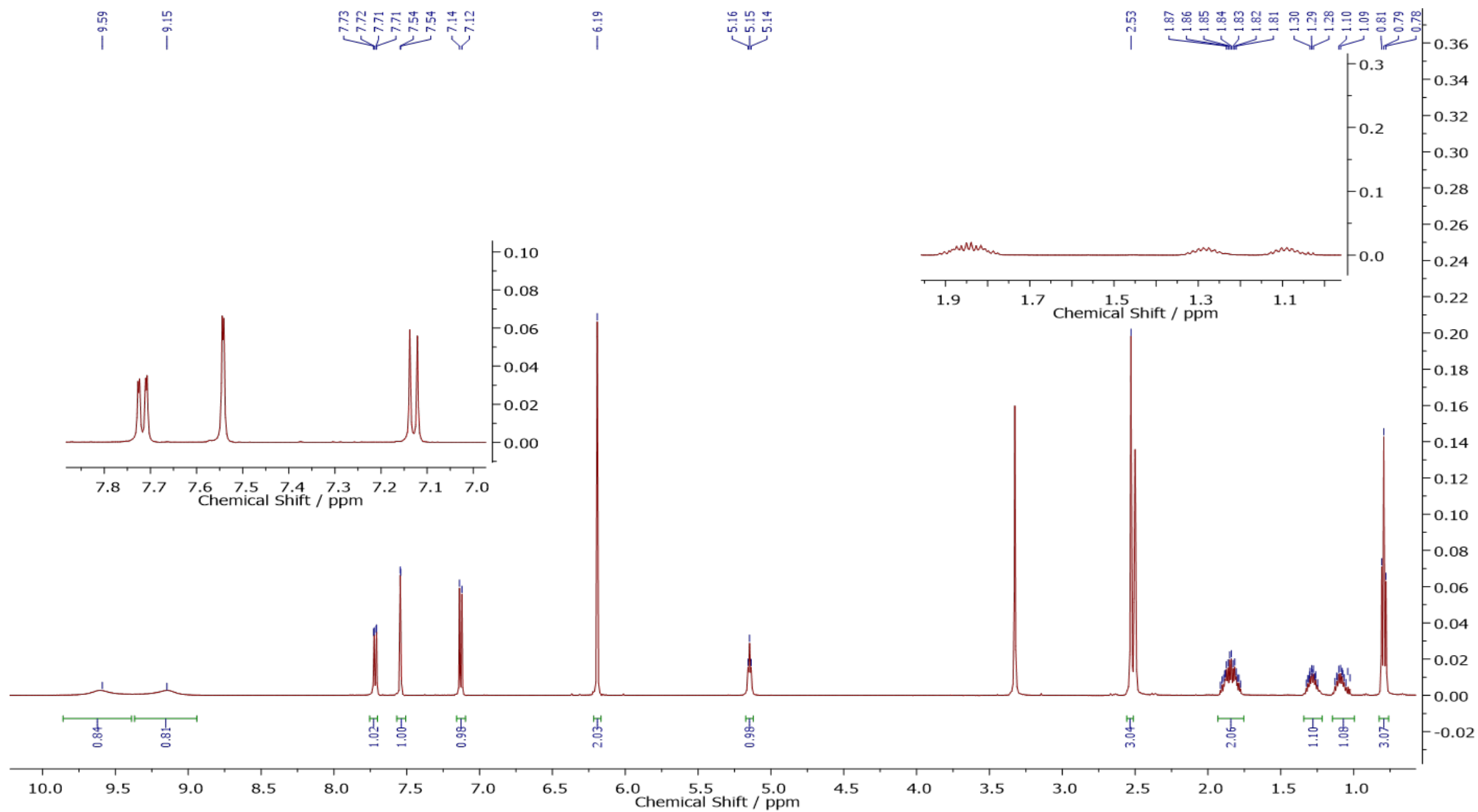


Figure 6: ^1H NMR spectrum of **8a** acquired in DMSO-d_6

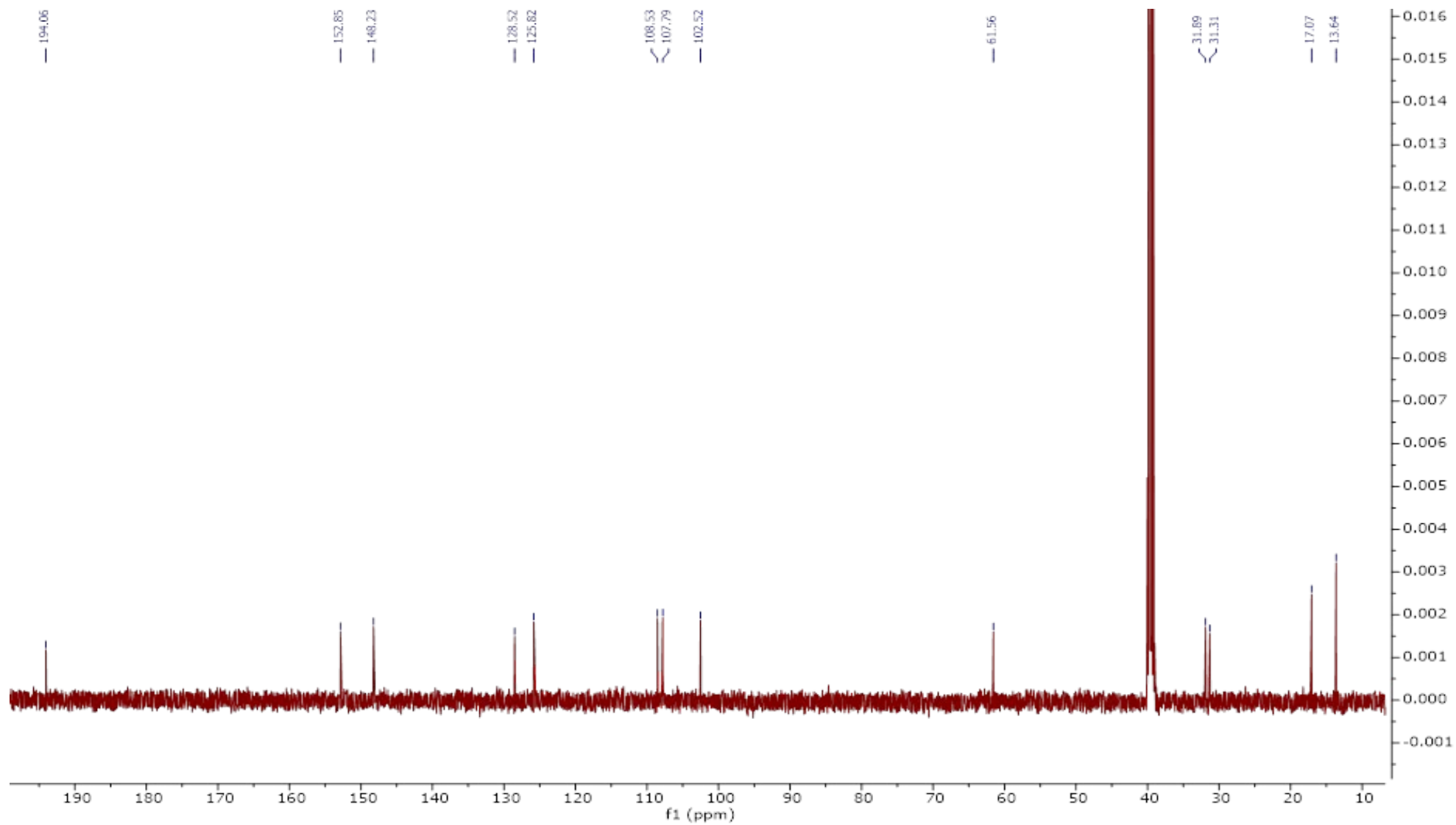


Figure 7: $^{13}\text{C}\{^1\text{H}\}$ NMR spectrum of **8a** acquired in DMSO-d_6 .

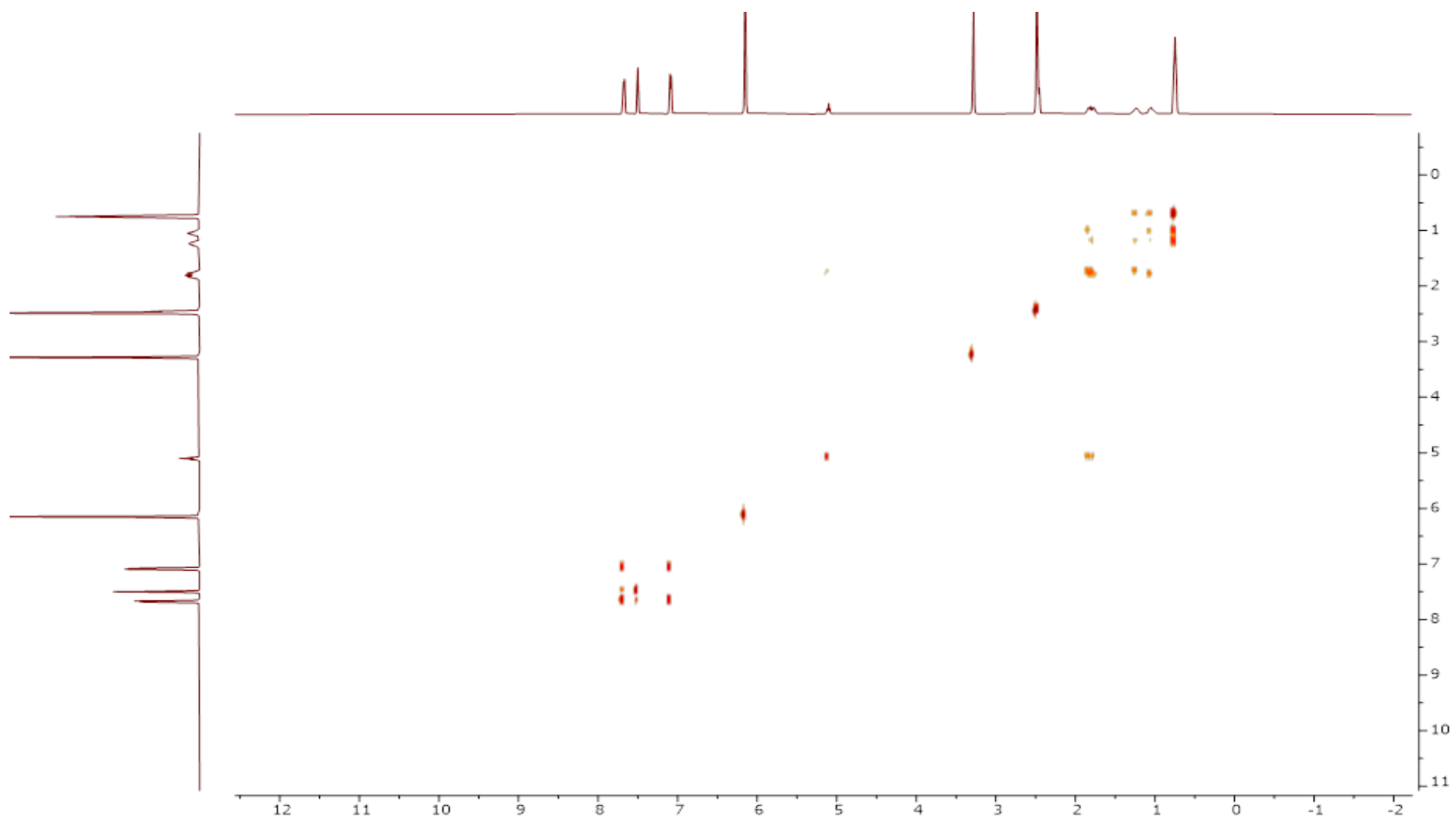


Figure 8: ^1H - ^1H COSY NMR spectrum of **8a** in DMSO-d_6 .

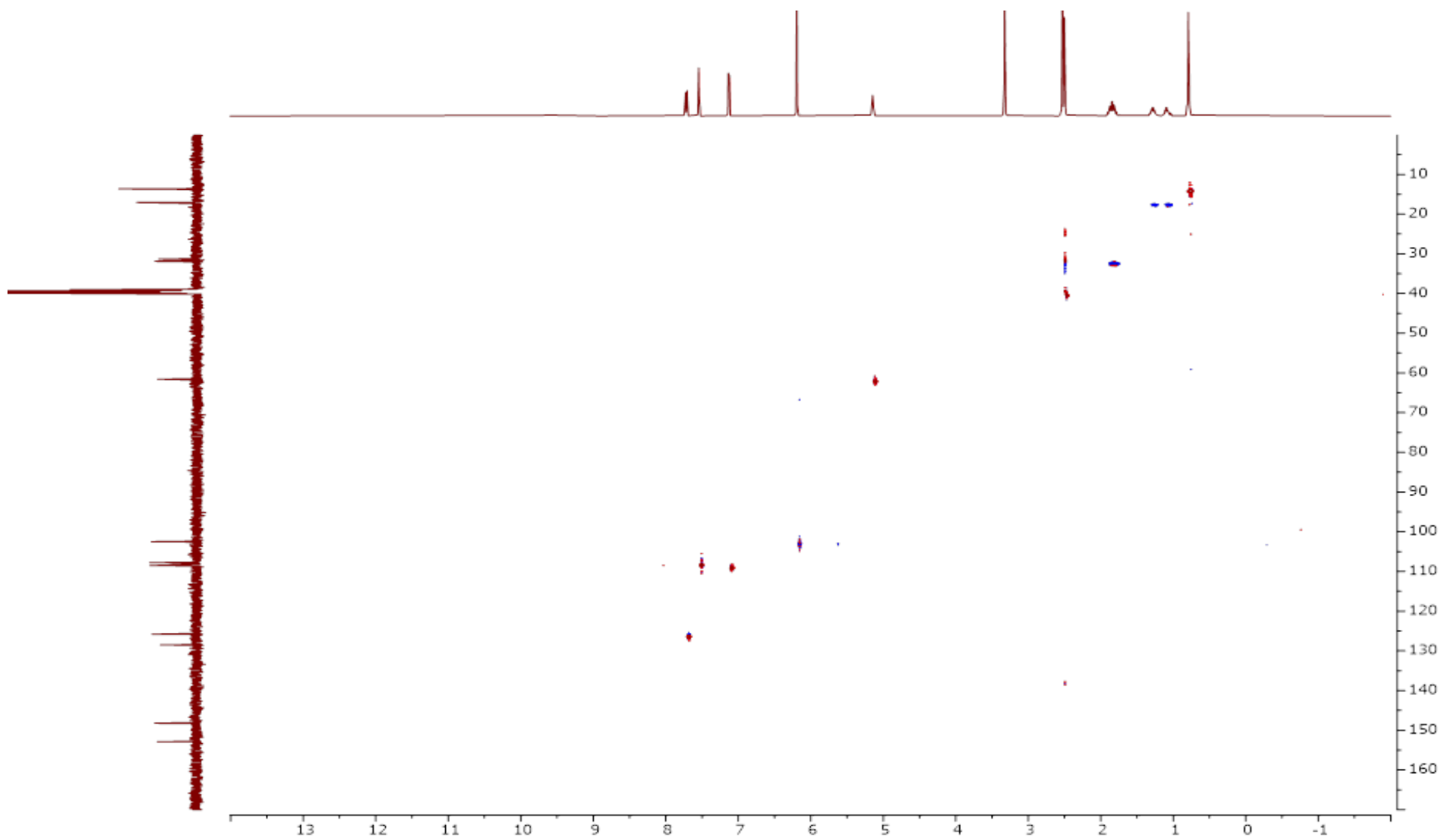


Figure 9: ^1H - $^{13}\text{C}\{^1\text{H}\}$ HSQC NMR spectrum of **8a** in DMSO-d_6 .

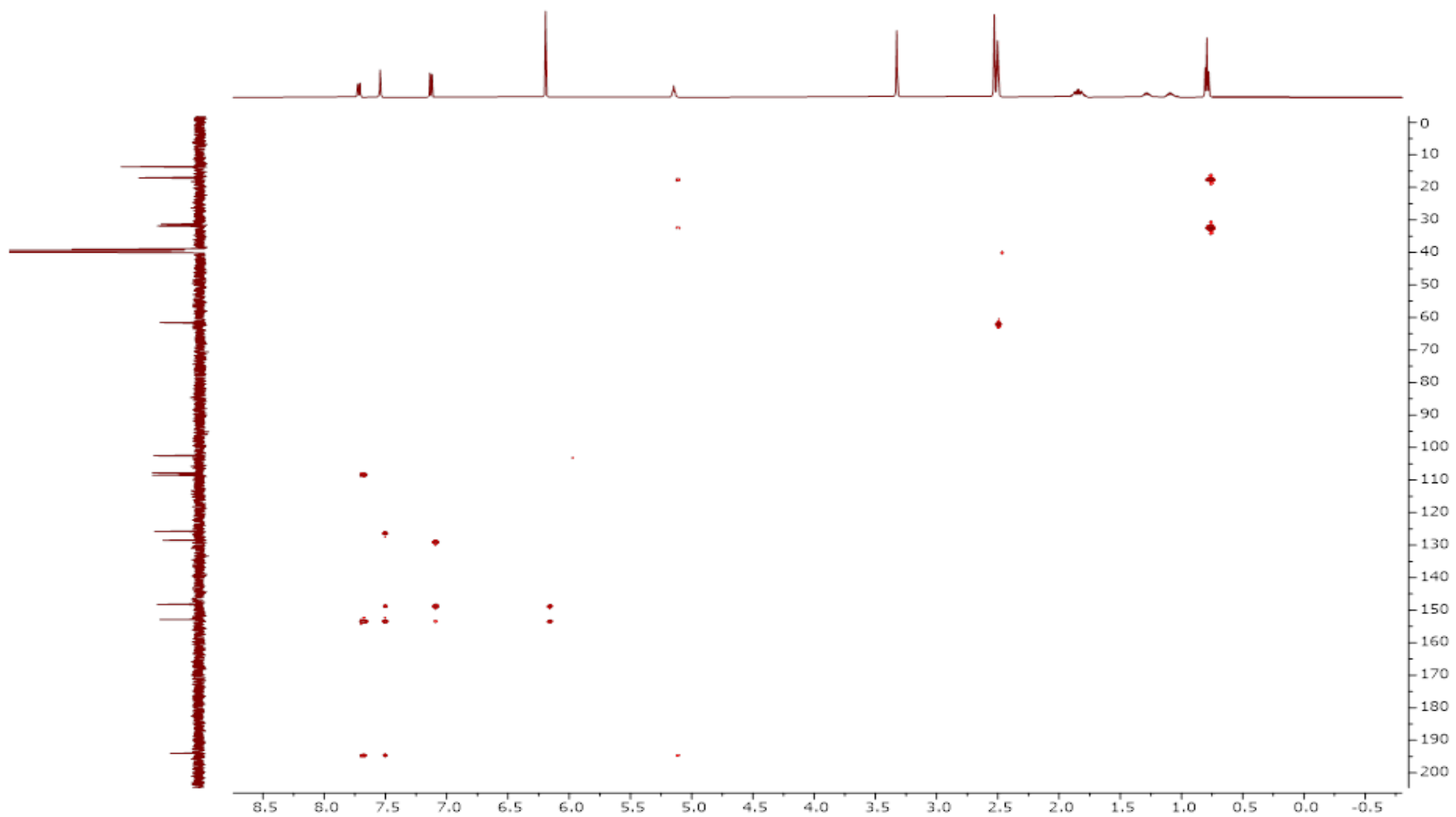


Figure 10: ^1H - $^{13}\text{C}\{^1\text{H}\}$ HMBC NMR spectrum of **8a** in DMSO-d_6

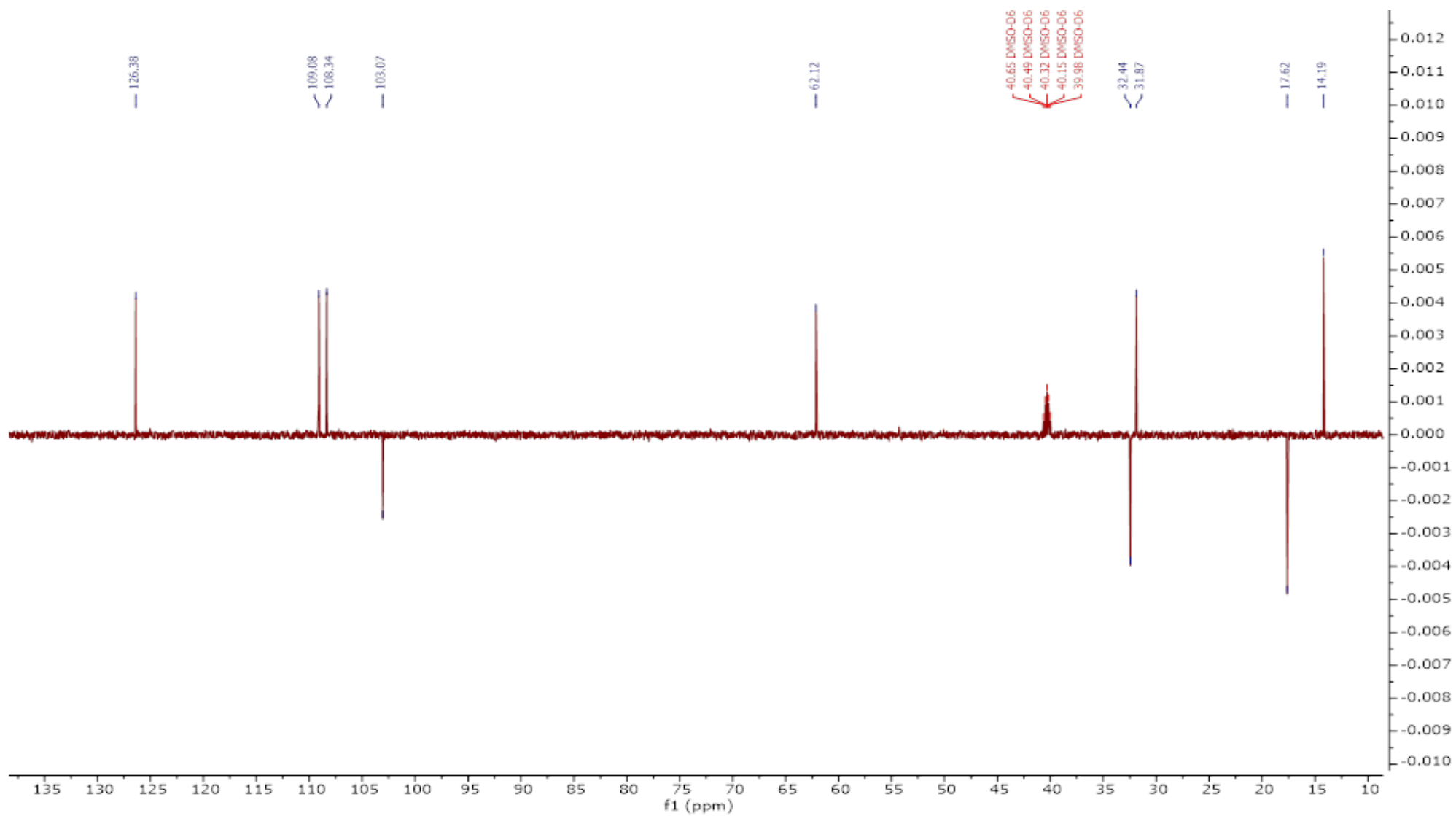


Figure 11: DEPT-135 NMR spectrum of **8a** in DMSO-d₆.

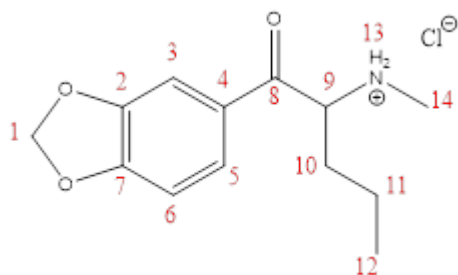


Figure 12: Chemical structure of **8a** with positions numbered.

Table 1: Chemical shifts for signals in the ^1H and $^{13}\text{C}\{^1\text{H}\}$ NMR spectra of **8a**. ^aFor each signal, J-coupling values are reported in Hertz (if present), as well as the integral value.

^bAbsorptive and emissive peaks are recorded as +ve and -ve respectively.

Position	^1H / ppm ^a	$^{13}\text{C}\{^1\text{H}\}$ / ppm	HSQC	DEPT-135 ^b
1	6.19 (s, 2H)	102.5	B (CH ₂)	-ve
2	-	148.2	-	-
3	7.54 (d, ⁴ J=1.77, 1H)	107.8	R (CH ₃ or CH)	+ve
4	-	128.5	-	-
5	7.72 (dd, ⁴ J= 1.77, ³ J= 8.24, 1H)	125.8	R (CH ₃ or CH)	+ve
6	7.13 (d, ³ J= 8.24, 1H)	108.5	R (CH ₃ or CH)	+ve
7	-	152.8	-	-
8	-	194.1	-	-
9	5.15 (t, ³ J= 5.38, 1H)	61.6	R (CH ₃ or CH)	+ve
10	1.75-1.93 (m, 2H)	31.9	B (CH ₂)	-ve
11	1.0-1.15 (m 1H) and 1.22-1.34 (m, 1H)	17.1	B (CH ₂)	-ve
12	0.79 (t, ³ J= 7.3, 3H)	13.6	R (CH ₃ or CH)	+ve
13	9.19 (s, 1H) and 9.59 (s, 1H)	-	-	-
14	2.53 (s, 3H)	31.3	R (CH ₃ or CH)	+ve

The high-field (500 MHz) ^1H NMR spectrum of compound **8a** in DMSO-*d*₆ is presented in **Fig. 6**. The spectrum possesses 12 signals in total. At δ 9.59 and δ 9.19, two broad singlets were observed and identified as the NH protons. The NH₂ protons are diastereotopic and therefore give rise to an individual signal each. Their broad nature indicates that are exchangeable on the NMR timescale. The aromatic protons of the 3,4-methylenedioxy ring are indicated by signals at δ 7.72 (doublet of doublets), δ 7.54 (doublet) and δ 7.13 (doublet). The signal at δ 7.72 possesses a ⁴J_{H5H3}-couplings of 1.77 Hz and a ³J_{H5H6} of 8.24

Hz and is assigned to position 5. A reciprocal $^4J_{\text{H5H3}}$ coupling at 1.77 Hz is also possessed by the signal at δ 7.54 (position 3), and likewise a $^3J_{\text{H5H6}}$ of 8.24 Hz was measured for the signal at δ 7.13 (position 6). These couplings imply a 1,3,4-tri-substituted ring system, which corresponds exactly to **8a**. Evidence for these $^3J_{\text{HH}}$ coupling interactions was also obtained from the ^1H ^1H COSY NMR spectrum in **Fig 9** as the two signals at δ 7.72 and 7.13 show cross peaks to one another. The $^4J_{\text{HH}}$ is not readily observed in the ^1H - ^1H COSY NMR spectrum and this might be due to the smaller J-coupling value of the interaction.

The 3,4-methylenedioxy protons (position 1) appear as a singlet at δ 6.19 with an integral of 2H. These protons are heavily deshielded due to being adjacent to two oxygen atoms. The 3,4-methylenedioxy and aromatic protons of **8a** correspond well to the reported chemical shifts of methylenedioxymethamphetamine (MDMA).³⁸ This is expected given that the two structures possess the same core structure but have differing tail moieties.

The proton attached to the chiral centre (position 9) is identified at δ 5.15 as a triplet with a J-coupling at 5.38 Hz indicating a 3-bond coupling to the methylene protons of position 10. The ^1H - ^1H COSY spectrum shows a cross-peak between the chiral centre with a signal between δ 1.93 and 1.75, which appears as a multiplet. The multiplet shows two cross-peaks to two individual multiplets at δ 1.34-1.22 and 1.15-1.00. This is due to the presence of diastereotopic protons which are inequivalent and as such they give rise to two unique signals in the ^1H NMR spectrum. These multiplets possess further cross-peaks in the ^1H - ^1H COSY NMR spectrum to a triplet at δ 0.79 with a $^3J_{\text{HH}}$ -coupling of 7.3 Hz. As the signal at δ 0.79 integrates to 3H, this is the terminal methyl group of the pentyl chain. In a separate environment, the methyl group attached to the amine presents itself as a singlet at δ 2.53 with an integration of 3H. It is more deshielded than the terminal methyl group of the pentyl chain due to the fact it is bonded to nitrogen which is more electronegative. Thus, all signals for **8a** are accounted for in the ^1H NMR spectrum.

The $^{13}\text{C}\{^1\text{H}\}$ NMR spectrum (**Figure 7**) displays 13 signals for **8a** which matches the number of signals that should be present. All the signals are, therefore, unique. The most deshielded signal at δ 194.1, corresponds to the carbonyl carbon, and its quaternary nature was confirmed by DEPT due to the absence of this signal in the spectrum. There are seven aromatic signals present in the $^{13}\text{C}\{^1\text{H}\}$ NMR spectrum. Three of the signals (δ 152.8, δ 148.2 and δ 128.5), as indicated by their lack of presence in the HSQC and DEPT-135 spectra, are quaternary. The two most downfield signals were assigned to two

quaternary carbons directly bonded to oxygen (positions 2 and 7). The remaining signal at δ 128.5 is the quaternary carbon to which the pentane chain is attached. The signal present at δ 102.5, which is relatively deshielded, is assigned to the methylene carbon bonded to two oxygens (position 1). This signal is also emissive in the DEPT-135 NMR spectrum which further reinforces its assignment. The remaining signals in the aromatic region at δ 125.8, 108.5 and 107.8 are all CH environments which is reflected by these signals being adsorptive in the DEPT-135 NMR. From HSQC data, the signal at δ 125.8 shows a cross peak to a ^1H NMR signal at δ 7.72 and was therefore assigned to position 5. The two signals at δ 108.5 and 107.8 were assigned similarly to position 6 and 3, respectively.

In the aliphatic region, the most deshielded signal is at δ 61.6. This signal is adsorptive in the DEPT-135 spectrum. It is assigned as the chiral proton attached to position 9. HSQC data confirms the cross peak to the ^1H NMR signal at δ 5.15.

The remaining four signals belong to the remaining three carbons in the pentyl chain and are located at δ 31.9, 17.1 and 13.6. The latter signal is terminal methyl group (adsorptive in the DEPT-135 NMR spectrum), whereas the other two signals are assigned to positions 10 (δ 17.1) and 11 (δ 13.36). Lastly, the signal at δ 31.3 is assigned to the methyl group directly bonded to the nitrogen. This assignment correlates with the signals for the two sets of methyl protons in the ^1H NMR spectrum; the *N*-methyl protons are more deshielded than the terminal methyl protons of the pentyl chain due to being directly bonded to nitrogen.

5.1.2 Dimethylpentylone hydrochloride (**8b**)

The synthesised standard of dimethylpentylone hydrochloride (**8b**) was synthesised, purified via recrystallization using acetone, dried and obtained as a pale beige powder (Scheme 1, 9 % overall yield from intermediate) using an adaption of previously reported protocols in Santali *et al.*³⁷ **8b** was analysed by ¹H, ¹³C, ¹H-¹H COSY, ¹H-¹³C HSQC and DEPT-135 NMR to assist in its full characterisation. ¹H and ¹³C{¹H} NMR spectra of compound **8b** are shown in **Figures 13** and **14**, respectively. ¹H-¹H COSY, ¹H-¹³C HSQC, HMBC and DEPT-135 NMR spectra of compound **8b** are shown in **Figures S1-S4**. The full assignment of ¹H and ¹³C {¹H} NMR signals **8b** is presented in **Table 2**.

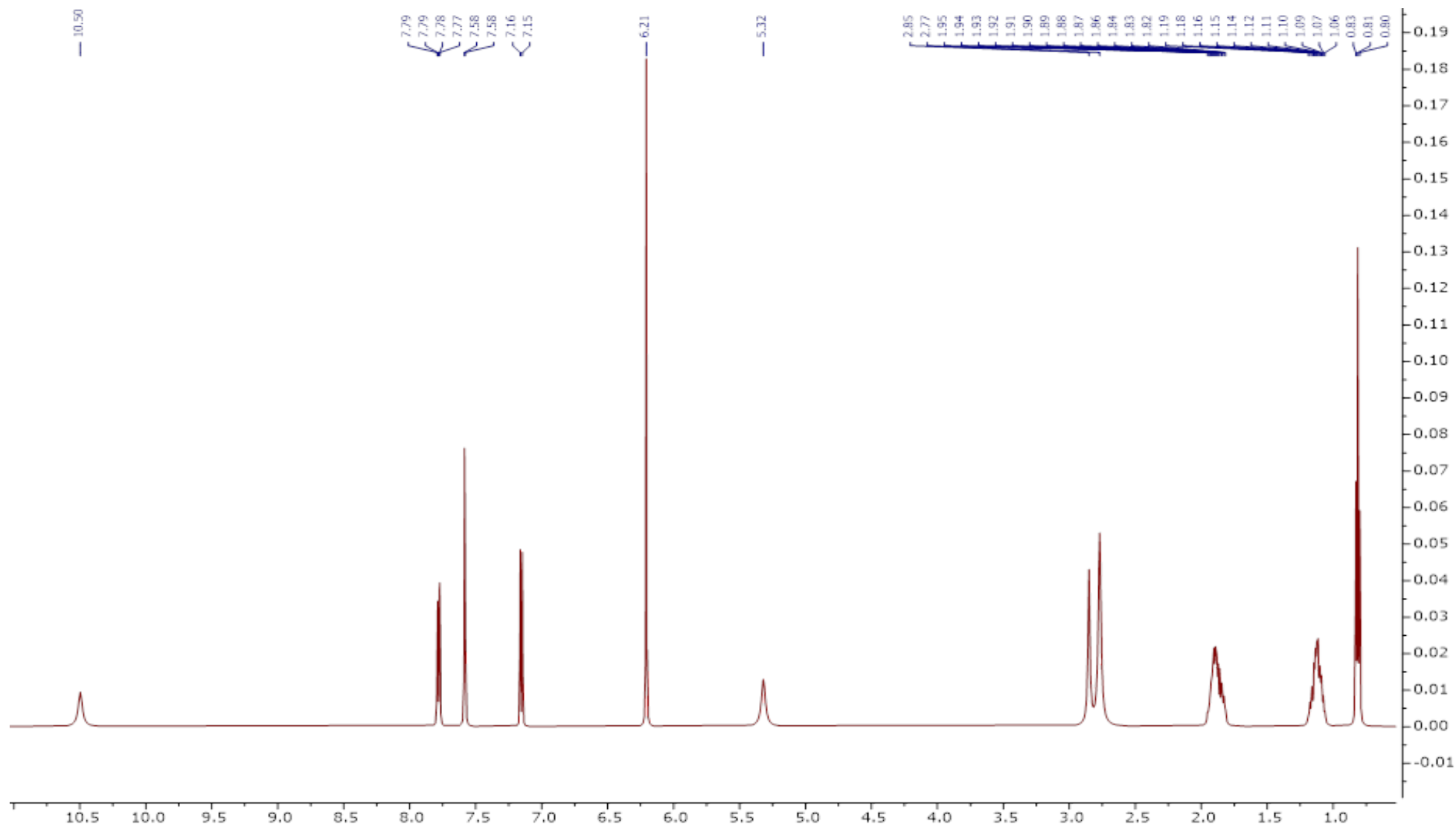


Figure 13: ^1H NMR spectrum of **8b** acquired in DMSO-d_6

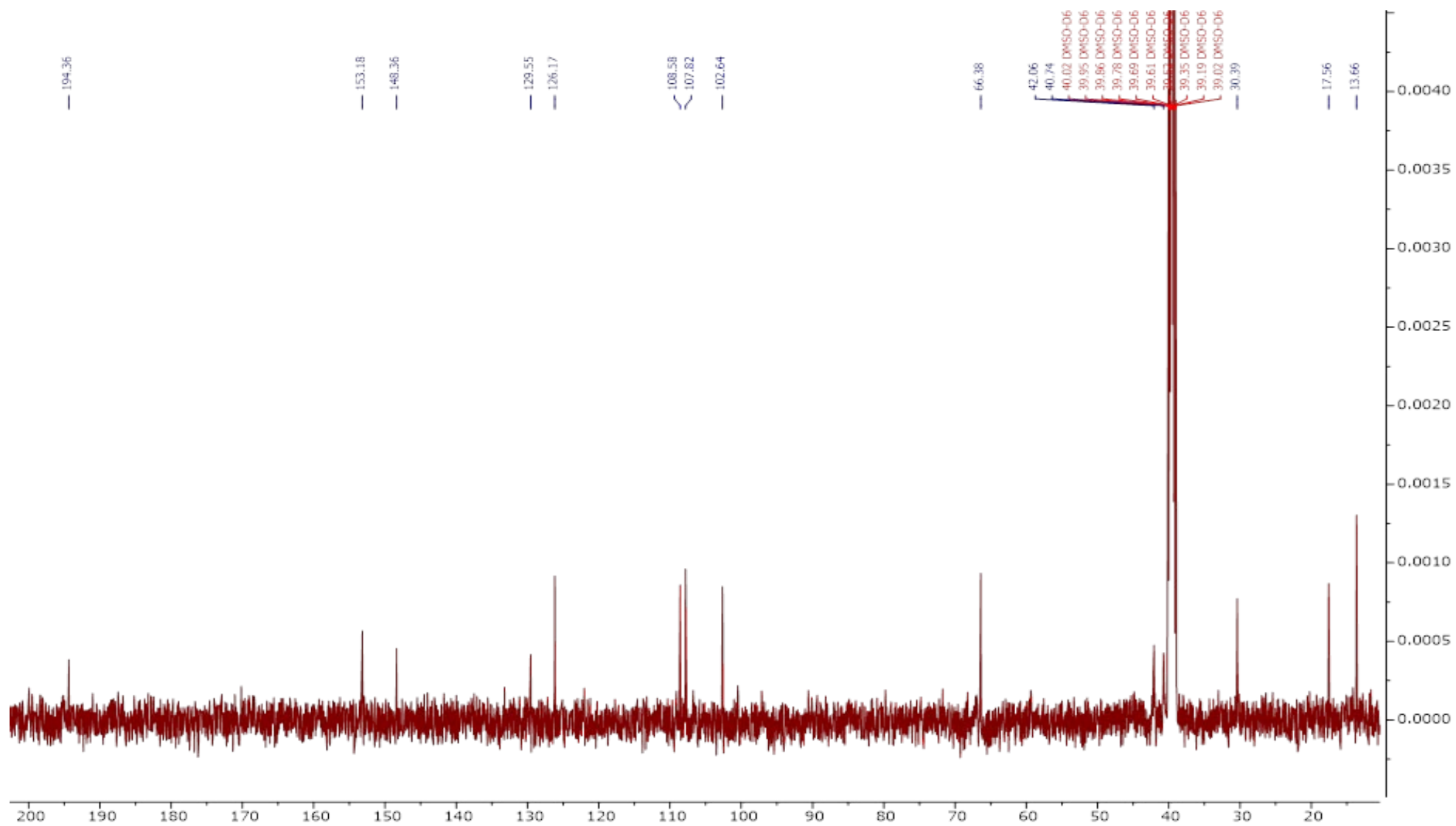


Figure 14: $^{13}\text{C}\{^1\text{H}\}$ NMR spectrum of **8b** acquired in DMSO- d_6 .

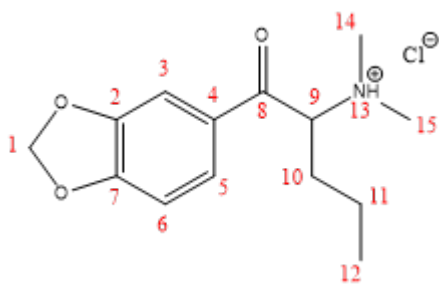


Figure 15: Chemical structure of **8b** with positions numbered.

Table 2: Chemical shifts for signals in the ^1H and $^{13}\text{C}\{^1\text{H}\}$ NMR spectra of **8b**. ^aFor each signal, J-coupling values are reported in Hertz (if present), as well as the integral value.

^bAbsorptive and emissive peaks are recorded as +ve and -ve respectively.

Position	^1H / ppm ^a	$^{13}\text{C}\{^1\text{H}\}$ / ppm	HSQC	DEPT-135 ^b
1	6.21 (s, 2H)	102.6	B (CH ₂)	-ve
2	-	148.4	-	-
3	7.58 (d, ⁴ J=1.65, 1H)	107.8	R (CH ₃ or CH)	+ve
4	-	129.6	-	-
5	7.72 (dd, ⁴ J= 1.65, ³ J= 8.25, 1H)	126.2	R (CH ₃ or CH)	+ve
6	7.15 (d, ³ J= 8.25, 1H)	108.6	R (CH ₃ or CH)	+ve
7	-	153.2	-	-
8	-	194.3	-	-
9	5.32 (s, 1H)	66.4	R (CH ₃ or CH)	+ve
10	1.80 -1.97 (m, 2H)	30.4	B (CH ₂)	-ve
11	1.04 -1.21 (m, 2H)	17.6	B (CH ₂)	-ve
12	0.81 (t, ³ J= 7.3, 3H)	13.6	R (CH ₃ or CH)	+ve
13	10.5 (s, 1H)	-	-	-
14	2.77 (s, 3H)	42.1	R (CH ₃ or CH)	+ve
15	2.85 (s, 3H)	40.8	R (CH ₃ or CH)	+ve

The high-field (500 MHz) ^1H NMR spectrum of compound **8b** in DMSO- d_6 is presented in **Fig. 13**. The spectrum possesses 11 signals in total. Nine signals within the spectrum are identical to the ^1H NMR spectrum of compound **8a** with the exception of two signals. At δ 10.5, a singlet was observed and identified as the NH proton. This contrasts to **8a** which possessed two singlet signals. Given the rigid nature of the structure in **8b**, the NH has poor proton exchange, producing a sharper NMR signal in comparison to compound **8a** where there is a broad peak due to the increased proton exchange from both protons.

The addition of a dimethylamine to the **5** is confirmed via the two singlets located at δ 2.77 and δ 2.85 caused because the methyl groups are chemically equivalent (or nearly equivalent). The similarity in the chemical shift of the two signals are a result of the diastereotopic centre causing the methyl groups to become inequivalent. ^1H - ^1H COSY NMR confirms no cross-peak interactions for these two signals.

The $^{13}\text{C}\{^1\text{H}\}$ NMR spectrum (**Figure 14**) displays 14 signals for **8b** which matches the number of signals that should be present. Given the similarity to **8a** the only expected change to the spectrum is a difference in the methyl groups (positions 14 and 15) attached to the nitrogen. The two methyl groups correspond to the signals at 42.1 and 40.8 ppm, which are both absorptive in the DEPT-135 NMR spectrum. ^1H - $^{13}\text{C}\{^1\text{H}\}$ HSQC NMR confirms the cross-peak interaction between the protons and carbons at positions 14 and 15. The signal at position 14 shows up downfield on the spectrum due to the interaction between the aromatic protons when the structure rotates at the pivotal chiral centre (position 9).

5.1.3 N-ethylpentylone hydrochloride (8c)

The synthesised standard of N-ethylpentylone hydrochloride (**8c**) was synthesised, purified via recrystallization using acetone, dried and obtained as a white powder (Scheme 3, 28 % overall yield from intermediate) using an adaption of previously reported protocols in Santali *et al.*³⁷ **8c** was analysed by ¹H, ¹³C, ¹H-¹H COSY, ¹H-¹³C HSQC and DEPT-135 NMR to assist in its full characterisation. ¹H and ¹³C{¹H} NMR spectra of compound **8c** are shown in **Figures 16** and **17**, respectively. ¹H-¹H COSY, ¹H-¹³C HSQC, HMBC and DEPT-135 NMR spectra of compound **8c** are shown in **Figures S5-S8**. The full assignment of ¹H and ¹³C{¹H} NMR signals **8c** is presented in **Table 3**.

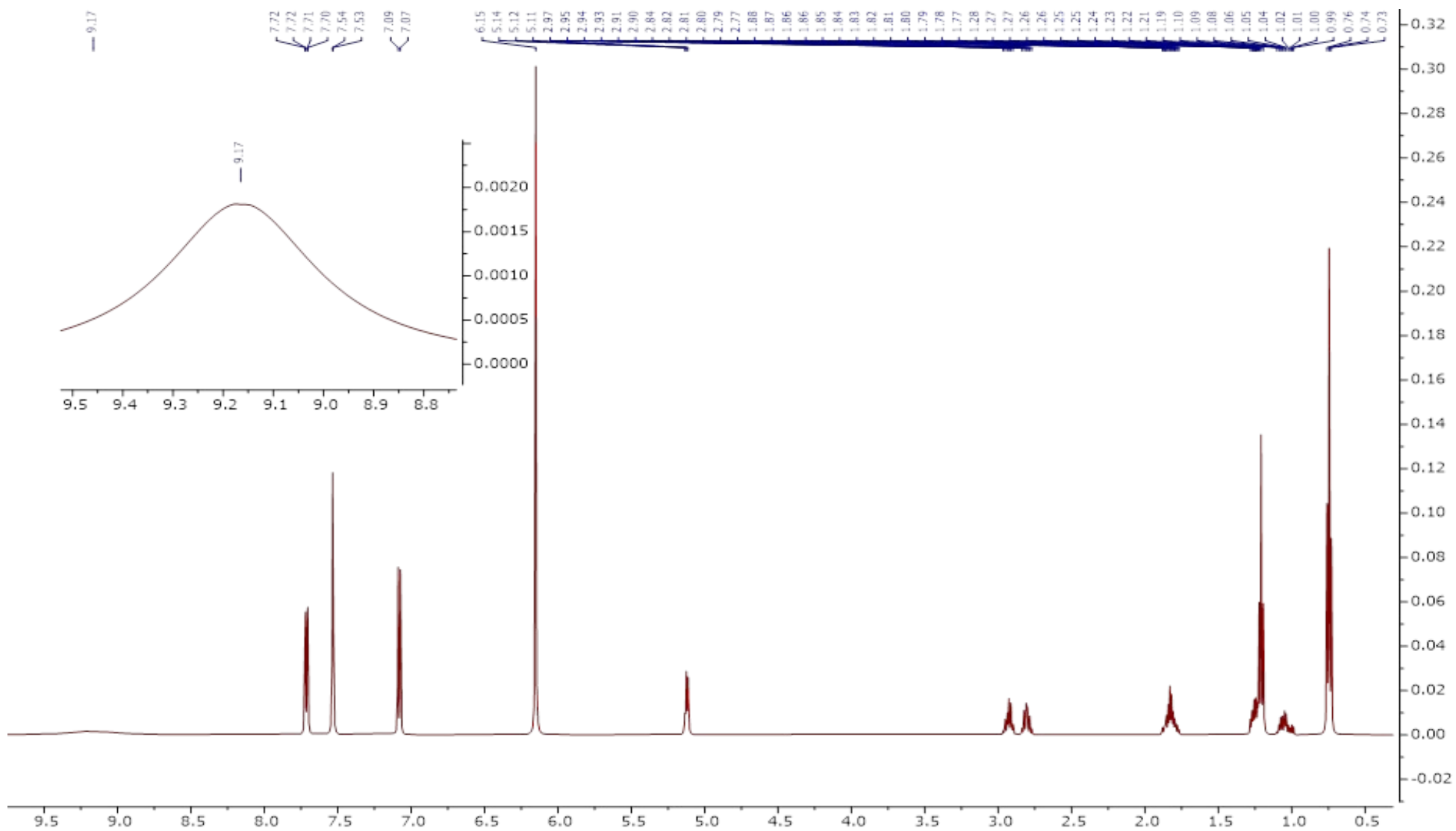


Figure 16: ^1H NMR spectrum of **8c** acquired in DMSO-d_6

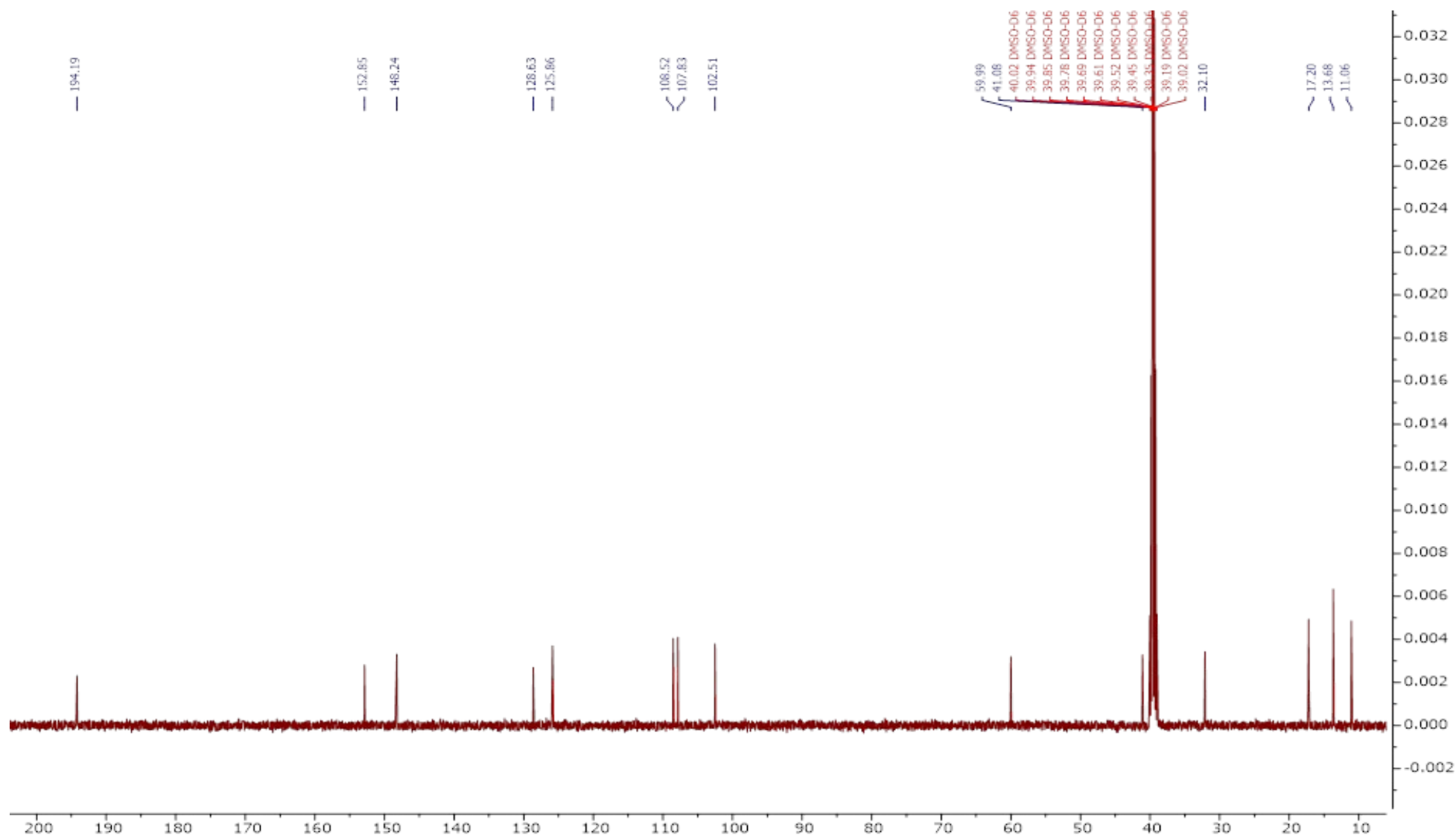


Figure 17: $^{13}\text{C}\{^1\text{H}\}$ NMR spectrum of **8c** acquired in DMSO-d_6 .

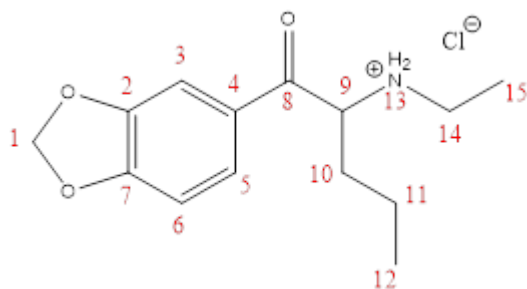


Figure 18: Chemical structure of **8c** with positions numbered.

Table 3: Chemical shifts for signals in the ^1H and $^{13}\text{C}\{^1\text{H}\}$ NMR spectra of **8c**. ^aFor each signal, J-coupling values are reported in Hertz (if present), as well as the integral value.

^bAbsorptive and emissive peaks are recorded as +ve and -ve respectively.

Position	^1H / ppm ^a	$^{13}\text{C}\{^1\text{H}\}$ / ppm	HSQC	DEPT-135 ^b
1	6.15 (s, 2H)	102.5	B (CH ₂)	-ve
2	-	148.2	-	-
3	7.53 (d, ⁴ J=1.83, 1H)	108.5	R (CH ₃ or CH)	+ve
4	-	128.6	-	-
5	7.71 (dd, ⁴ J= 1.83, ³ J= 8.25, 1H)	125.9	R (CH ₃ or CH)	+ve
6	7.08 (d, ³ J= 8.25, 1H)	107.9	R (CH ₃ or CH)	+ve
7	-	152.9	-	-
8	-	194.2	-	-
9	5.12 (t, ³ J= 5.58, 1H)	60.0	R (CH ₃ or CH)	+ve
10	1.75-1.98 (m, 2H)	32.1	B (CH ₂)	-ve
11	0.97-1.10 (m, 1H), 1.23-1.29 (m, 1H)	17.2	B (CH ₂)	-ve
12	0.74 (t, ³ J= 7.34, 3H)	11.06	R (CH ₃ or CH)	+ve
13	9.17 (s, 2H)	-	-	-
14	2.78-2.97 (m, 2H)	41.08	B (CH ₂)	-ve
15	1.21 (t, ³ J= 7.26, 3H)	13.68	R (CH ₃ or CH)	+ve

The high-field (500 MHz) ^1H spectrum of compound **8c** in DMSO- d_6 is presented in **Fig. 16**. The spectrum comprises of 12 signals in total. In comparison to compound **8a** there are three signals that show are shifted within the spectrum. At δ 9.17, a broad singlet was observed and identified as the NH protons. The broad nature indicates they are exchangeable on the NMR timescale. The signal s presenting itself as a singlet instead of 2 two individual signals indicating that the two NH protons are chemically equivalent

making the signals overlap in the ^1H NMR spectrum. In the same environment, an ethyl group attached to the amine presents itself as two signals. The multiplet at δ 2.97-2.78 (position 14), with an integration of 2H, shows a cross-peak to the triplet at δ 1.21. The triplet is observed at δ 1.21 (position 15) with a $^3J_{\text{HH}}$ -coupling of 7.3 Hz. As the signal at δ 1.21 integrates to 3H, this can only be a terminal methyl. Both signals are more deshielded than the expected carbonyl chain protons due to the ethyl group being directly attached to the nitrogen, which is more electronegative, hence the signals being shifted further downfield on the NMR spectrum.

The $^{13}\text{C}\{^1\text{H}\}$ NMR spectrum (**Fig 17**) displays 14 signals. In comparison to the spectra for compound 8a, the compounds share 12 out of the 14 signals. The ethyl group attached to the amine presents itself as two signals on the spectra for 8c. The signal at δ 41.08, showing as more downfield on the spectra is a result of the CH_2 bonded to the nitrogen atom with makes it more electronegative. DEPT-135 confirms the CH_2 by its emissive peak. The HMBC confirms interaction from the CH_2 with just the terminal methyl group at δ 13.68. HSQC shows a cross peak between this signal and the CH_3 protons, also confirmed by its absorptive signal on the DEPT spectrum. Thus, all signals accounted for.

5.1.4 Butylone hydrochloride (9a)

The synthesised standard of butylone hydrochloride (**9a**) was synthesised, purified via recrystallization using acetone, dried and obtained as a white powder (Scheme 3, 16 % overall yield from intermediate) using an adaption of previously reported protocols in Santali *et al.*³⁷ **9a** was analysed by ^1H , ^{13}C , ^1H - ^1H COSY, ^1H - ^{13}C HSQC and DEPT-135 NMR to assist in its full characterisation. ^1H and $^{13}\text{C}\{^1\text{H}\}$ NMR spectra of compound **9a** are shown in **Figures 19** and **20**, respectively. ^1H - ^1H COSY, ^1H - ^{13}C HSQC, HMBC and DEPT-135 NMR spectra of compound **9a** are shown in **Figures S9-S12**. The full assignment of ^1H and $^{13}\text{C}\{^1\text{H}\}$ NMR signals **9a** is presented in **Table 4**.

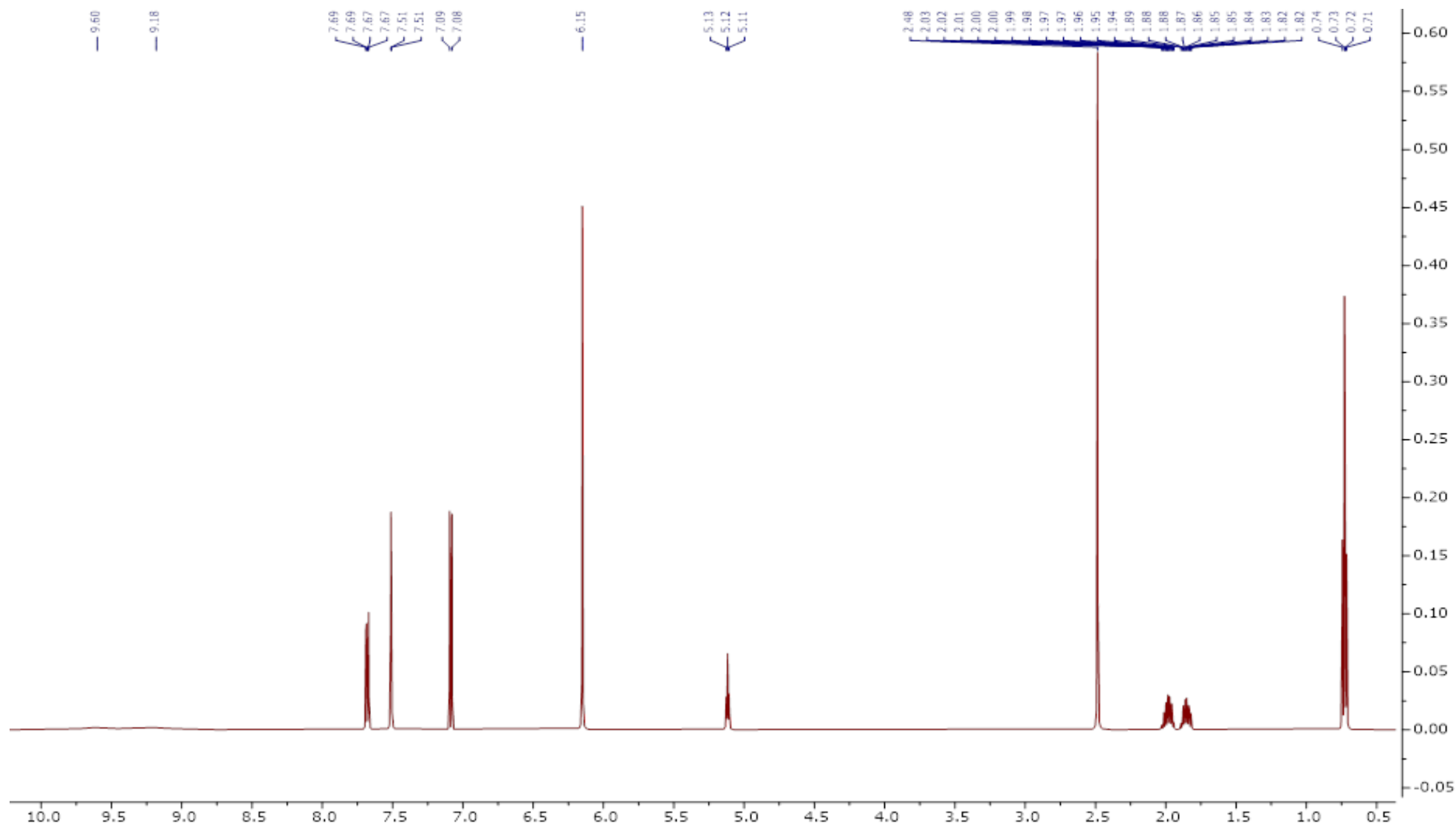


Figure 19: ^1H NMR spectrum of **9a** acquired in DMSO-d_6

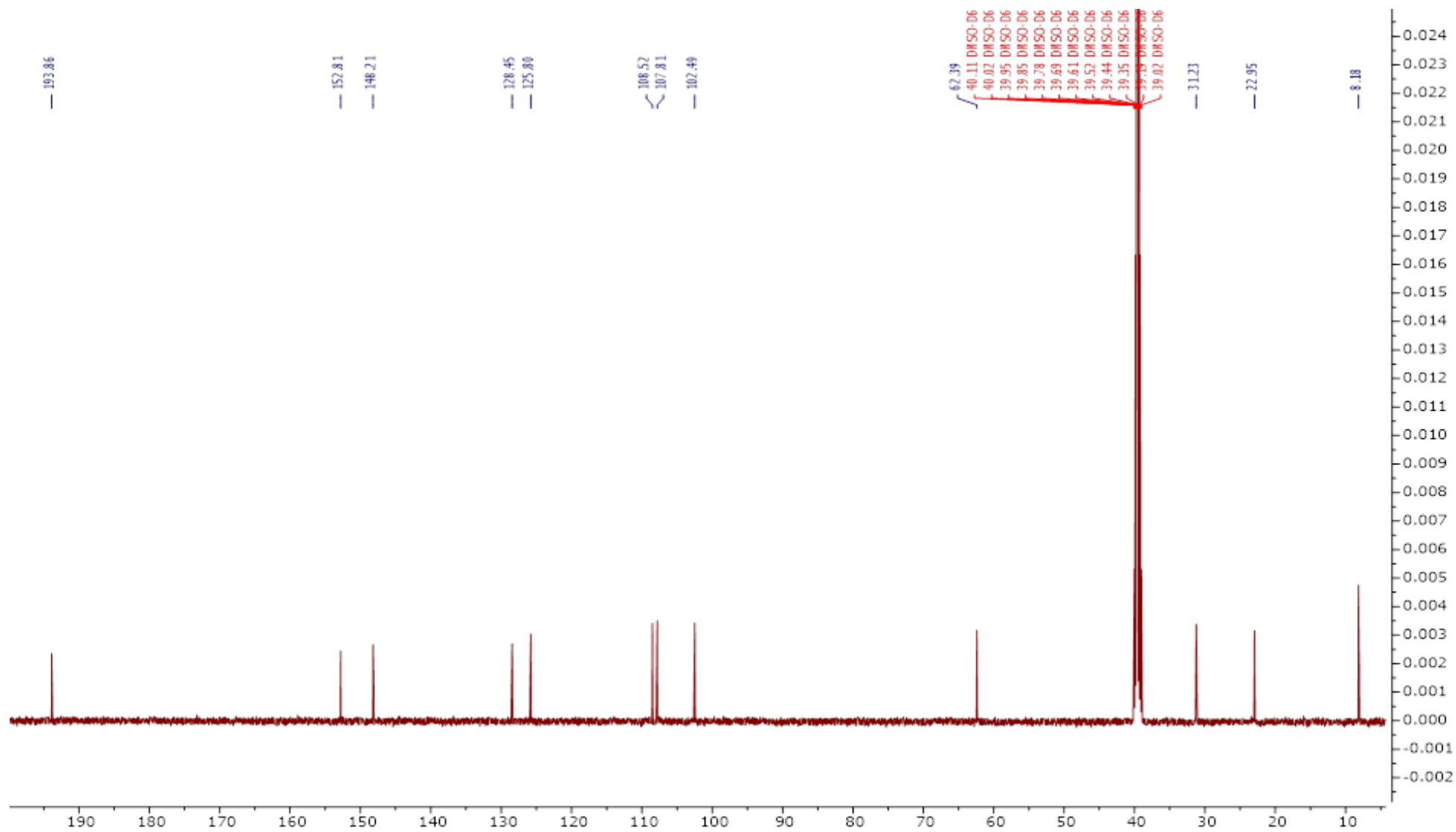


Figure 20: $^{13}\text{C}\{^1\text{H}\}$ NMR spectrum of **9a** acquired in DMSO-d_6 .

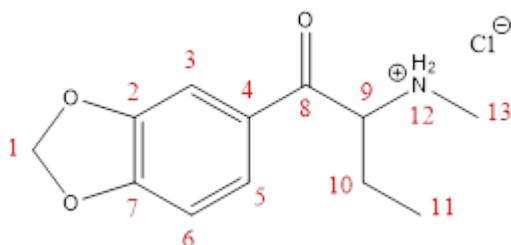


Figure 21: Chemical structure of **9a** with positions numbered.

Table 4: Chemical shifts for signals in the ^1H and $^{13}\text{C}\{^1\text{H}\}$ NMR spectra of **9a**. ^aFor each signal, J-coupling values are reported in Hertz (if present), as well as the integral value.

^bAbsorptive and emissive peaks are recorded as +ve and -ve respectively.

Position	^1H / ppm ^a	$^{13}\text{C}\{^1\text{H}\}$ / ppm	HSQC	DEPT-135 ^b
1	6.15 (s, 2H)	102.49	B (CH ₂)	-ve
2	-	148.21	-	-
3	7.51 (d, ⁴ J=1.83, 1H)	107.81	R (CH ₃ or CH)	+ve
4	-	128.45	-	-
5	7.68 (dd, ⁴ J= 1.83, ³ J= 8.25, 1H)	125.8	R (CH ₃ or CH)	+ve
6	7.09 (d, ³ J= 8.25, 1H)	108.52	R (CH ₃ or CH)	+ve
7	-	152.81	-	-
8	-	193.86	-	-
9	5.12 (t, ³ J= 5.20, 1H)	62.39	R (CH ₃ or CH)	+ve
10	1.74-1.94 (m, 1H), 1.94-2.06 (m, 1H)	22.95	B (CH ₂)	-ve
11	0.73 (t, ³ J= 7.55, 3H)	8.18	R (CH ₃ or CH)	+ve
12	9.18 (d, 1H), 9.60 (s, 1H)	-	-	-
13	2.48 (s, 3H)	31.23	R (CH ₃ or CH)	+ve

The high-field (500 MHz) ^1H NMR spectrum of compound **9a** in DMSO-*d*₆ is presented in **Fig. 19**. The spectrum possesses 12 signals in total. Nine signals within the spectrum are identical to compound **8a** spectrum except for three signals in the **9a** NMR spectrum. With the additional proton on the amine the spectrum displays three singlets, one identical to compound **8a**, responsible for one NH and the other due to the additional protonation. The additional NH presents as two singlets at δ 9.60 and 9.18. COSY confirms there are no additional interaction from other environments. Due to the diastereotopic nature of the NH protons, it gives rise to two singlets. In comparison to compound **8a**

spectrum, within the aliphatic region the only signal different is the terminal methyl bonded to the nitrogen. With the CH₃ being directly bonded to the Nitrogen atom, the methyl is more electronegative shifting the signal more downfield. COSY confirmed no other proton interaction between different environments and so it's an isolated group within the compounds.

The ¹³C{¹H} NMR spectrum (**Fig 20**) displays 12 signals matching butylone molecular structure. In comparison to compound **8a**, all signals are similar the only structural difference that can be seen within the spectrum is the absence of a carbon between 15 and 40 ppm as the butyl chain consists of only four carbons instead of five like 8a. The methyl group bonded directly to the nitrogen atom can be seen at δ 31.23. Due to the electronegativity from the nitrogen atom the signal is shifted more downfield in comparison to the terminal methyl of the butyl chain at δ 8.18. HSQC confirms the cross peak between the downfield CH₃ protons at δ 2.48 as well as the isolated environment with no additional interactions. Thus, all peaks accounted for in ¹H and ¹³C NMR.

5.1.5 Putylone hydrochloride (9b)

The synthesised standard of putylone hydrochloride (**9b**) was synthesised, purified via recrystallization using acetone, dried and obtained as a white crystalline powder (Scheme 3, 65 % overall yield from intermediate) using an adaption of previously reported protocols in Santali et *al.*³⁷ **9b** was analysed by ¹H, ¹³C, ¹H-¹H COSY, ¹H-¹³C HSQC and DEPT-135 NMR to assist in its full characterisation. ¹H and ¹³C{¹H} NMR spectra of compound **9b** are shown in **Figures 22** and **23**, respectively. ¹H-¹H COSY, ¹H-¹³C HSQC, HMBC and DEPT-135 NMR spectra of compound **9b** are shown in **Figures S13-S16**. The full assignment of ¹H and ¹³C{¹H} NMR signals **9b** is presented in **Table 5**.

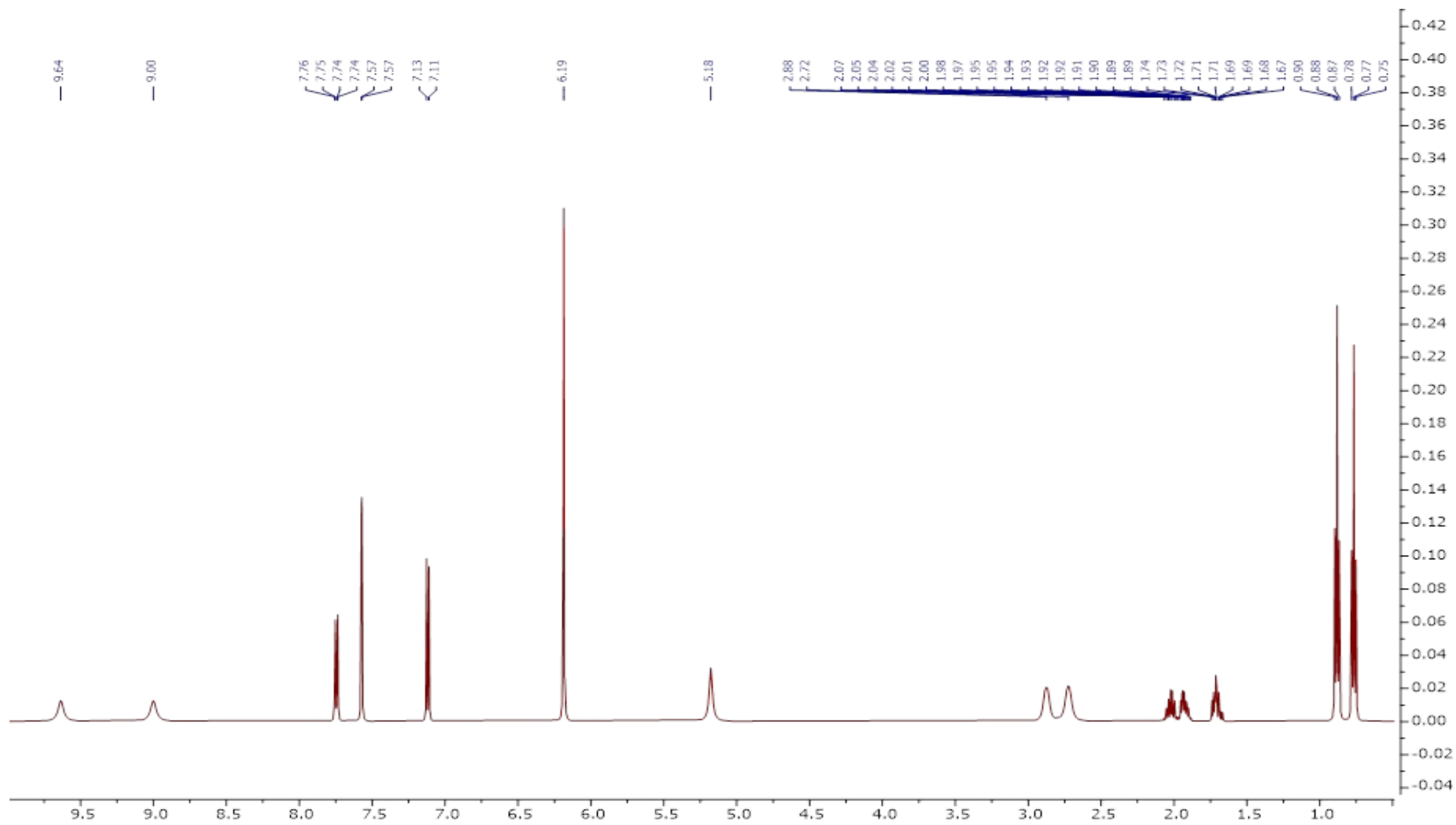


Figure 22: ^1H NMR spectrum of **9b** acquired in DMSO-d_6

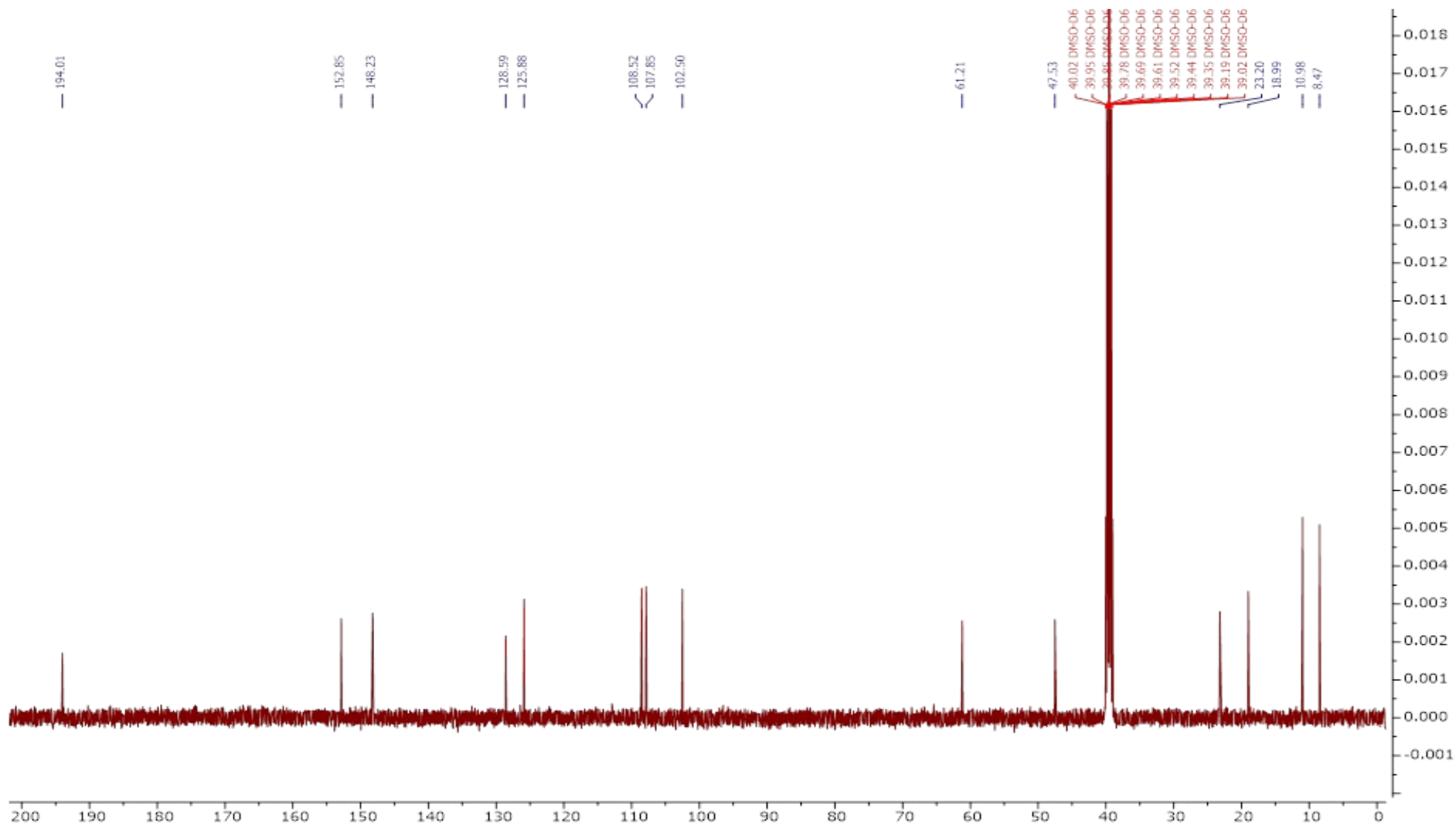


Figure 23: $^{13}\text{C}\{^1\text{H}\}$ NMR spectrum of **9b** acquired in DMSO-d_6 .

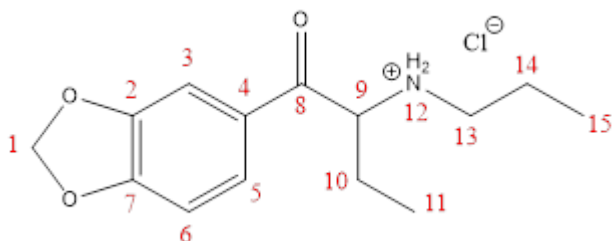


Figure 24: Chemical structure of **9b** with positions numbered.

Table 5: Chemical shifts for signals in the ^1H and $^{13}\text{C}\{^1\text{H}\}$ NMR spectra of **9b**. ^aFor each signal, J-coupling values are reported in Hertz (if present), as well as the integral value.

^bAbsorptive and emissive peaks are recorded as +ve and -ve respectively.

Position	^1H / ppm ^a	$^{13}\text{C}\{^1\text{H}\}$ / ppm	HSQC	DEPT-135 ^b
1	6.19 (s, 2H)	102.5	B (CH ₂)	-ve
2	-	148.2	-	-
3	7.57 (d, ⁴ J=1.83, 1H)	107.9	R (CH ₃ or CH)	+ve
4	-	128.6	-	-
5	7.75 (dd, ⁴ J= 1.83, ³ J= 8.17, 1H)	125.9	R (CH ₃ or CH)	+ve
6	7.12 (d, ³ J= 8.17, 1H)	108.5	R (CH ₃ or CH)	+ve
7	-	152.9	-	-
8	-	194.1	-	-
9	5.20 (s, 1H)	61.2	R (CH ₃ or CH)	+ve
10	1.65-1.77 (m, 2H)	19.0	B (CH ₂)	-ve
11	0.77 (t, ³ J= 7.57, 3H)	8.5	R (CH ₃ or CH)	+ve
12	9.00 (s, 1H), 9.64 (s, 1H)	-	-	-
13	2.72 (s, 1H), 2.88 (s, 1H)	47.6	B (CH ₂)	-ve
14	1.88-1.97 (m, 1H), 1.97-2.09 (m, 1H)	23.2	B (CH ₂)	-ve
15	0.88 (t, 3J= 7.49, 3H)	11.0	R (CH ₃ or CH)	+ve

The high-field (500 MHz) ^1H NMR spectrum of compound **9b** in DMSO- d_6 is presented in **Fig. 22**. The spectrum possesses 14 signals in total. In comparison to **8a**, **9a** has one less carbon on the carbonyl chain and an extension of functional group attached to the nitrogen to a propyl chain. These are presented as followed; with only 1 chain on the amin the nitrogen already has an existing proton and is protonated by the salt as well giving rise to two signals at δ 9.64 and 9.00. Due to the diastereotopic nature of these protons it gives

rise to 2 individual singlets with an integration of 1 each. COSY confirms this is an isolated environment with the lack of proton interaction from other environments. Due to the propyl chain being directly bonded to the nitrogen which is more electronegative the signals will shift more down field where there are two singlets found at δ 2.88 and 2.72 with and integrations of 1H for each signal. The presence of two singlet peaks is due to the diastereotopic nature of the protons, giving rise to two individual peaks. COSY confirms further interaction with two multiplet up field at δ 1.97-2.09 and 1.88-1.97, each with an integration of 1H. In comparison to both triplet signals upfield, the triplet with a slight shift downfield is the final interaction with the CH₂ propyl chain. The triplet is present at δ 0.88 with an integration of 3H and a coupling of $^3J = 7.49$. Coupling confirms the 3-bond interaction between the CH₂ and CH₂. These protons are all in the same environment within the COSY spectrum confirming they are bonded together. Thus, all signals accounted for.

The $^{13}\text{C}\{^1\text{H}\}$ NMR spectrum (**Figs 23**) displays 14 signals. In comparison to the spectra for compound **8a**, the compounds share 11 out of the 14 signals. With the loss of the methyl from the butyl chain there is an increase in signals within the aliphatic region, responsible for the propyl chain bonded to the nitrogen atom. The electronegativity causes the signals to shift more downfield, allowing them to be distinguished between the carbonyl chain. The most downfield signal from the propyl chain is at δ 47.6, with an emissive signal on the DEPT and a cross peak to the two singlet signals at δ 2.72 and 2.88 (position 13). The signal at δ 23.2 also has an emissive peak with a cross peak on the HSQC with the other two CH₂ protons between δ 1.88-2.09. Finally, the terminal carbon on the propyl chain can be seen at δ 11.0 with an absorptive signal on the DEPT, confirming the CH₃ environment. A cross peak between the 3H protons 0.88 confirm the terminal CH₃ on the propyl chain.

5.1.6 MDPHP hydrochloride (10a)

The standard of the novel compound MDPHP hydrochloride provided by MANDRAKE (**10a**) was purified via recrystallization using acetone, dried and obtained as a white powder. **10a** was analysed by ^1H , ^{13}C , ^1H - ^1H COSY, ^1H - ^{13}C HSQC and DEPT-135 NMR to assist in its full characterisation. ^1H and $^{13}\text{C}\{^1\text{H}\}$ NMR spectra of compound **10a** are shown in **Figures 25** and **26**, respectively. ^1H - ^1H COSY, ^1H - ^{13}C HSQC, HMBC and DEPT-135 NMR spectra of compound **9b** are shown in **Figures S17-S20**. The full assignment of ^1H and $^{13}\text{C}\{^1\text{H}\}$ NMR signals **10a** is presented in **Table 6**.

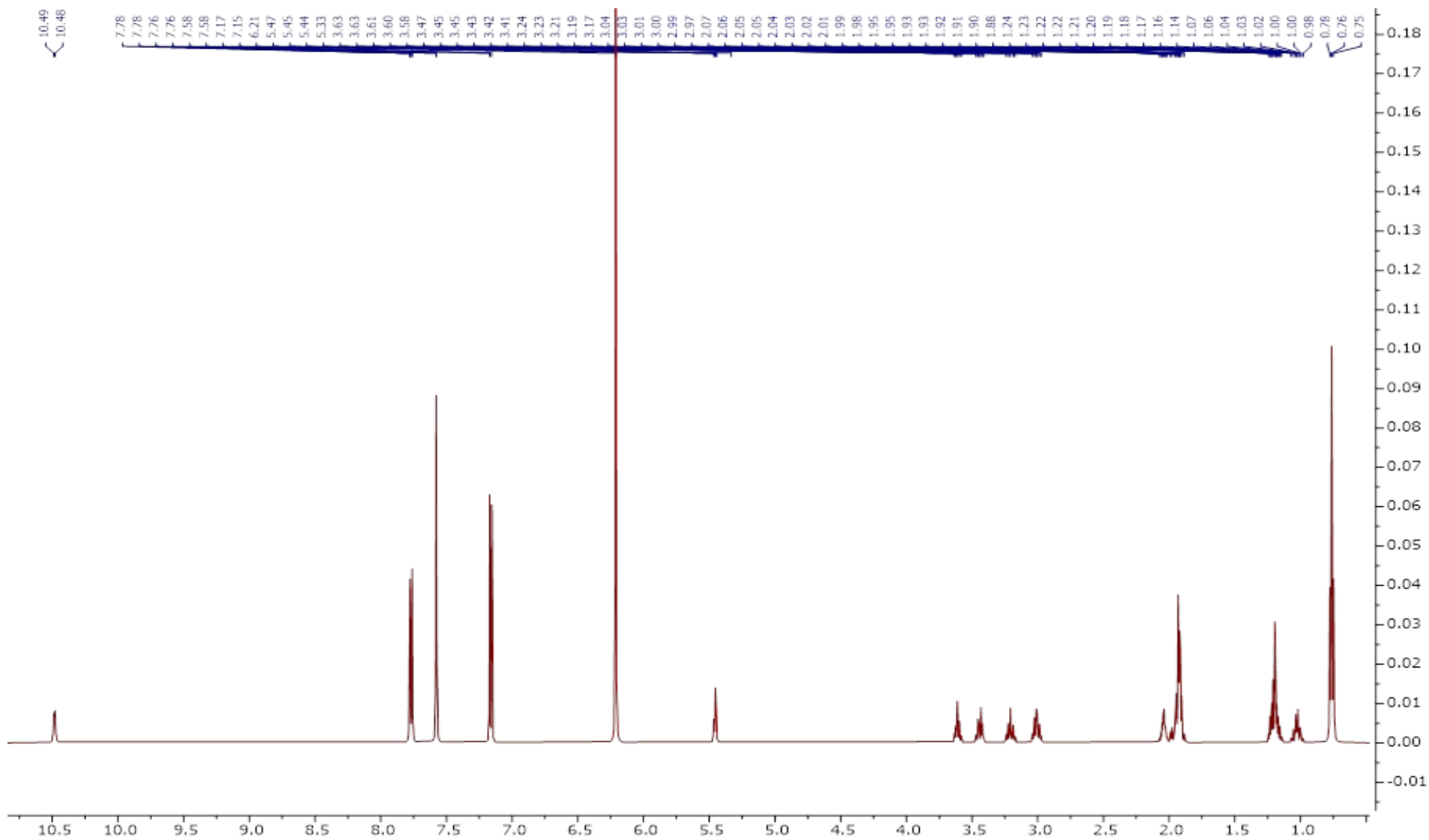


Figure 25: ^1H NMR spectrum of **10a** acquired in DMSO-d_6

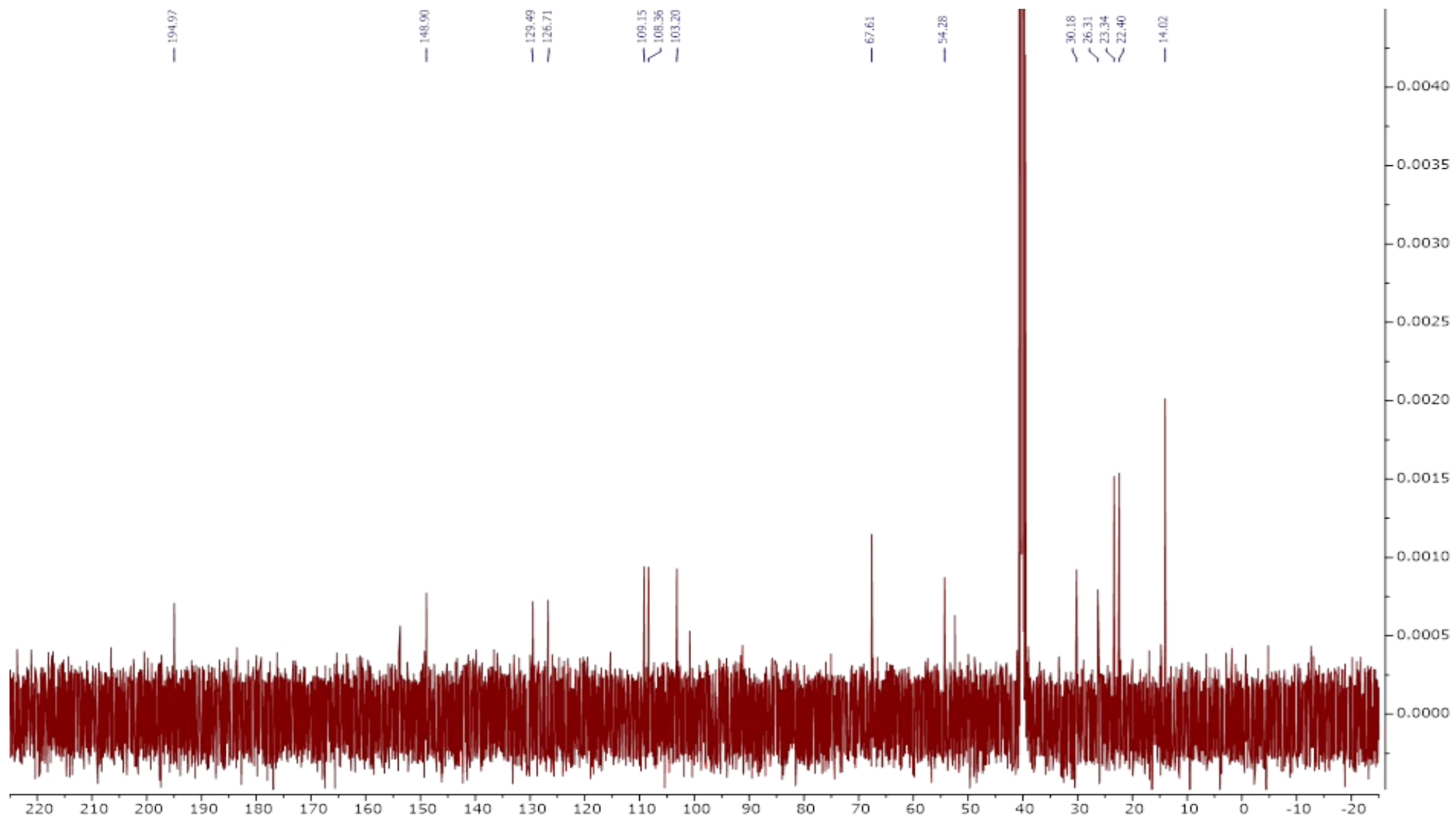


Figure 26: $^{13}\text{C}\{^1\text{H}\}$ NMR spectrum of **10a** acquired in DMSO-d_6 .

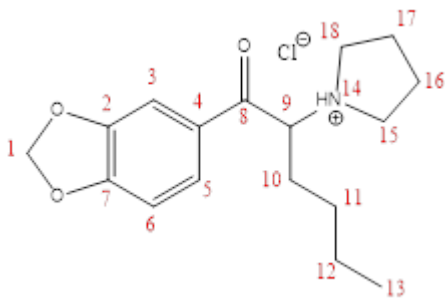


Figure 27: Chemical structure of **10a** with positions numbered.

Table 6: Chemical shifts for signals in the ^1H and $^{13}\text{C}\{^1\text{H}\}$ NMR spectra of **10a**. ^aFor each signal, J-coupling values are reported in Hertz (if present), as well as the integral value.

^bAbsorptive and emissive peaks are recorded as +ve and -ve respectively.

Position	^1H / ppm ^a	$^{13}\text{C}\{^1\text{H}\}$ / ppm	HSQC	DEPT-135 ^b
1	6.17 (s, 2H)	103.20	B (CH ₂)	-ve
2	-	148.90	-	-
3	7.52 (d, ⁴ J= 1.62, 1H)	108.36	R (CH ₃ or CH)	+ve
4	-	129.49	-	-
5	7.71 (dd, , ⁴ J= 1.62, ³ J= 8.25, 1H)	126.71	R (CH ₃ or CH)	+ve
6	7.12 (d, ³ J= 8.25, 1H)	109.15	R (CH ₃ or CH)	+ve
7	-	153.48	-	-
8	-	194.97	-	-
9	5.35 (t, ³ J= 5.42, 1H)	67.61	R (CH ₃ or CH)	+ve
10	1.8-2.05 (m, 2/6H)	30.18	B (CH ₂)	-ve
11	0.9-1.23 (m, 2/4H)	26.31	B (CH ₂)	-ve
12	0.9-1.23 (m, 2/4H)	22.40	B (CH ₂)	-ve
13	0.72 (³ J= 7.09, 3H)	14.02	R (CH ₃ or CH)	+ve
14	10.3 (s, 1H)	-	-	-
15	3.50-3.62 (m, 1H), 3.09-3.20 (m, 1H)	52.46	B (CH ₂)	-ve
16	1.8-2.05 (m, 2/6H)	33.3	B (CH ₂)	-ve
17	1.8-2.05 (m, 2/6H)	33.1	B (CH ₂)	-ve
18	3.33-3.43 (m, 1H), 2.88-2.99 (m, 1H)	54.28	B (CH ₂)	-ve

The high-field (500 MHz) ^1H NMR spectrum of compound **10a** in DMSO- d_6 is presented in **Fig. 25**. The spectrum possesses 15 signals in total. Six signals within the spectrum are identical to compound **8a** spectrum with the exception of nine signals in the **10a** NMR

spectrum. Given the similarity to **8a** the only expected change to the spectrum should reflect the single protonation of the amine; the extension of the pentyl chain to a hexenyl chain and the pyrrolidine ring. With that the signal at δ 10.3, with an integration of 1H is present due to the protonation of the amine (position 14) the hydrochloride salt. COSY confirmed the isolated environment and so there is no additional proton interaction. The four signals at δ 3.50-3.62, δ 3.33- 3.43, δ 3.09-3.20 and δ 2.88-2.99, with an integration of 1H for each individual peak, are responsible for the first two CH₂ (position 18 and 15) in the pyrrolidine ring. With them being bonded to the nitrogen atom the protons are more electronegative, shifting them more downfield on the spectrum. COSY shows small cross-peaks with the remaining CH₂ protons in the ring at a small signal at δ 1.8-2.05. This signal presents as partially split from another signal with an integration of 6H overall. The 4H are the remaining protons in the ring (position 16 and 17). As they are further away from the Nitrogen atom, they don't experience the electronegative effects, so they remain in the aliphatic region.

As for the remaining hexenyl chain, the signals are present up field in the aliphatic region. The sharp multiplet signal at δ 1.8-2.05 with a remaining integration of 2H from the 6H, is responsible for the CH₂ protons attached to the chiral centre at position 10. COSY confirms cross peaks to the remaining CH₂ signal (position 11 and 12) at 0.9-1.23 with a shared integration of 4H. These protons signals overlap as they are chemically equivalent and so they present as the same signal. COSY confirms the cross peak from the CH₂ signals to the terminal methyl at δ 0.72.

The ¹³C{¹H} NMR spectrum (**Fig 26**) displays 17 signals for **10a** which matches the number of signals that should be present. In comparison with the spectrum for **8a**, eight signals are identical. The remaining signals reflect the structural changes in the amine derivative and the aliphatic groups. The two CH₂ groups directly bonded to the nitrogen atom (positions 15 and 18) are more electronegative than the remaining CH₂ in the pyrrolidine ring (position 16 and 17) and so they shift downfield where they are found at δ 54.28 and 52.46, as two signals with emissive signals on the DEPT. HSQC confirms the cross-peak to the signals between δ 2.88-3.62. The remaining CH₂ groups (position 16 and 17) are found at δ 33.3 and 33.1, with emissive signals on the DEPT and the signals on the C NMR are merged, forming a doublet. The HSQC confirms cross-peak between the CH₂ groups at δ 1.8-2.05 on the ¹H NMR spectrum.

The peaks from the hexenyl chain can be seen between δ 30.2-14.04, where they present as 4 signals. The CH₂ bonded directly to the chiral centre (position 10) presents as an emissive signal at 30.2, with a cross-peak on the HSQC to the multiplet at δ 1.8-2.05. The CH₂ signals for positions 11 and 12 are present as emissive signals at δ 26.31 and 22.40. HMBC identifies the cross peak between the multiplet at δ 0.9-1.23 as well as the interaction between the terminal methyl which presents as an absorptive signal at δ 14.02 (position 13). HSQC shows the cross peak between the terminal CH₃ protons at δ 0.72, thus, accounting for all signals.

5.2 Attenuated Total Reflectance-Fourier Transform Infra Red (FT-IR) Spectroscopy

The synthetic cathinone products **9a-10a** were analysed by FT-IR to assist in its full characterisation. The FT-IR spectra for compound **8a** is shown in **Figure 28**, the remaining compounds are shown in **Figures S21 -S25**, respectively. The full assignment of functional group peaks is presented in **Table 7** for compounds **8a-10a**. The assignment relied on measuring the absorption of infrared light at various wavelengths, providing a molecular fingerprint of the sample, allowing identification of specific function groups and bonding patterns.

The infrared spectra of compounds **9a-10a** showed the characteristic bands associated with the hydrochloride salts of 3,4-methyldioxymethcathinones such as MDPV . The spectra all show strong, broad bands between 2400 and 3100 cm^{-1} , corresponding to a combination of aromatic and aliphatic C-H stretches and N-H absorption bands from the ammonium salt. A strong absorbance between 1600 and 1700 cm^{-1} for the carbonyl group in conjugation with the 3,4-methylenedioxy moiety is observed. Furthermore, vibration bands are observed between 1500 and 1600 cm^{-1} because of the aromatic nucleus. In addition, a medium C-N stretching vibration between 1200 and 1350 cm^{-1} from the amine functionalities and a strong C-O stretching vibration from the 3,4-methylenedioxy group between 1000 and 1300 cm^{-1} is observed. A summary of all these observations is presented in **Table 7** for comparison.

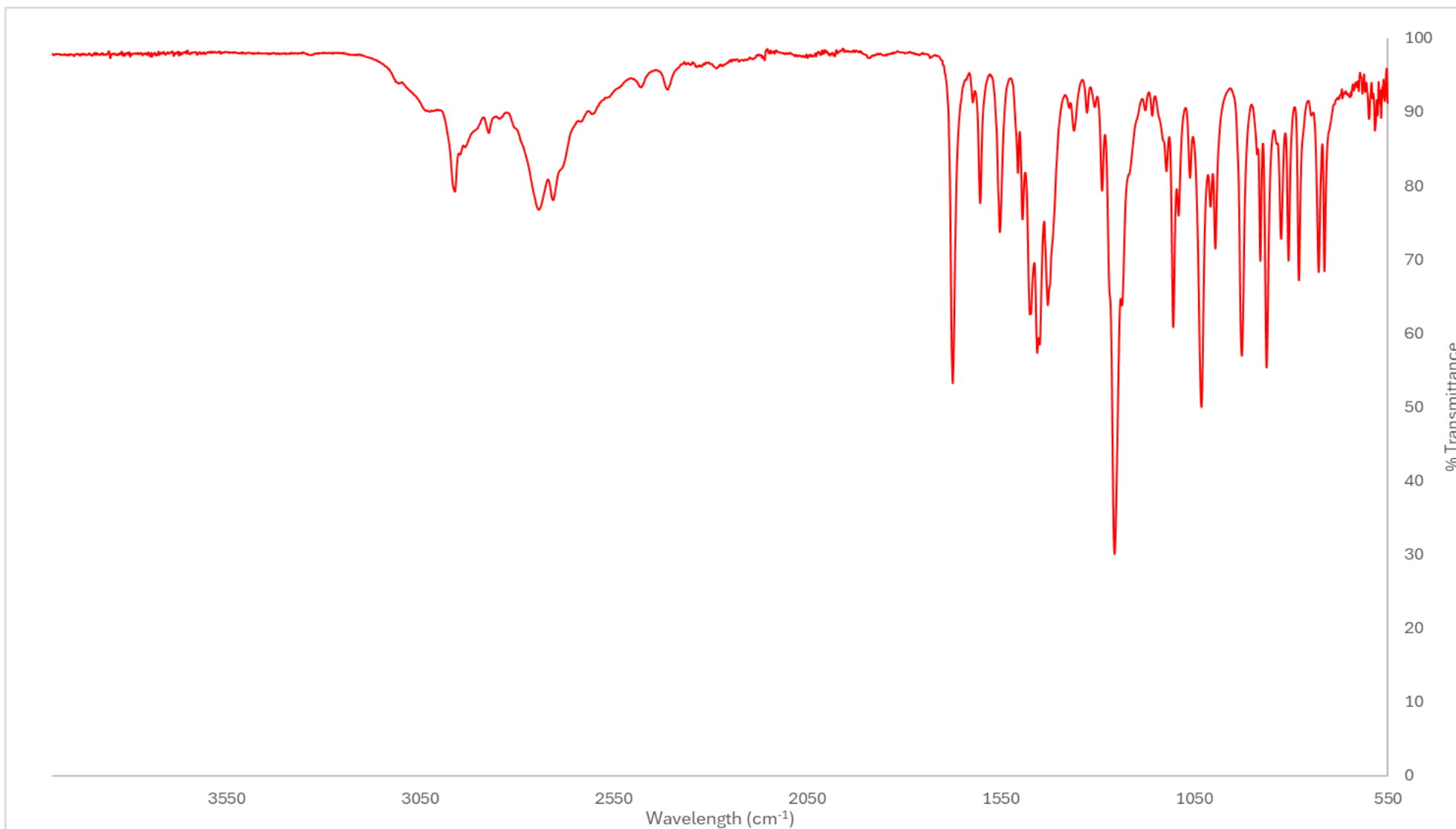


Figure 28: ATR FT-IR spectrum of pentylone hydrochloride (**8a**)

Table 7: Functionalities in the FT-IR spectra for compounds **8a-10a**. All common functional group have been recorded with their peak values, respectively.

Compound	Absorption (cm⁻¹)				
	N-H & C-H	C=O	C=C	C-O	C-N
8a	3053 - 2526	1674	1605	1253	1030
8b	3077 - 2438	1673	1612	1258	1035
8c	3053 - 2523	1672	1602	1253	1035
9a	3006 - 2397	1664	1603	1264	1034
9b	3116 - 2496	1668	1604	1263	1034
10a	3106-2368	1683	1607	1257	1033

5.3 Gas Chromatography-Mass Spectrometry (GC-MS)

The qualitative GC-EI-MS method utilized, with a runtime of approximately 10 minutes, which involved a simple solubilization of the samples in methanol (70 µg/mL), followed by direct injection into the GC-MS system. No derivatization steps were necessary. A representative total ion chromatogram (TIC) illustrates the separation of stock solution 1 including (in order of peaks from shortest to longest retention time); butylone ($t_R = 4.662$, **9a**), caffeine ($t_R = 4.901$), pentylone ($t_R = 4.946$, **8a**), dimethylpentylone ($t_R = 5.041$, **8b**), putylone ($t_R = 5.143$), MDPV ($t_R = 5.903$), and MDPHP ($t_R = 6.171$), alongside the separation of stock solution 2 including (in order of peaks going left to right); dimethylpentylone ($t_R = 5.041$, **8b**) and N-ethylpentylone ($t_R = 5.093$, **8c**), as shown in **Figures 29 and 30**

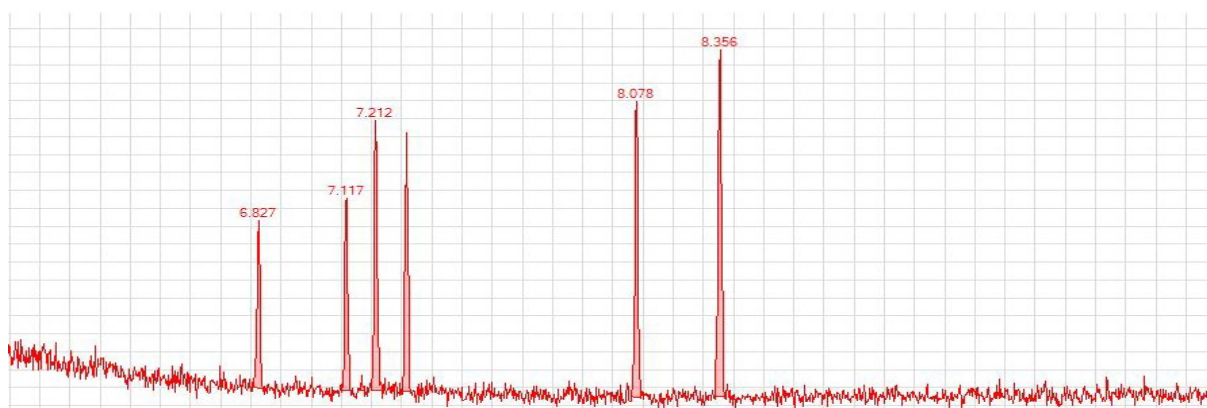


Figure 29: Gas chromatograph of compounds **8a,8b,9a,9b** and **10a** in stock solution 1.

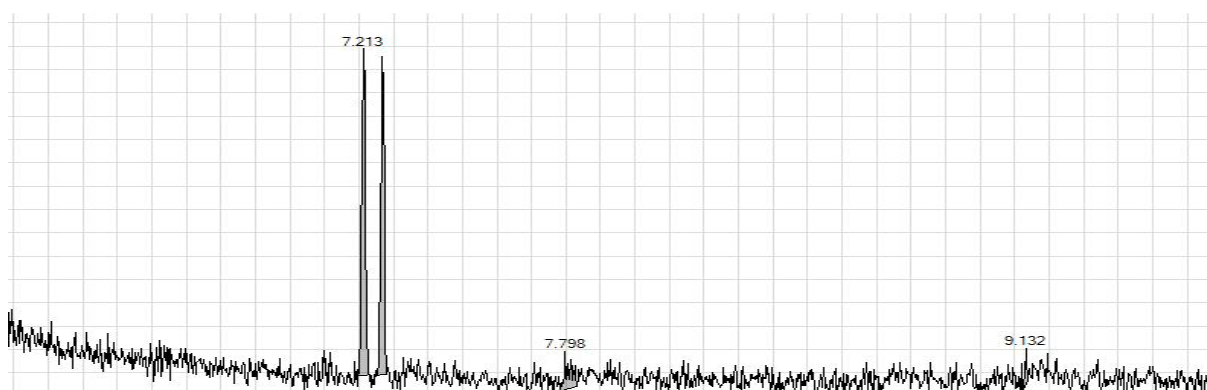


Figure 30: Gas chromatograph of compounds **8b** and **8c** from stock solution 2.

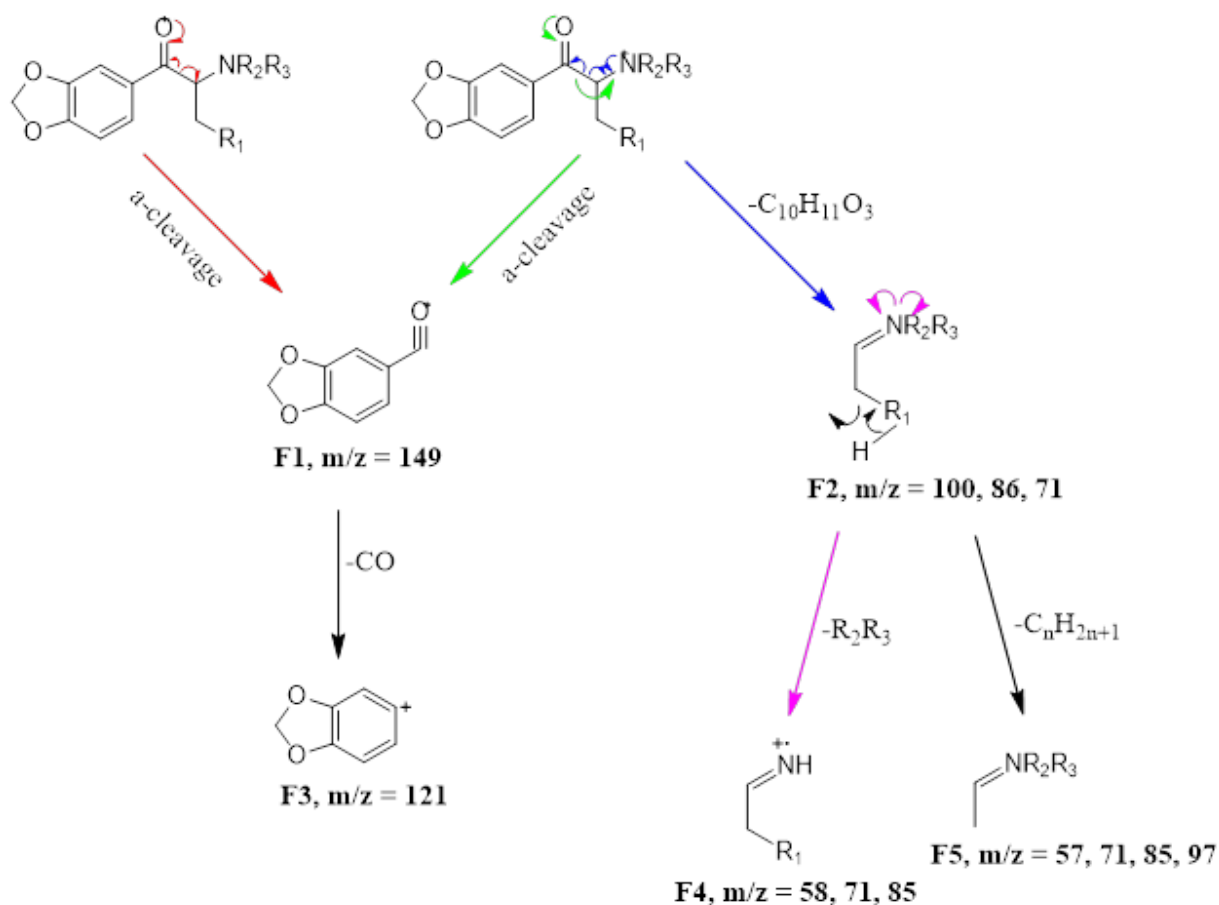
The corresponding electron ionization (EI) mass spectra for pentylone (**8a**) is displayed in **Figure 31** and the remaining synthesised compounds can be found in **Figures S26-S30**. The data acquired in full scan mode, confirmed the presence of a single component for each synthesised product: pentylone ($t_R = 4.946$), dimethylpentylone ($t_R = 5.041$), *N*-

ethylpentylone ($t_R = 5.093$), butylone ($t_R = 4.662$), putylone ($t_R = 5.143$), and MDPHP ($t_R = 6.171$). A comparison of the EI spectra with the NISTDRUGS and SWGDRUGS libraries further corroborated the successful synthesis of each targeted compound. The application of GC-EI-MS enabled detailed visualization of the mass spectral data for all synthetic cathinones within the stock solution, exemplified by the mass spectrum of pentylone hydrochloride in **Figure 31**.



Figure 31: Mass spectrum of pentylone hydrochloride (**8a**).

A general molecular ion structure for cathinones **8a-10a** and their respective fragment ions are illustrated in a **Scheme 2**. The proposed fragmentation pathways for these cathinones are consistent with those previously reported for 3,4-methylenedioxyphenylacetyl ions, such as MDPV. Notably, the dominant fragmentation pathways include the formation of the 3,4-methylenedioxyphenylacylium ion (**F1**, $m/z = 149$, red pathway) and the iminium ion (**F2**, $m/z = 100$, blue pathway), which are key characteristic ions of synthetic cathinones.



Scheme 2: Proposed GC-MS general fragmentation pathway for methylenedioxyphenylacetone derivatives that compounds **8a-10a** follow.³⁹

The following inductive cleavage of carbon monoxide from the 3,4-methylenedioxyphenylacylium ion (**F1**) results in the formation of the 3,4-methylenedioxyphenylium ion (**F3**) at $m/z = 121$. Additionally, the formation of the 3,4-methylenedioxyphenylacylium ion (**F1**) occurs through an α -cleavage of the bond between the carbonyl carbon and the adjacent α -carbon, a process facilitated or stabilized by a lone electron pair on the oxygen atom (green pathway). The methylenedioxyphenylacylium ion (**F1**) at $m/z = 149$ is a prominent SIM ion for six of the seven synthesised cathinones. The methylenedioxyphenylium ion (**F3**) at $m/z = 121$ is a prominent SIM ion in only butylone and pentylone hydrochloride. The iminium ion (**F2**) represents the most prominent ion (base peak) in most mass spectra and is generated via α -cleavage of the bond between the carbonyl carbon and the α -carbon of the aminopropyl group. The subsequently leads to the iminium ion pathway forming secondary fragments through 4- or 6-center eliminations along the alkyl chain (**F5**, black pathway) and radical-directed cleavage (**F4**, gold pathway).³⁹

Table 8: GC-EI-MS validation data (selective ion monitoring mode) for the quantification of butylone, caffeine, pentylone, dimethylpentylone, *N*-ethylpentylone, putylone, MDPV and MDPHP. *Note:* Methyl stearate: $t_R = 9.08$ min; SIM ions (base peak indicated in bold) = **74.0**, 87.0 and 143.0.

Parameter	Analyte								
	Butylone	Caffeine	Pentylone	DP 1	Putylone	MDPV	MDPHP	DP2	NEP
SIM Ions (for quantification)	72.1 , 121.0, 148.9	67.0, 109.0, 194.0	86.0 , 121.0, 149.0	71.0, 100.0 , 148.9	58.0, 100.0 , 149.0	65.0, 126.0 , 149.0	65.0, 140.0 , 149.0	71, 100.0 , 148.9	58.0, 100.0 , 149.0
t_R / min	4.662	4.901	4.946	5.039	5.143	5.903	6.171	5.041	5.093
RRt	0.79	0.83	0.84	0.85	0.87	1.00	1.05	0.99	1.00
Rs	-	7.0	1.1	2.6	3.9	8.7	8.7	-	1.57
As	1.1	1.4	1.3	1.9	0.9	1.0	0.7	1.45	1.18
N (plates)	339517	292409	195463	538110	609969	655064	584405	639832	829395
H (mm)	8.8E-05	1.0E-04	1.5E-04	5.6E-05	4.9E-05	4.6E-05	5.1E-05	4.7E-05	3.6E-05
Linearity (r^2)	0.9981	0.9981	0.9973	0.9978	0.9978	0.9996	0.9970	0.9994	0.9994
LOD (ug/mL)	2.48	2.45	2.92	2.66	2.63	3.07	3.09	1.39	1.41
LOQ (ug/mL)	7.53	7.42	8.86	8.07	7.98	9.31	9.36	4.22	4.27
Precision (%RSD, n = 6)									
10 ug/mL	0.30	0.12	1.55	1.22	0.11	0.16	0.18	0.28	0.73
20 ug/mL	0.56	0.47	1.39	0.68	0.51	0.52	0.46	0.36	0.85
30 ug/mL	0.55	0.65	0.70	0.69	0.57	0.51	0.55	0.18	0.34
40 ug/mL	0.40	0.35	0.55	0.35	0.46	0.48	0.42	0.18	0.35
50 ug/mL	0.89	0.85	0.71	0.85	0.87	0.86	0.83	1.26	1.10
60 ug/mL	0.55	0.53	0.45	0.51	0.59	0.59	0.54	0.60	0.77
70 ug/mL	0.28	0.29	0.31	0.38	0.30	0.37	0.26	0.60	0.35
Assay Recovery (% , n = 3)									
30 ug/mL (80%)	97.3	97.5	95.6	96.5	98.1	97.8	97.3	100.46	100.36
40 ug/mL (100%)	99.3	100.5	98.0	99.0	100.4	101.1	101.4	97.67	98.13
50 ug/mL (120%)	98.1	99.3	95.0	98.4	99.7	100.4	99.5	98.54	99.01
Average Recovery	98.2	99.1	96.2	98.0	99.4	99.7	99.4	98.89	99.20
%RSD	0.01	0.52	0.23	0.03	0.11	0.71	0.51	0.02	0.45
Relative Error (%)	1.78	0.91	3.81	2.05	0.57	0.27	0.61	1.11	0.80

A quantitative GC-MS method utilizing selective ion monitoring (SIM) was developed and validated. Three characteristic ions for each analyte were selected as seen in **Table 8**, and calibration standards were prepared. All seven analytes—namely butylone, pentylone, dimethylpentylone, *N*-ethylpentylone, putylone, MDPV, MDPHP, and caffeine—exhibited linear responses ($r^2 = 0.997$ – 0.999) over a concentration range of 10.0–70.0 $\mu\text{g/mL}$ (with 20.0 $\mu\text{g/mL}$ methyl stearate as internal standard). Repeatability (RSD = 0.11–1.55%, $n = 6$) was satisfactory. Limits of detection (LOD) and quantification (LOQ) were calculated in SIM mode, based on the standard deviation of the response and the slope of the calibration curve, with values ranging from 2.45 to 3.09 $\mu\text{g/mL}$ for LOD and 4.22 to 9.36 $\mu\text{g/mL}$ for LOQ, respectively.

The accuracy of the method was determined through a percentage recovery study, in which samples were spiked in triplicate at three concentration levels (80–120% of the target concentration, 40 µg/mL). The experimentally determined concentrations were compared to the theoretical values using the developed calibration curve. Relative error was assessed to indicate divergence from the expected 100% assay recovery. The method demonstrated good repeatability (%RSD) and recovery rates for all analytes: butylone ($98.2 \pm 0.01\%$), caffeine ($99.1 \pm 0.52\%$), pentylone ($96.2 \pm 0.23\%$), dimethylpentylone ($98.0 \pm 0.03\%$), *N*-ethylpentylone ($99.2 \pm 0.45\%$), putylone ($99.4 \pm 0.57\%$), MDPV ($99.7 \pm 0.71\%$), and MDPHP ($99.4 \pm 0.51\%$).

The GC-EI-MS technique proved effective for the analysis of the synthesized compounds, particularly in cases where either *N*-ethylpentylone or putylone were present in the stock solution. However, due to the identical major SIM ions and nearly indistinguishable retention times of *N*-ethylpentylone and putylone, the peaks of these compounds overlapped significantly in the chromatogram, complicating their differentiation during analysis. As a result, the decision was made to separate the compounds into two distinct stock solutions to improve the accuracy and resolution of their detection. This approach highlights the importance of adjusting analytical conditions to account for challenges in peak overlap and co-elution when analysing structurally similar compounds. The method optimization ensured that both compounds could be individually assessed and characterized in subsequent analyses. It also be noted that, given the small sample size ($n = 3$), the method may not accurately reflect the typical prevalence or concentrations of samples containing these synthetic cathinones on a larger scale. Nevertheless, these findings demonstrate that the 10 minute GC-EI-MS method, employing selective ion monitoring as described, shows great potential for the routine screening of suspect samples containing this novel cathinone.

5.4 Cytotox Evaluation

5.4.1 Assay 1: Four Compounds, 0 - 1.8 μ M in LX-2 Cell lines

The cytotoxic profile of the synthetic cathinones **8a-c,9b** and **10a** were analysed through the changes in membrane integrity that occur due to cell death in the CellTox™ assays (performed at 24 hrs).

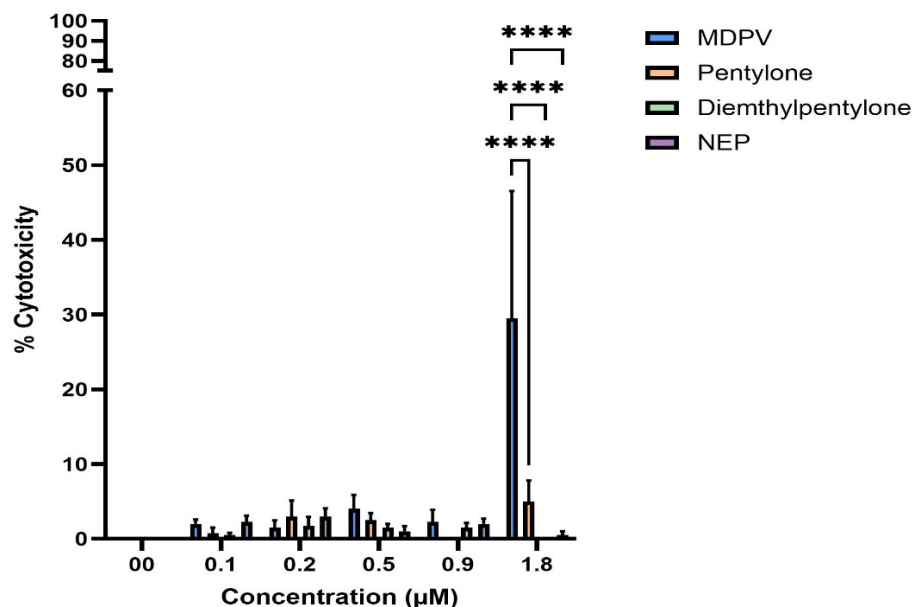


Figure 32: Cytotoxic effects of synthetic methylenedioxycathinones (MDPV, pentylone, dimethylpentylone and NEP) 24hrs after dosing at concentrations of 0.00–1.8 μ M on LX-2 hepatic stellate cell lines. LX-2 cells were treated in quadruplicate (n=4) with increasing concentrations (0.00–1.8 μ M) of the synthetic cathinones MDPV, pentylone, dimethylpentylone, and N-ethylpentylone (NEP). Readings were taken 24 hours after dosing. Cytotoxicity was assessed using a viability assay and expressed as a percentage relative to the maximum response induced by Promega Lysis Buffer, which served as the positive control (100% cytotoxicity). Data represent mean \pm standard error of mean (n = 4 independent experiments). MDPV induced a concentration-dependent increase in cytotoxicity, with a significant elevation observed at 1.8 μ M compared to all other compounds (****p < 0.0001; one-way ANOVA followed by multiple comparisons).

The cytotoxicity profile of the four synthesised methylenedioxycathinones—MDPV, pentylone, dimethylpentylone, and N-ethylpentylone (NEP)—were evaluated in LX-2

hepatic stellate cell lines over a concentration range of 0 to 1.8 μM . As illustrated in **Figure 32**, MDPV (blue) exhibited a significant, concentration-dependent increase in cytotoxicity, with a elevated response observed at 1.8 μM , where cell death approached approximately 50% of the maximal cytotoxic response (relative to the positive control achieved using Promega Lysis buffer). Statistical analysis using two-way ANOVA confirmed that MDPV at a concentration of 1.8 μM induced significantly greater cytotoxicity than all other compounds tested (**** $p < 0.0001$). In contrast, pentylone (orange), dimethylpentylone (green), and NEP (purple) presented marginal cytotoxicity across all concentrations as shown in **Figure 33**, with average cell death consistently below 10% and within the range of baseline variability.

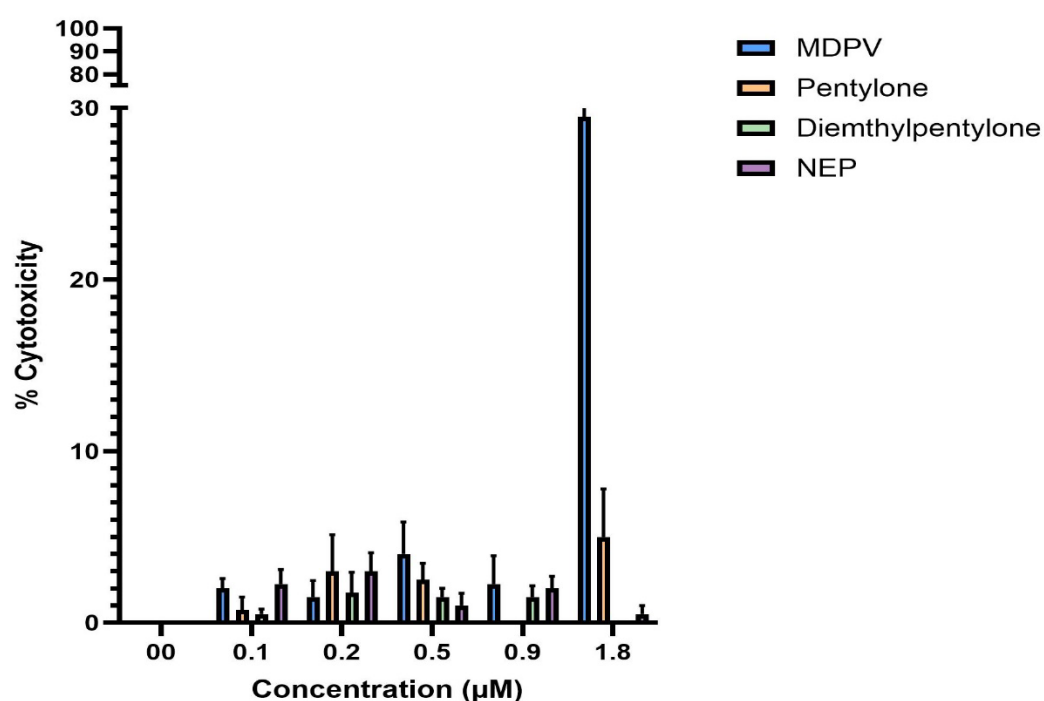


Figure 33: Cytotoxic effects of synthetic methylenedioxy cathinones (MDPV, pentylone, dimethylpentylone and NEP) 24 hrs after dosing at concentrations of 0.00–1.8 μM on LX-2 hepatic stellate cell lines. An expanded view of **Figure 32**, highlighting the minor peaks within the cytotoxic profile. Statistical results further supported these observations, indicating a significant effect of concentration on cytotoxicity ($p < 0.05$), a significant effect of compound identity ($p < 0.05$), and a highly significant interaction between compound and concentration ($p < 0.006$). These findings underscore the distinct toxicological behaviour of MDPV compared to structurally related analogues.

The results suggested that among the methylenedioxcathinones evaluated, MDPV exhibited a distinctly higher hepatotoxic potential in LX-2 cell lines. The pronounced response at 1.8 μM emphasises the relevance of including MDPV in targeted toxicological screening panels, particularly in the context of liver-related adverse responses. LX-2 cell lines, as an established model of hepatic stellate cell activation and liver injury, offer restricted insight into potential fibrogenic or hepatotoxic effects. The lack of cytotoxicity observed for pentylone, dimethylpentylone, and NEP suggests either a lower intrinsic toxicity or reduced interaction with pathways critical to stellate cell viability under the conditions tested.

Taken together, these findings reinforce the compound-specific nature of hepatotoxicity among methylenedioxy-substituted cathinones. The data supports the use of LX-2 cells as a sensitive in vitro model for preliminary screening of synthetic cathinone toxicity, while highlighting MDPV as a priority for further mechanistic and dose-response investigations.

5.4.2 Assay 2: Four Compounds, 0 - 7.3 μM in HepG2 Cell lines

An initial cytotoxicity assay using concentrations ranging between 0.4 to 7.3 μM (concentrations recorded in various post mortem papers) of the four methylenedioxcathinones analogues (MDPV, pentylone, dimethylpentylone and NEP) with data recorded 24 hours after dosing revealed no observable signs of cytotoxicity in HepG2 cell lines, with all compounds exhibiting no cell death relative to the positive control (Promega Lysis buffer, representing 100% cytotoxicity).²² The lack of significant cytotoxic response at these concentrations suggested that the compounds were either not sufficiently potent to induce acute toxicity of that HepG2 cell lines or that the HepG2 cell lines possessed a tolerance threshold above this range on concentrations initially tested. As a result, subsequent experiments employed increased concentrations to better evaluate the toxicological profiles of the compounds, particularly to determine whether higher exposure levels could produce measurable cytotoxic effects and provide clear differentiation between the compounds toxic potential.

5.4.3 Assay 3 Four Compounds, 0 - 2000 mM in HepG2 Cell lines

The cytotoxic effects of the four methylenedioxy-substituted cathinones—MDPV, pentylone, dimethylpentylone, and N-ethylpentylone (NEP)—were assessed in HepG2 cell lines over a concentration range (0 to 2 mM), as shown in **Figure 34**. Cytotoxicity was expressed as a percentage relative to the maximum cytotoxic response produced by the positive control (Promega Lysis buffer) . All compounds exhibited varying degrees of cytotoxicity, with the most prominent responses occurring at 1 mM, where pentylone showed the highest mean cytotoxicity (25%), followed closely by dimethylpentylone, MDPV, and NEP, all of which displayed cytotoxicity between 10–20%.

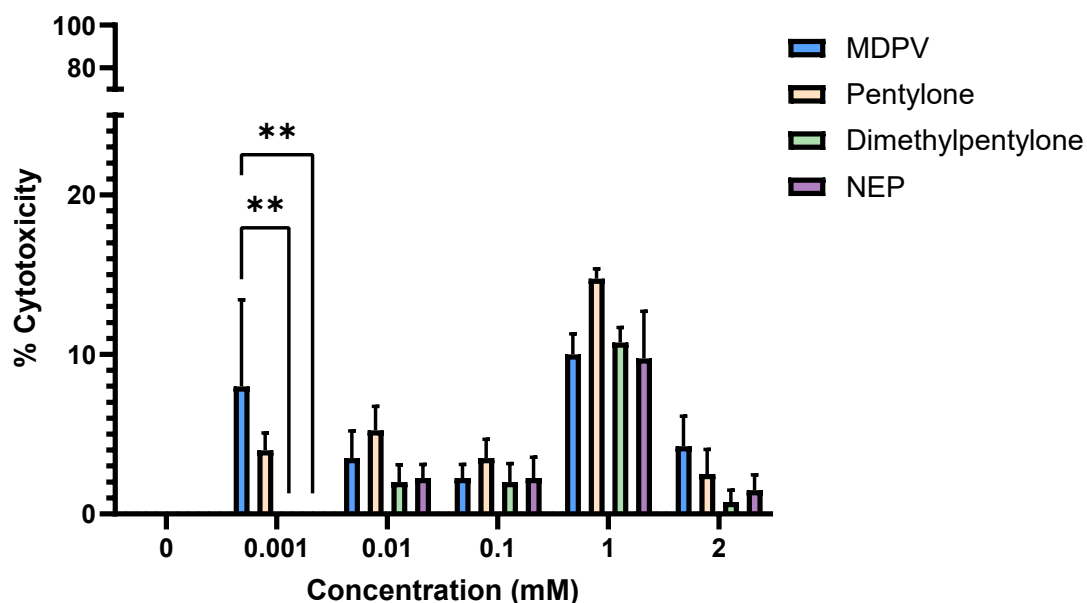


Figure 34: Cytotoxicity of four methylenedioxcathinones (MDPV, pentylone, dimethylpentylone, NEP) in invitro HepG2 cells, readings 24hrs after dosage (1-2000 μ M). Bar chart depicting the percentage of cytotoxicity induced by MDPV (blue), pentylone (orange), dimethylpentylone (green), and NEP (purple) in HepG2 cell lines after 24 hours of exposure to concentrations ranging from 1 mM to 2000 mM. Cytotoxicity was assessed via a standard cell viability assay and expressed as a percentage relative to the maximum cytotoxic response obtained using Promega Lysis Buffer (set as 100%). Data represent mean \pm SEM from four independent experiments (n = 4). Two-way ANOVA revealed a highly significant effect of concentration on cytotoxicity ($p < 0.0001$) and a significant effect of compound identity ($p < 0.05$), while no significant interaction was observed between concentration and compound. Statistically significant differences were observed between MDPV and both dimethylpentylone and NEP at 1 μ M (** $p < 0.005$). These findings indicate concentration-dependent cytotoxic responses and highlight MDPV's enhanced potency at low micromolar levels in HepG2 cells.

MDPV demonstrated a distinct elevation in cytotoxicity at the lowest concentration (0.001 mM), significantly differing from both dimethylpentylone and NEP at the same dose (** $p < 0.005$). This suggests a higher sensitivity of HepG2 cell lines to MDPV at reduced levels, although this early peak was not maintained at intermediate concentrations. All synthetic

cathinones showed similar toxicity profiles between 0.01 and 1 mM, followed by a reduction in cytotoxicity at 2 mM, possibly indicative of cellular adaptation, compound degradation, or assay saturation effects at higher concentrations.

Two-way ANOVA confirmed that concentration had a highly significant effect on cytotoxicity ($p < 0.0001$), while differences among the four compounds were also statistically significant ($p < 0.05$). However, there was no significant interaction between compound type and concentration, indicating that although both variables independently influenced cytotoxicity, the pattern of response across concentrations did not differ significantly between compounds.

These findings highlight small differences in the cytotoxic profiles of structurally related cathinones in HepG2 cell lines. MDPV's continuous enhanced toxicity at low concentrations in LX-2 and HepG2 cell lines may reflect its higher potency or unique metabolic interactions, while the relatively similar mid-range effects across all compounds suggest a shared mechanism of cytotoxicity at higher exposures. Further mechanistic studies would be valuable in confirming whether the observed effects are linked to oxidative stress, mitochondrial dysfunction, or other hepatotoxic pathways.

5.4.4 Assay 4: 2 Compounds, 0 - 2000 mM in HepG2 cell lines.

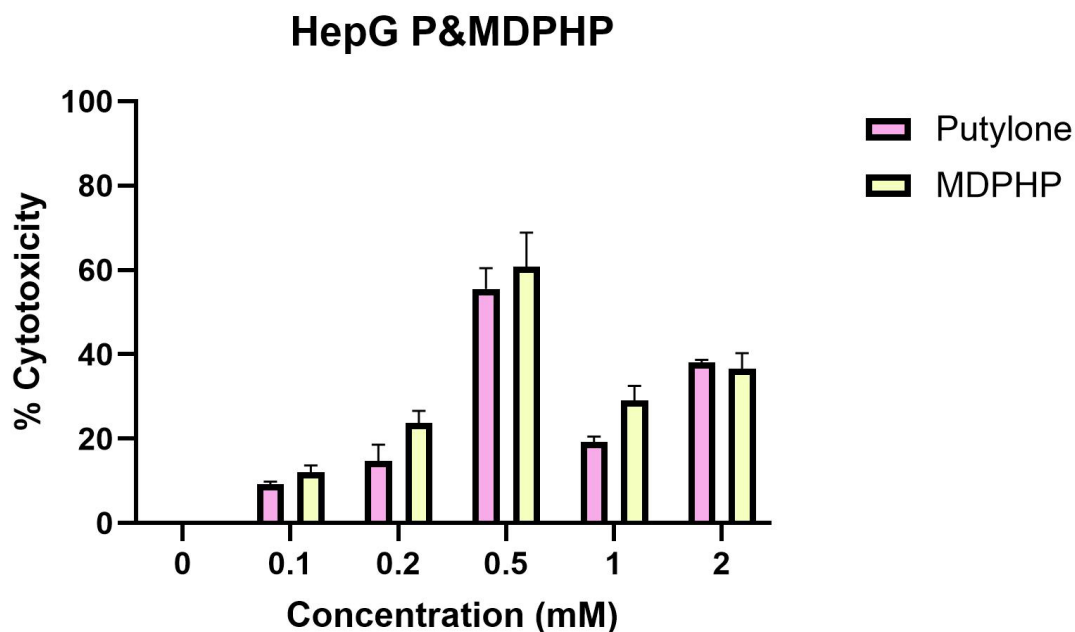


Figure 35: Cytotoxic effects of MDPHP and Putylone at concentration between 0 to 2 mM on HepG2 cell lines. HepG2 cells were treated with increasing concentrations (0–2 mM) of MDPHP (yellow) and Putylone (pink) and their fluorescence was recorded after 24hrs of dosage. Cytotoxicity was assessed in quadruplicate (n=4) and expressed as a percentage of cell death relative to the positive control also known as 100% maximum cytotoxicity (Promega lysis buffer). Both compounds exhibited concentration-dependent cytotoxicity, with maximal effects observed at 0.5 mM. Data represent mean \pm standard error mean (SEM) with a replication of 4 dosages of each compound. Statistical analysis indicated a significant effect of concentration ($p < 0.0001$) and a significant main effect of compound ($p < 0.05$), with no significant interaction ($p < 0.05$), with no significant interaction between compound and concentration.

This assay investigated the cytotoxic effects of the synthetic cathinones MDPHP and Putylone on HepG2 cell lines across a concentration range of 0 to 2 mM. Both compounds exhibited a clear dose-dependent cytotoxic response shown in **Figure 35**, with the most pronounced toxicity observed at 0.5 mM, after which a decline was noted at 1 mM, followed by a slight increase at 2 mM. This unusual pattern could suggest cellular adaptation or saturation effects at higher concentrations. Statistical analysis revealed a

highly significant effect of concentration on cytotoxicity ($P < 0.0001$), underscoring the potency of both substances in compromising HepG2 cell viability as exposure increases.

Although MDPHP consistently demonstrated slightly higher cytotoxicity than Putylone across most concentrations, this difference was noticeable, with a statistically significant effect on the compound type ($P < 0.05$) but no significant interaction between compound and concentration. This lack of interaction indicates that the two substances produce cytotoxic effects in a similar concentration-dependent manner. These findings are consistent with existing literature on synthetic cathinones, which highlights their hepatotoxic potential and mechanisms involving oxidative stress and mitochondrial dysfunction.

The comparable toxicity profiles suggest that both compounds may share overlapping mechanisms of cellular damage, likely involving disruption of mitochondrial integrity, generation of reactive oxygen species, or interference with detoxification pathways in hepatocytes. Given the liver's central role in xenobiotic metabolism, the HepG2 cell line serves as a relevant invitro model for predicting potential hepatotoxic risks associated with synthetic cathinone exposure. These findings support the need for further mechanistic studies to delineate the pathways of toxicity and to assess potential cumulative or synergistic effects with other substances of abuse.

6 Conclusion

This study reports the successful synthesis, isolation, purification, and comprehensive analytical profiling (^1H , $^{13}\text{C}\{^1\text{H}\}$ NMR, ATR-FTIR and GC-EI-MS) of prevalent synthetic cathinones derivatives (pentylone, dimethylpentylone, *N*-ethylpentylone and butylone) and two novel synthetic cathinone derivatives (putylone and MDPHP). In addition to spectral data and detailed characterisation and structural elucidation, this thesis details the development of a rapid and validation GC-EI-MS method using selected ion monitoring (SIM) for the detection and quantitative analysis of the cathinones. The GC-EI-MS method has a detection of 8 minutes, exhibiting a limit of detection (LOD) of up to 3.09 $\mu\text{g}/\text{mL}$ and a limit of quantification of up to 9.36 $\mu\text{g}/\text{mL}$, making it suitable for processing samples in large concentrations. The data presented serves as a valuable reference for the future identification of this novel 3,4-methylenedioxy-*N*-alkyl cathinone and related compounds as they become more prevalent within the night-time economy.

In the cytotoxicity assays, the synthetic cathinones did not show cytotoxicity levels exceeding the positive controls (Promega Lysis buffer), indicating they are not highly cytotoxic under the tested conditions. At higher concentrations, beyond typical ingestion or injection doses, potential for cytotoxicity was observed. At lower concentrations, consistent with post-mortem reports, MDPV was the only compound with noticeable effects. No significant cytotoxic effects were detected in the remaining compounds, suggesting these cathinones are unlikely to cause hepatotoxicity in liver cells. However, further studies are required to evaluate long-term exposure and potential cumulative effects.

One limitation of the cytotoxicity assays in this study is the exclusive use of single cell lines for each assay, which does not replicate the complexity of multicellular organs such as the liver, the primary focus of this research. The liver consists of various cell types, and interactions between these cells are crucial for an accurate representation of *in vivo* effects. While the metabolites of the synthetic cathinones may not directly cause hepatocyte damage, they could still pose potential risks (HSC activation), potentially leading to liver fibrosis and other long-term complications. Further studies using multicellular models are necessary to fully assess these risks.

7 Future Work

Future work should prioritize incorporating the presented analytical data into existing databases as reference points for future analysis of these and related synthetic cathinones. Further characterization and structural elucidation of *N*-butyl and *N*-hexenyl cathinone derivatives will add critical reference points for emerging drug analogues. The qualitative and quantitative data presented in this thesis, particularly through GC-MS analysis, provides a solid foundation. However, acquiring complementary HPLC data would enhance the robustness of the analysis, and utilizing HPLC alongside GC-MS would enable more comprehensive compound profiling.

Further investigation into GC-EI-MS methods is necessary to improve the separation of *N*-ethylpentylone and putylone, as co-elution and the shared major mass ions and retention times reported in this study complicate their distinct identification. Optimizing these methods would significantly enhance the accuracy of drug detection in routine testing. Finally, for greater reliability in forensic testing, low-field benchtop NMR analysis of the 3,4-methylenedioxy cathinone derivatives could be conducted, with spectral data compared against high-field NMR results to ensure consistency and reproducibility.

Optimization of the synthetic route could be achieved by enhancing both the reaction rate and yield using alternative, well-studied methods. For instance, employing solvents with higher boiling points, such as benzene, in place of DCM, may improve reaction conditions. However, the use of acetone as a recrystallization solvent should remain unchanged, as it has proven effective for purification in the method described in this thesis.

Given that both putylone and MDPHP are novel compounds, future research should focus on further cytotoxic testing at doses typically administered *in vivo*, as this study primarily examined high concentrations that could be considered lethal. Additional biological testing is also recommended for all cathinones to establish a more comprehensive understanding of their cytotoxic potential in LX2 and HepG2 cells. Moreover, future studies should identify the specific enzymes involved in the metabolism of these compounds to provide deeper insights into their pharmacokinetic behaviour. Given that one of dimethylpentylone's primary metabolites has been identified as pentylone, further investigation into the pharmacokinetic profiles of both compounds is warranted.

References

1. Luethi, D., Liechti, M. E. & Krahenbuhl, S. 2017. Mechanisms of hepatocellular toxicity associated with new psychoactive synthetic cathinones. *Toxicol*, 387, 57-66.
2. Peacock, A., Bruno, R., Gislev, N., Degenhardt, L., Hall, W., Sedefoc, R., White, J., Thomas, K. V., Farrell, M. & Griffiths, P. 2019. New psychoactive substances: challenges for drug surveillance, control, and public health responses. *Lancet*, 394, 1668-1684.
3. Soussan, C. & Kjellgren, A. 2016. The users of Novel Psychoactive Substances: Online survey about their characteristics, attitudes and motivations. *Int. J. Drug Policy*, 32, 77-84.
4. Batisse, A., Eiden, C., Peyriere, H. & Djezzar, S. 2020. Use of new psychoactive substances to mimic prescription drugs: The trend in France. *NeuroToxicology*, 79, 20-24.
5. Karila, L., Megarbane, B., Cottencin, O. & Lejoyeux, M. 2015. Synthetic cathinones: a new public health problem. *Curr Neuropharmacol*, 13, 12-20.
6. Blum K., Foster Olive, M., Wang, K. K. W., Febo, M., Borsten, J., Giordano, J., Hauser, M. & Gold, M. S. 2013. Hypothesizing that designer drugs containing cathinones ("bath salts") have profound neuro-inflammatory effects and dangerous neurotoxic response following human consumption. *Med. Hypotheses*, 81, 450-455.
7. Zwartsen, A., Olijhoek, M. E., Westerink, R. H. S. & Honderbrink, L. 2020. Hazard Characterization of Synthetic Cathinones Using Viability, Monoamine Reuptake, and Neuronal Activity Assays. *Front Neurosci*, 14, 9.
8. Crime, U. N. O. O. D. A. 2022. UNODC Early Warning Advisory on New Psychoactive Substances.
9. Sumnall, H. & Atkinson, A. 2022. Chapter3 - Prevalence of use of novel psychoactive substances. In: DARGAN, P. & WOOD, D. (eds.) *Novel Psychoactive Substances (Second Edition)*. Boston: Academic Press.
10. Shafi, A., Berry, A. J., Sumnall, H., Wood, D. M. & Tracy, D. K. 2020. New psychoactive substances: a review and updates. *Ther Adv Psychopharmacol*, 10, 2045125320967197.
11. Pearlson, G. D. 1981. Psychiatric and medical syndromes associated with phencyclidine (PCP) abuse. *Johns Hopkins Med J*, 148, 25-33.
12. (NDARC), N. D. A. A. R. C. 2017. New and emerging psychoactive substances. *A Quick Guide to Drugs & Alcohol*, 3rd ed. State Library of NSW: Drug Info
13. Wire, G. H. N. 2023. Major Study Reveals Safest Way to Take Valium and Ativan. *Global Health News Wire*.
14. Baumann, M. H., Walters, H. M., Niello, M. & Sitte, H. H. 2018. Neuropharmacology of Synthetic Cathinones. *Handb Exp Pharmacol*, 252, 113-142.
15. Daziani, G., Lo Faro, A. F., Montana, V., Goteri, G., Persaresi, M., Bambagiotti, G., Montnari, E., Giorgetti, R. & Montana, A. 2023. Synthetic Cathinones and Neurotoxicity Risks: A Systematic Review. *Int. J. Mol. Sci.*, 24, 6230.
16. Soares, J., Costa, V. M., Bastos, M. D. L., Carvalho, F. & Capela, J. P. 2021. An updated review on synthetic cathinones. *Arch. Toxicol.*, 95, 2895-2940.
17. WEDINOS. 2024. *Sample Results* [Online]. <https://www.wedinos.org/sample-results#mylocation> [Accessed 23/05 2024].
18. Krotulski, A. J., Papsun, D. M., DE Martinis, B. S., Mohr, A. L. A. & Logan, B. K. 2018. N-Ethyl Pentylone (Ephylone) Intoxications: Quantitative Confirmation and Metabolite Identification in Authentic Human Biological Specimens. *J. Anal. Toxicol.*, 42, 467-475.

19. Wood, M. R., Bernal, I. & Lalancette, R. A. 2017. The hydrochloride hydrates of pentylone and dibutylone and the hydrochloride salt of ephylone: the structures of three novel designer cathinones. *Struct. Chem.*, 28, 1369-1376.
20. Dal Cason, T. A., Young, R. & Glennon, R. A. 1997. Cathinone: An Investigation of Several N-Alkyl and Methylenedioxy-Substituted Analogs. *Pharmacol Biochem Behav*, 58, 1109-1116.
21. Organisation, W. H. 2023. Critical Review Report: Dipentylone.
22. Jackson, G. 2022. Fragmentation Pathways Of Odd- And Even-electron N-alkylated Artificial Cathinones.
23. Kuroпка, P., Zawadzki, M. & Szpot, P. 2023. A review of synthetic cathinones emerging in recent years (2019–2022). *Forensic Toxicol*, 41, 25-46.
24. Westphal, F., Junge, T., Girreser, U., Greibl, W. & Doering, C. 2012. Mass, NMR and IR spectroscopic characterization of pentedrone and pentylone and identification of their isocathinone by-products. *Forensic Sci. Int.*, 217, 157-167.
25. Dasgupta, A. 2017. 3 - Designer drugs including bath salts and spices. In: Dasgupta, A. (ed.) *Alcohol, Drugs, Genes and the Clinical Laboratory*. Academic Press.
26. Simmler, L., Buser, T., Donzelli, M., Schramm, Y., Dieu, L.-H., Huwyler, J., Chaboz, S., Horner, M. & Liechti, M. 2013. Pharmacological characterization of designer cathinones in vitro. *Br. J. Pharmacol.*, 168, 458-470.
27. Nutt, D. J. 2008. Relationship of neurotransmitters to the symptoms of major depressive disorder. *J Clin Psychiatry*, 69 Suppl E1, 4-7.
28. Boyer, E. W. & Shannon, M. 2005. The Serotonin Syndrome. *NEJM*, 352, 1112-1120.
29. Angoa-Perez, M., Anneken, J. H. & Kuhn, D. M. 2017. Neurotoxicology of Synthetic Cathinone Analogs. *Curr Top Behav Neurosci*, 32, 209-230.
30. Valente, M. J., Araujo, A. M., Silva, R., Bastos, M. D. L., Carvalho, F., Guedes DD Pinho, P. & Carvalho, M. 2016. 3,4-Methylenedioxypropylone (MDPV): in vitro mechanisms of hepatotoxicity under normothermic and hyperthermic conditions. *Arch. Toxicol.*, 90, 1959-1973.
31. Anizan, S., Concheiro, M., Lehner, K. R., Bukhari, M. O., Suzuki, M., Rice, K. C., Baumann, M. H. & Huestis, M. A. 2016. Linear pharmacokinetics of 3,4-methylenedioxypropylone (MDPV) and its metabolites in the rat: relationship to pharmacodynamic effects. *Addict Biol*, 21, 339-47.
32. Araujo, A. M., Carvalho, M., Costa, V. M., Durrte, J. A., Dinis-Oliveira, R. J., Bastos, M. D. L., Guedes De Pinho, P. & Carvalho, F. 2021. In vivo toxicometabolomics reveals multi-organ and urine metabolic changes in mice upon acute exposure to human-relevant doses of 3,4-methylenedioxypropylone (MDPV). *Arch. Toxicol*, 95, 509-527.
33. Ryan, M. & Desmond, P. 2001. Liver toxicity: could this be a drug reaction? *Australian Family Physician*, 30, 427.
34. Xu, L., Hui, A. Y., Albanis, E., Arthur, M. J., O'Byrne, S. M., Blaner, W. S., Mukherjee, P., Friedman, S. L. & Eng, F. J. 2005. Human hepatic stellate cell lines, LX-1 and LX-2: new tools for analysis of hepatic fibrosis. *Gut*, 54, 142-151.
35. Aden, D. P., Fogel, A., Plotkin, S., Damjanov, I. & Knowles, B. B. 1979. Controlled synthesis of HBsAg in a differentiated human liver carcinoma-derived cell line. *Nature*, 282, 615-616.
36. Fulmer, G. R., Miller, A. J. M., Sherden, N. H., Gottlieb, H. E., Nudelman, A., Stoltz, B. M., Bercaw, J. E. & Goldberg, K. I. 2010. NMR Chemical Shifts of Trace Impurities: Common Laboratory Solvents, Organics, and Gases in Deuterated Solvents Relevant to the Organometallic Chemist. *Organometallics*, 29, 2176-2179.

37. Santali, E. Y., Cadogan, A.-K., Daeid, N. N., Savage, K. A. & Sutcliffe, O. B. 2011. Synthesis, full chemical characterisation and development of validated methods for the quantification of (\pm)-4'-methylmethcathinone (mephedrone): A new "legal high". *J. Pharm. Biomed. Anal.*, 56, 246-255.
38. Hussain, J. H., Gilbert, N., Costello, A., Schofield, C. J., Kemsley, E. K., Sutcliffe, O. B. & Mewis, R. E. 2020. Quantification of MDMA in seized tablets using benchtop 1H NMR spectroscopy in the absence of internal standards. *BC_FCHE*, 20, 100263.
39. Davidson, J. T., Sasiene, Z. J. & Jackson, G. P. 2020. Fragmentation pathways of odd- and even-electron N-alkylated synthetic cathinones. *Int. J. Mass Spectrom.*, 453, 116354.

Supplementary

Figure S1. ^1H - ^1H COSY NMR spectrum of 8b in DMSO- d_6	89
Figure S2. ^1H - $^{13}\text{C}\{^1\text{H}\}$ HMBC NMR spectrum of 8b in DMSO- d_6	90
Figure S3. ^1H - $^{13}\text{C}\{^1\text{H}\}$ HSQC NMR spectrum of 8b in DMSO- d_6	91
Figure S4: DEPT-135 NMR spectrum of 8b in DMSO- d_6	92
Figure S5: ^1H - ^1H COSY NMR spectrum of 8c in DMSO- d_6	93
Figure S6: ^1H - $^{13}\text{C}\{^1\text{H}\}$ HMBC NMR spectrum of 8c in DMSO- d_6	94
Figure S7: ^1H - $^{13}\text{C}\{^1\text{H}\}$ HSQC NMR spectrum of 8c in DMSO- d_6	95
Figure S8: DEPT-135 NMR spectrum of 8c in DMSO- d_6	96
Figure S9: ^1H - ^1H COSY NMR spectrum of 9a in DMSO- d_6	97
Figure S10: ^1H - $^{13}\text{C}\{^1\text{H}\}$ HMBC NMR spectrum of 9a in DMSO- d_6	98
Figure S11: ^1H - $^{13}\text{C}\{^1\text{H}\}$ HSQC NMR spectrum of 9a in DMSO- d_6	99
Figure S12: DEPT-135 NMR spectrum of 9a in DMSO- d_6	100
Figure S13: ^1H - ^1H COSY NMR spectrum of 9b in DMSO- d_6	101
Figure S14: ^1H - $^{13}\text{C}\{^1\text{H}\}$ HMBC NMR spectrum of 9b in DMSO- d_6	102
Figure S15: ^1H - $^{13}\text{C}\{^1\text{H}\}$ HSQC NMR spectrum of 9b in DMSO- d_6	103
Figure S16: DEPT-135 NMR spectrum of 9b in DMSO- d_6	104
Figure S17: ^1H - ^1H COSY NMR spectrum of 10a in DMSO- d_6	105
Figure S18: ^1H - $^{13}\text{C}\{^1\text{H}\}$ HMBC NMR spectrum of 10a in DMSO- d_6	106
Figure S19: ^1H - $^{13}\text{C}\{^1\text{H}\}$ HSQC NMR spectrum of 10a in DMSO- d_6	107
Figure S20: DEPT-135 NMR spectrum of 10a in DMSO- d_6	108
Figure S21: ATR FT-IR specrum of dipentylone hydrochloride (8b).....	109
Figure S22: ATR FT-IR specrum of N-ethylpentylone hydrochloride (8c).....	110
Figure S23: ATR FT-IR specrum of Butylone hydrochloride (9a).....	111
Figure 24: ATR FT-IR specrum of Putylone hydrochloride (9b).....	112
Figure S25: ATR FT-IR specrum of MDPHP Hydrochloride (10a).....	113
Figure S26: Mass spectrum of dimethylpentylone hydrochloride (8b).....	114
Figure S27: Mass spectrum of N-ethylpentylone hydrochloride (8c).....	115
Figure S28: Mass spectrum of butylone hydrochloride (9a).....	116
Figure S29: Mass spectrum of putylone hydrochloride (9b).....	117
Figure S30: Mass spectrum of MDPHP hydrochloride (10a).....	118

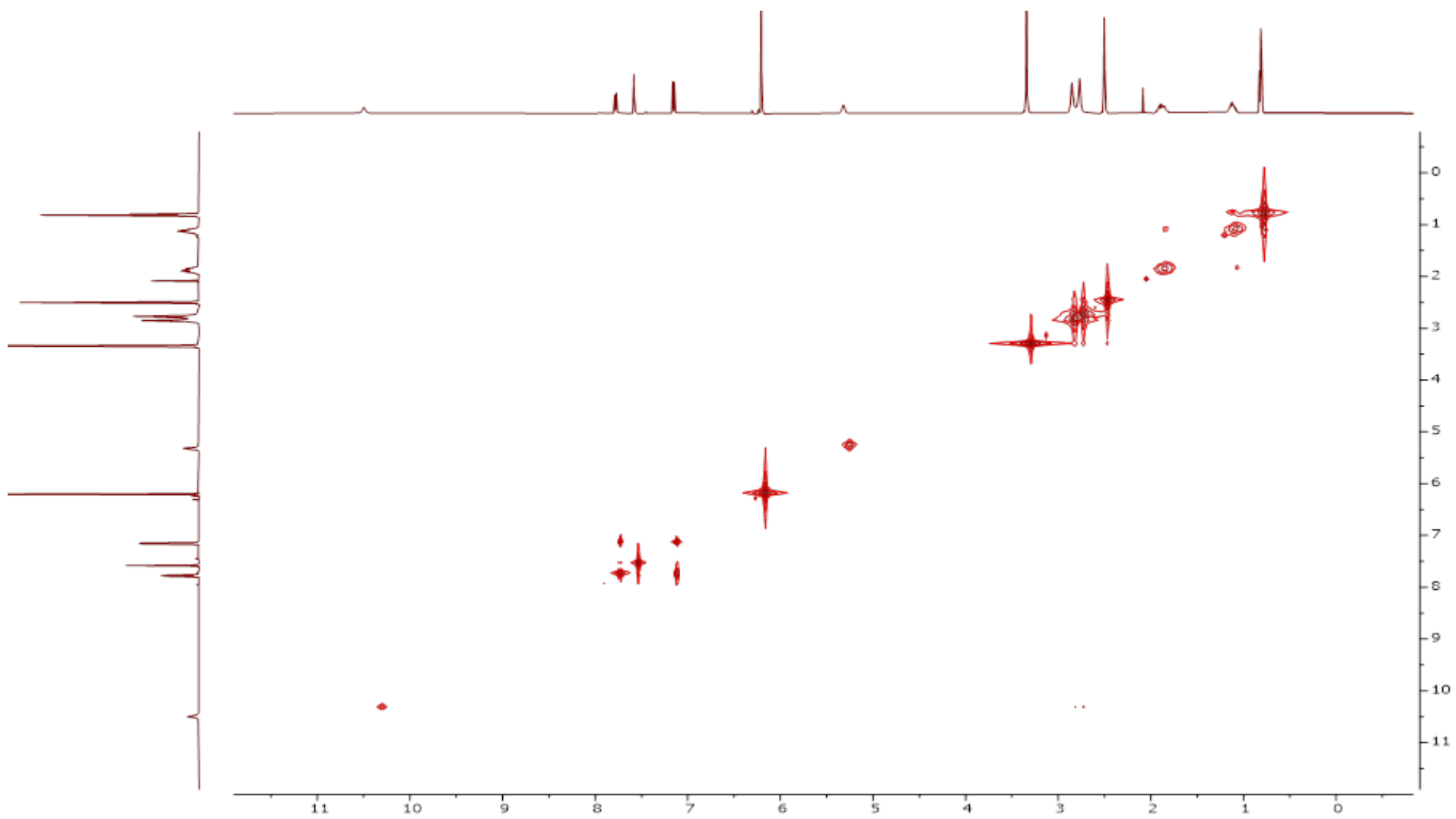


Figure S1: ^1H - ^1H COSY NMR spectrum of **8b** in DMSO-d_6 .

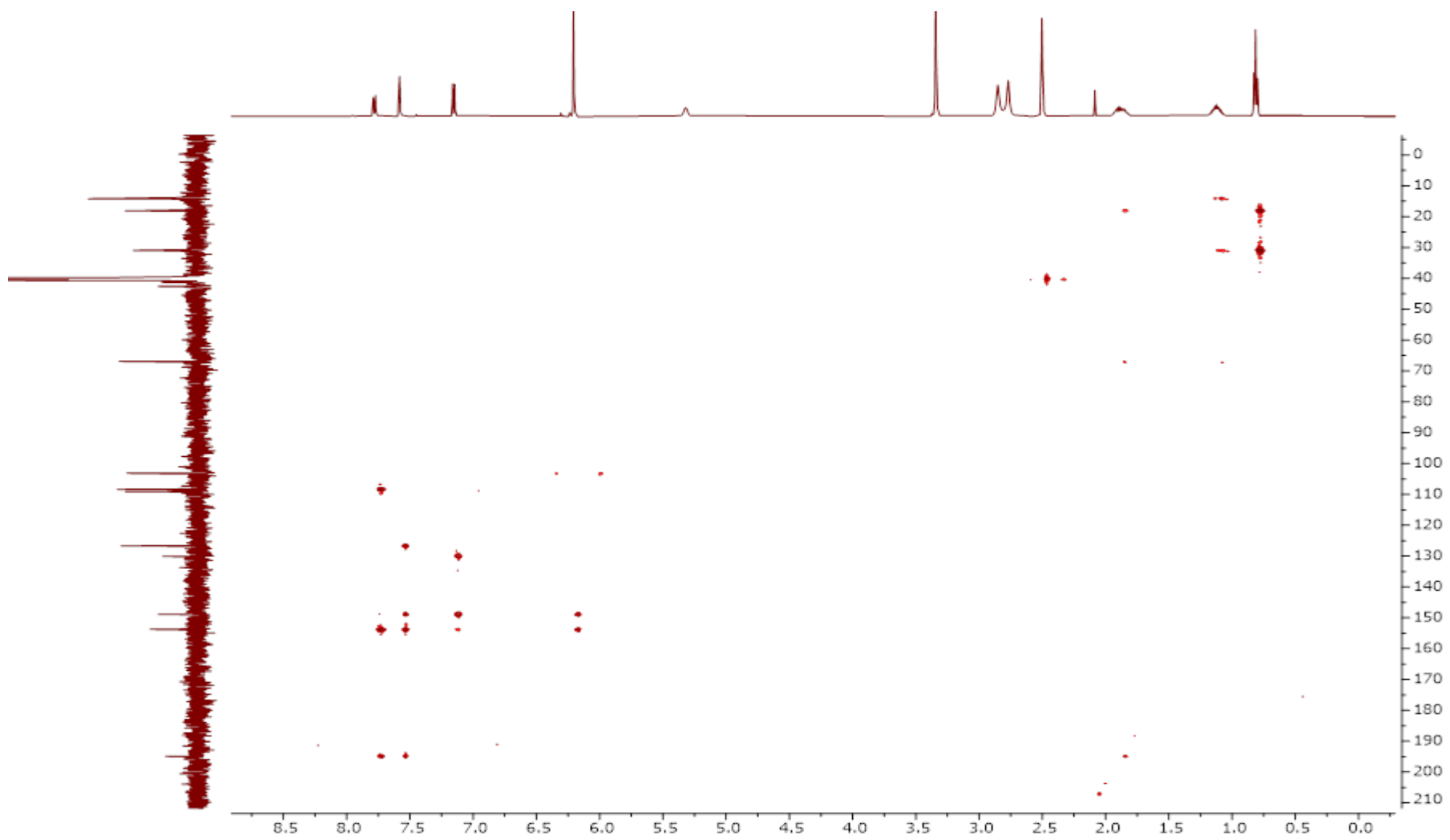


Figure S2: ^1H - $^{13}\text{C}\{^1\text{H}\}$ HMBC NMR spectrum of **8b** in DMSO-d_6 .

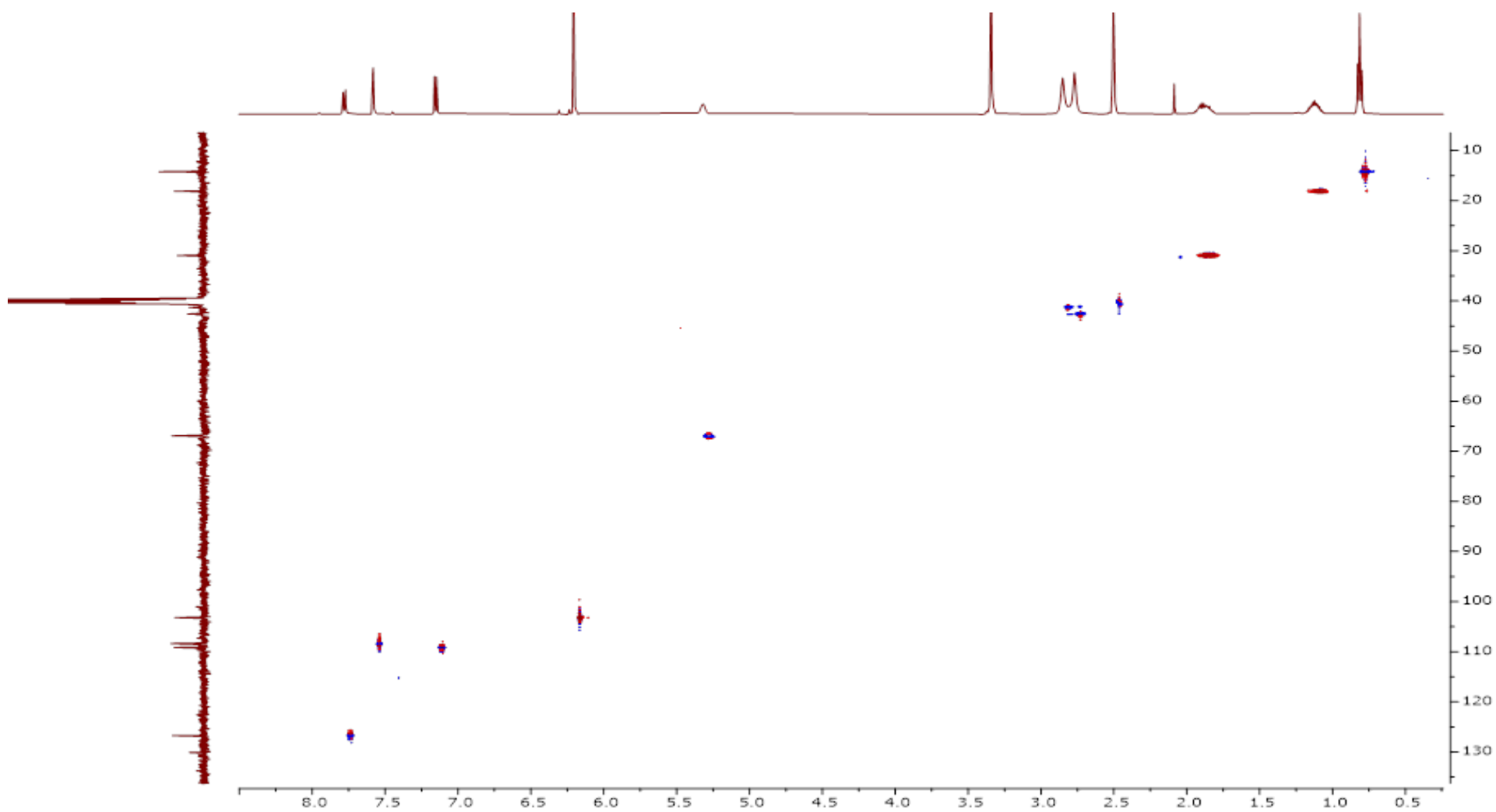


Figure S3: ^1H - $^{13}\text{C}\{^1\text{H}\}$ HSQC NMR spectrum of **8b** in DMSO-d_6 .

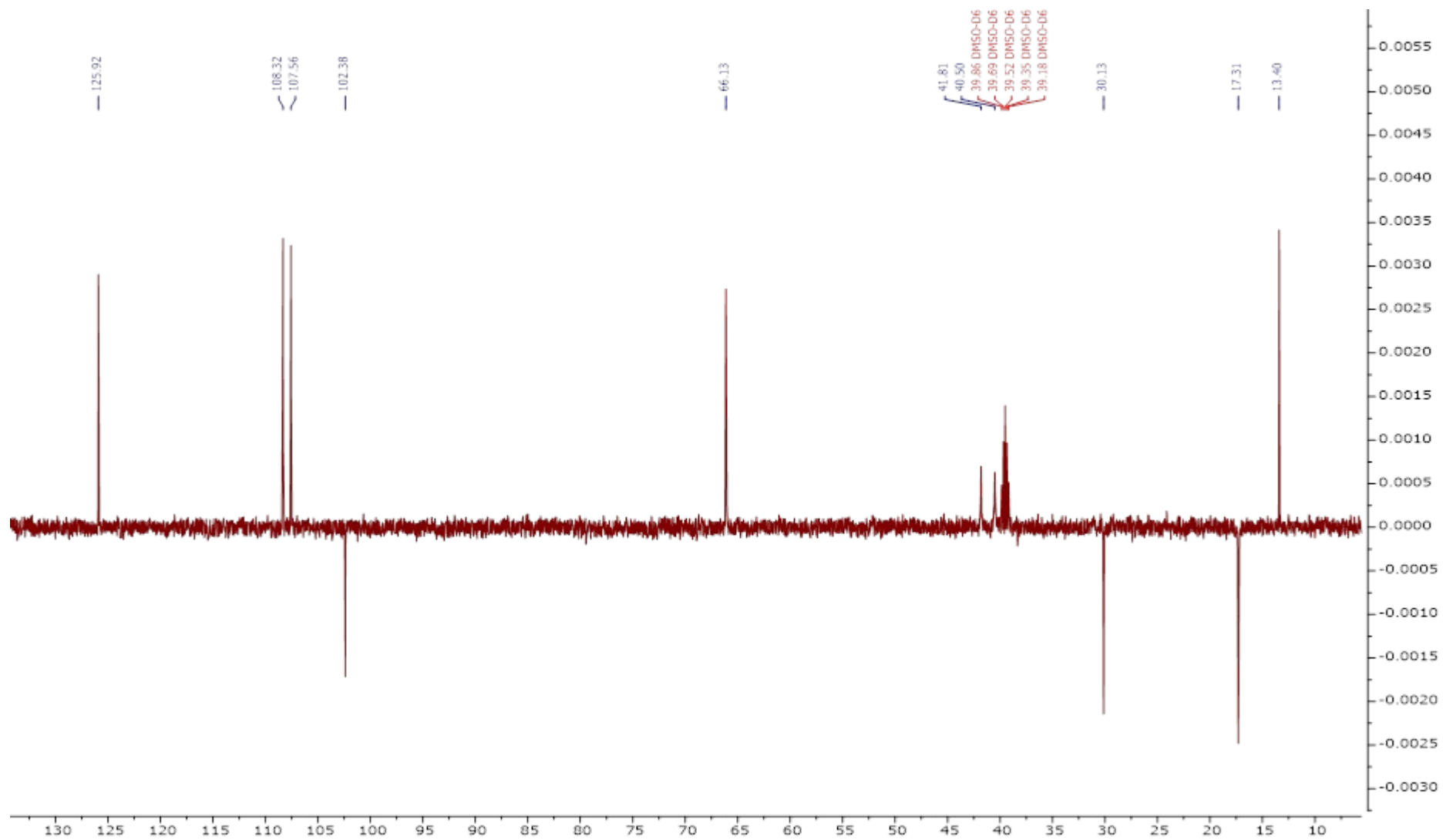


Figure S4: DEPT-135 NMR spectrum of **8b** in DMSO-d₆.

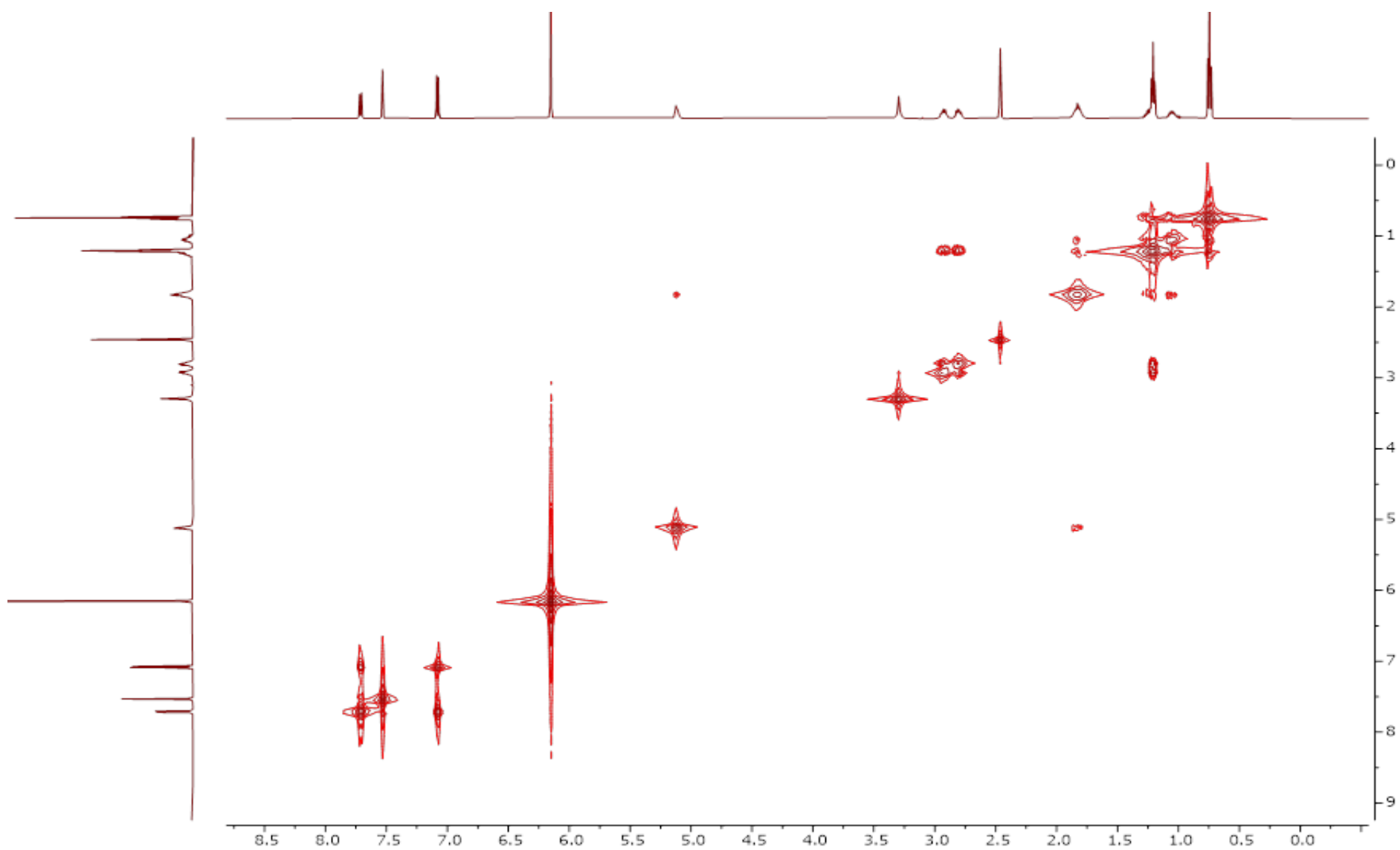


Figure S5: ^1H - ^1H COSY NMR spectrum of **8c** in DMSO-d_6 .

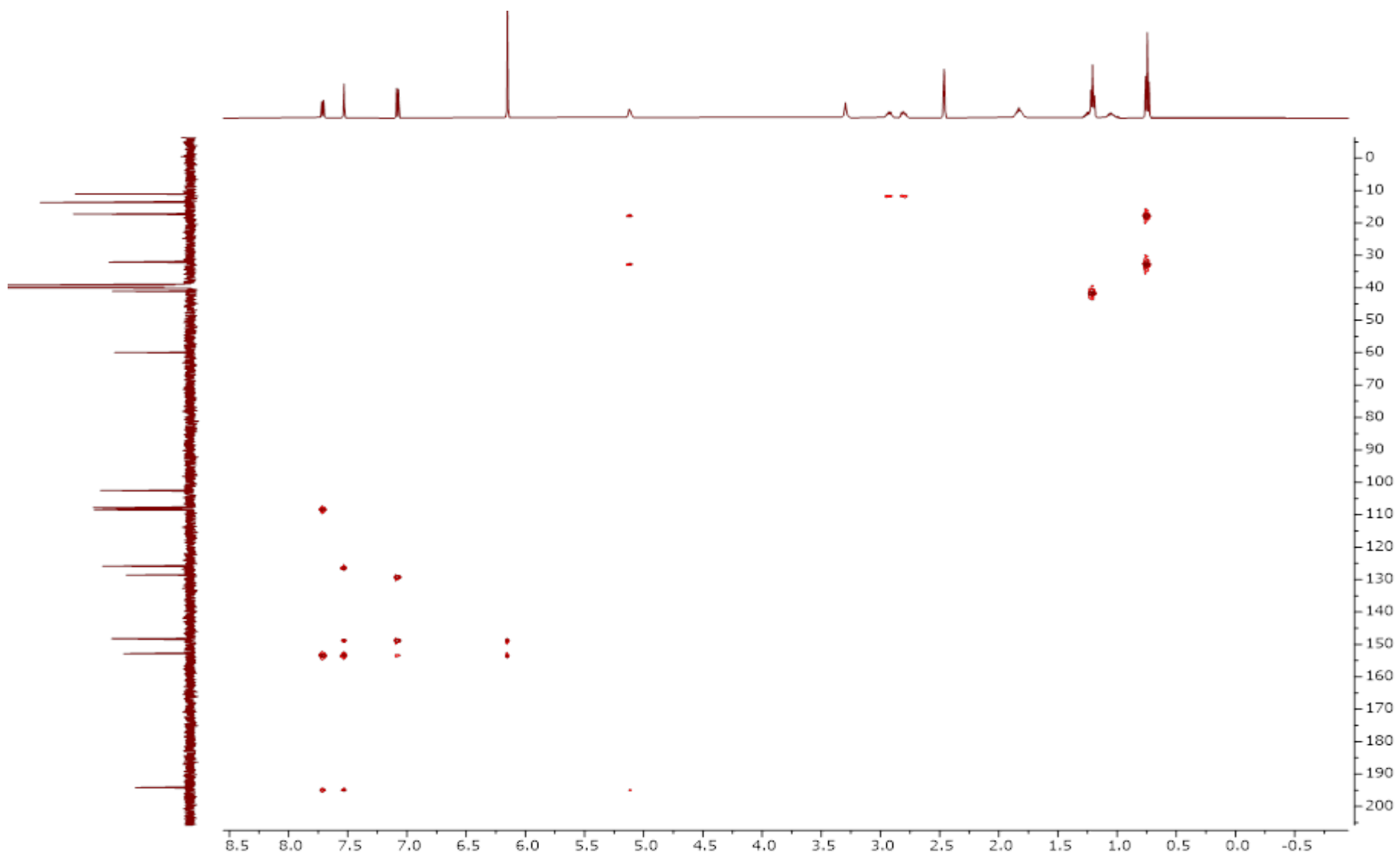


Figure S6: ^1H - $^{13}\text{C}\{^1\text{H}\}$ HMBC NMR spectrum of **8c** in DMSO-d_6 .

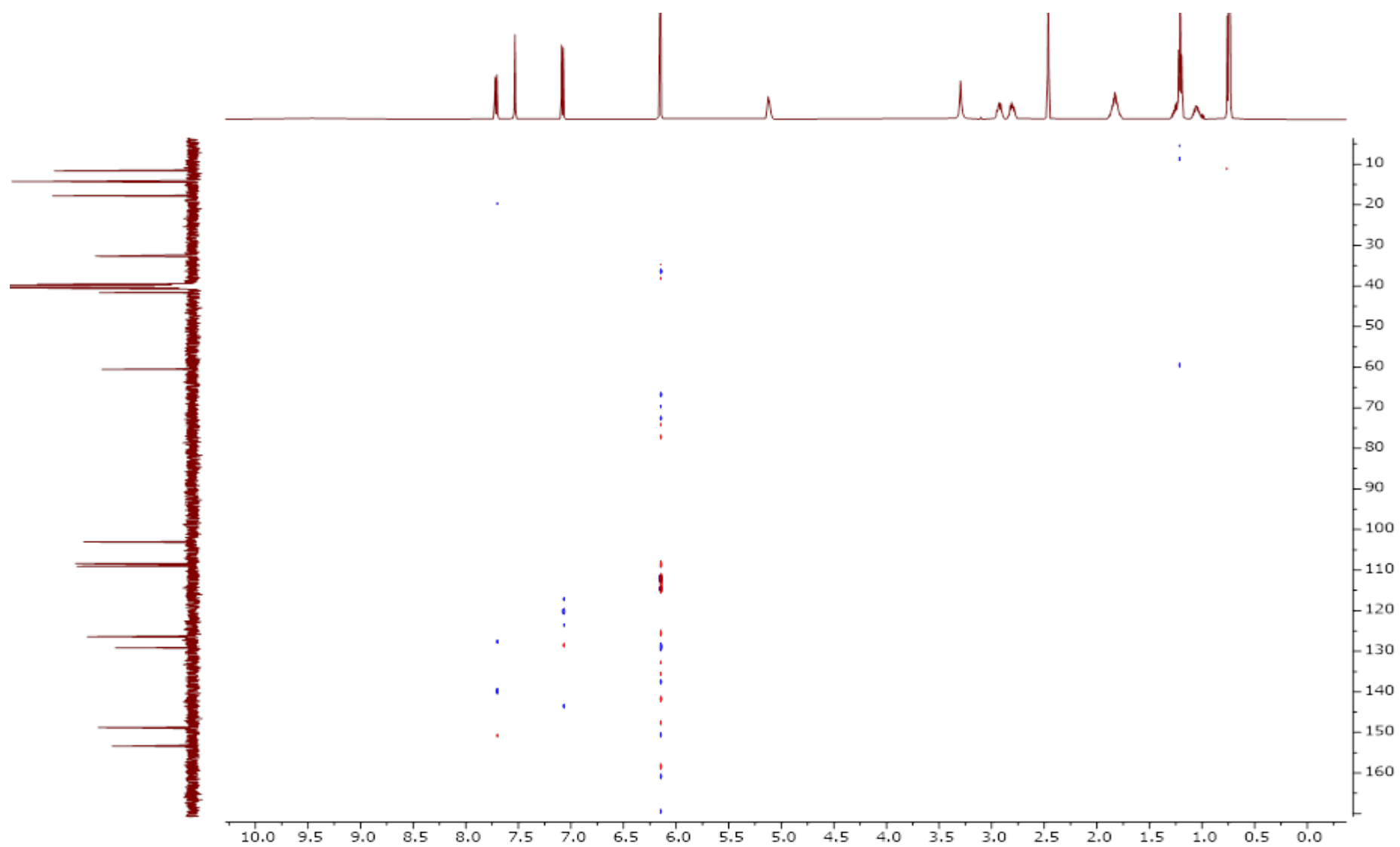


Figure S7: ^1H - $^{13}\text{C}\{^1\text{H}\}$ HSQC NMR spectrum of **8c** in DMSO-d_6 .

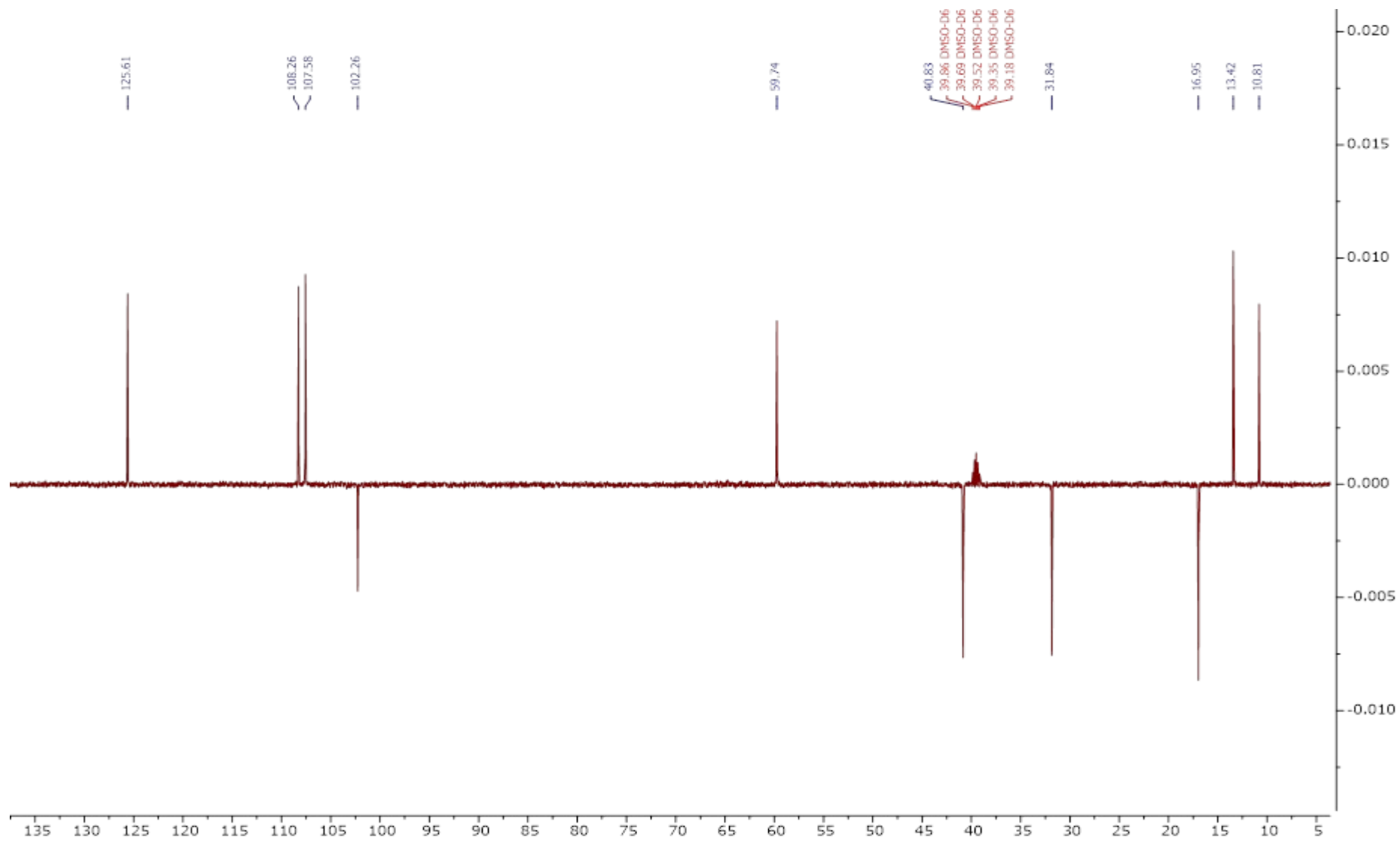


Figure S8: DEPT-135 NMR spectrum of **8c** in DMSO-d₆.

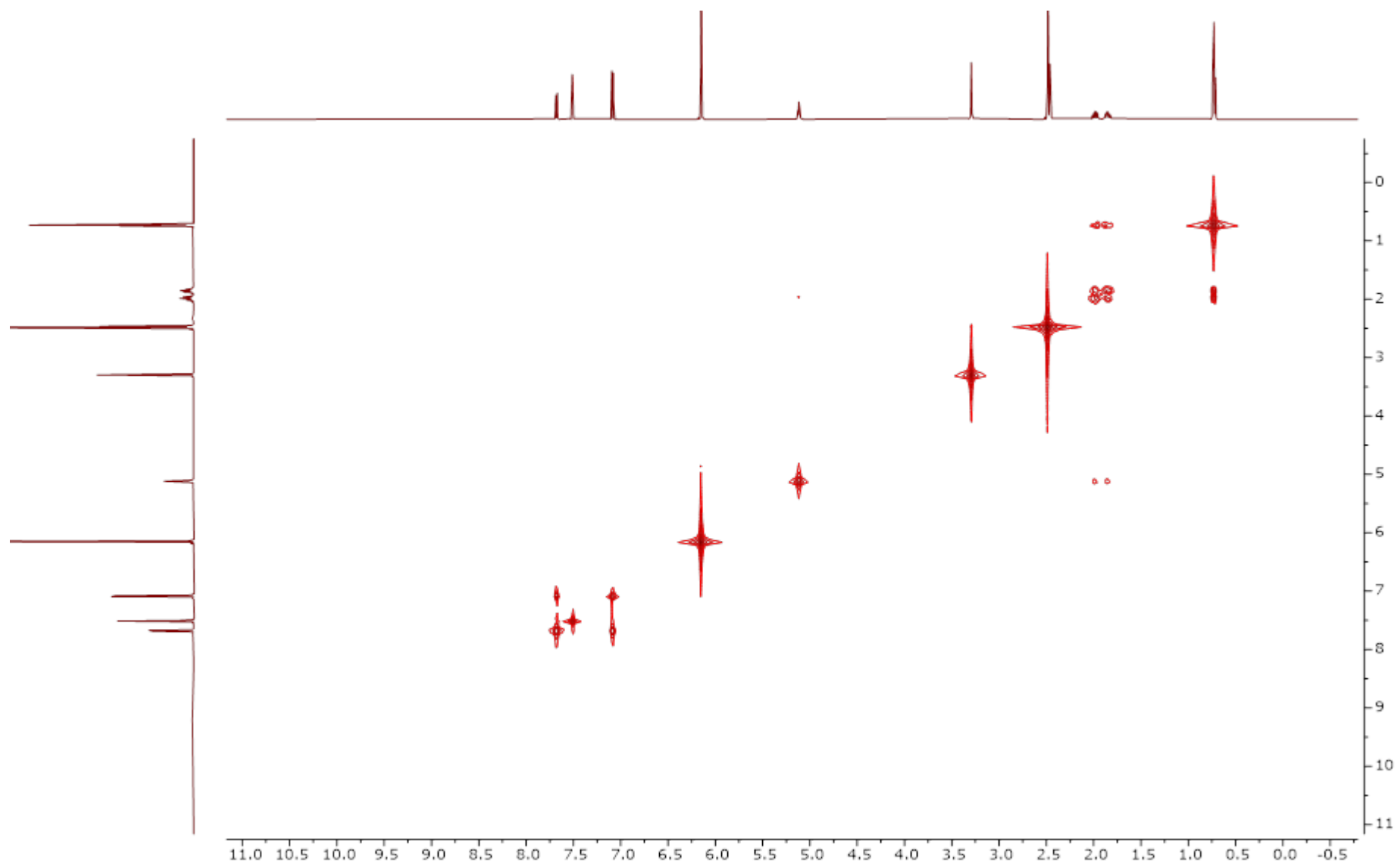


Figure S9: ^1H - ^1H COSY NMR spectrum of **9a** in DMSO-d_6 .

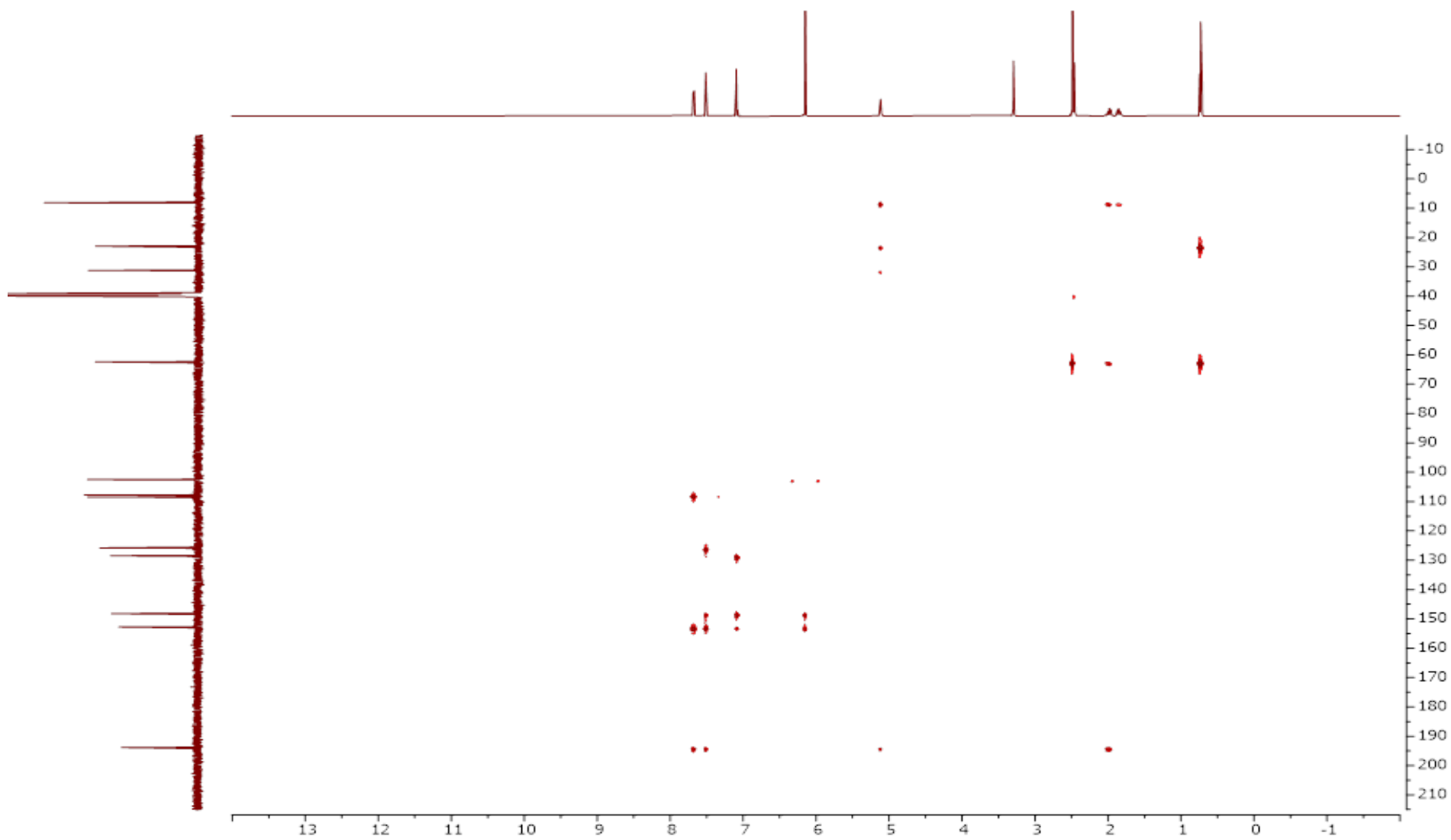


Figure S10: ^1H - $^{13}\text{C}\{^1\text{H}\}$ HMBC NMR spectrum of **9a** in DMSO-d_6 .

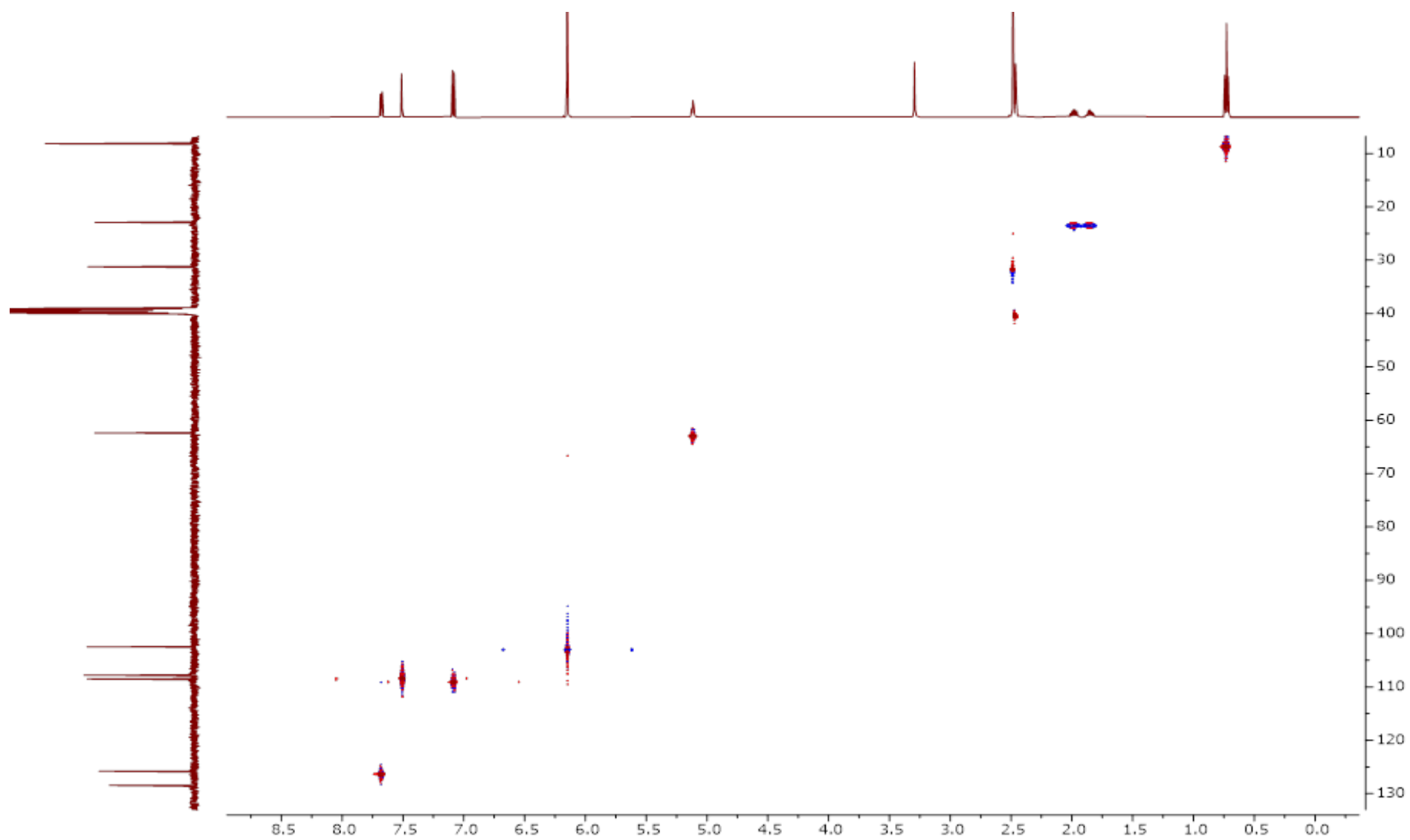


Figure S11: ^1H - $^{13}\text{C}\{^1\text{H}\}$ HSQC NMR spectrum of **9a** in DMSO-d_6 .

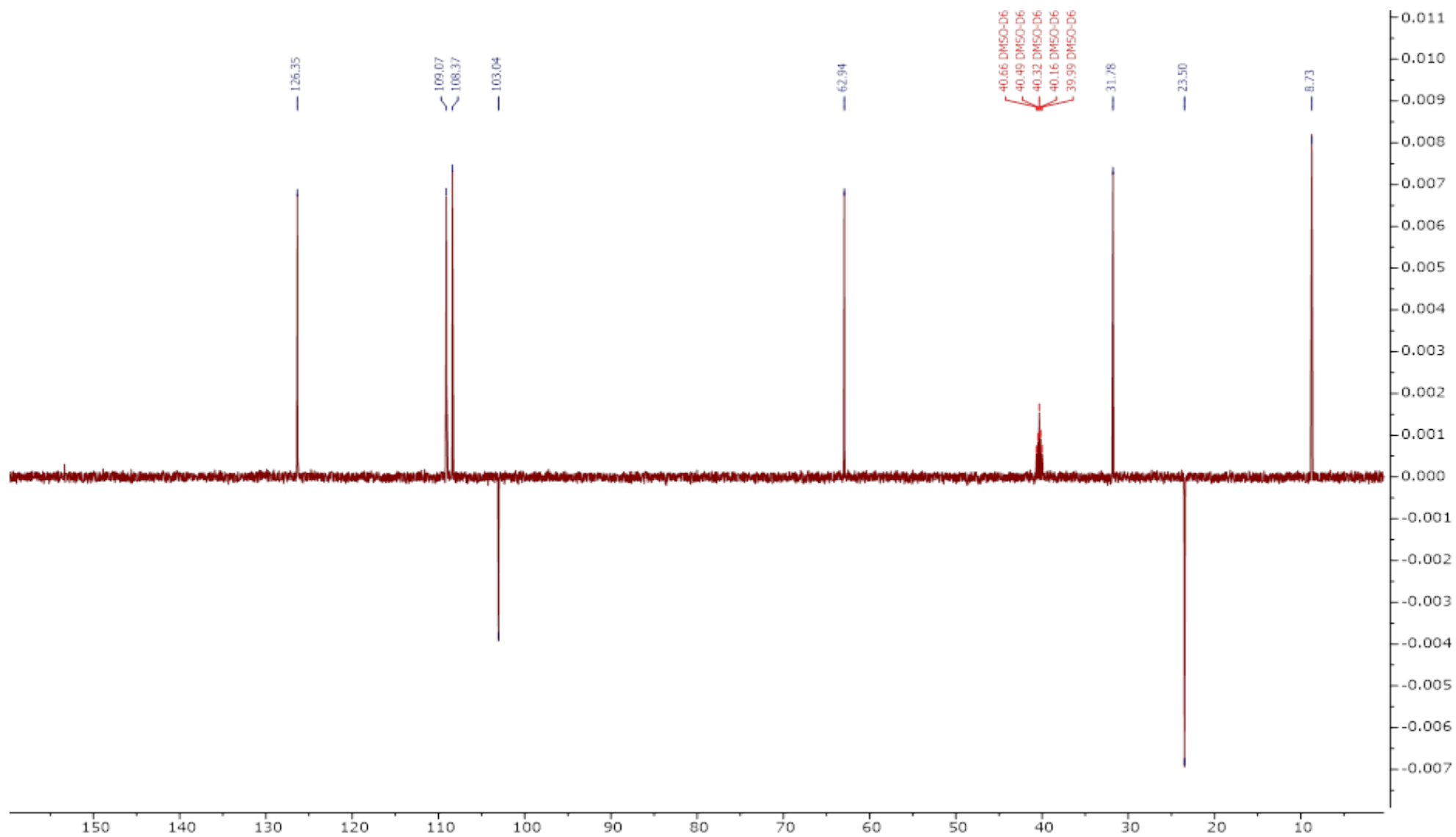


Figure S12: DEPT-135 NMR spectrum of **9a** in DMSO-d₆.

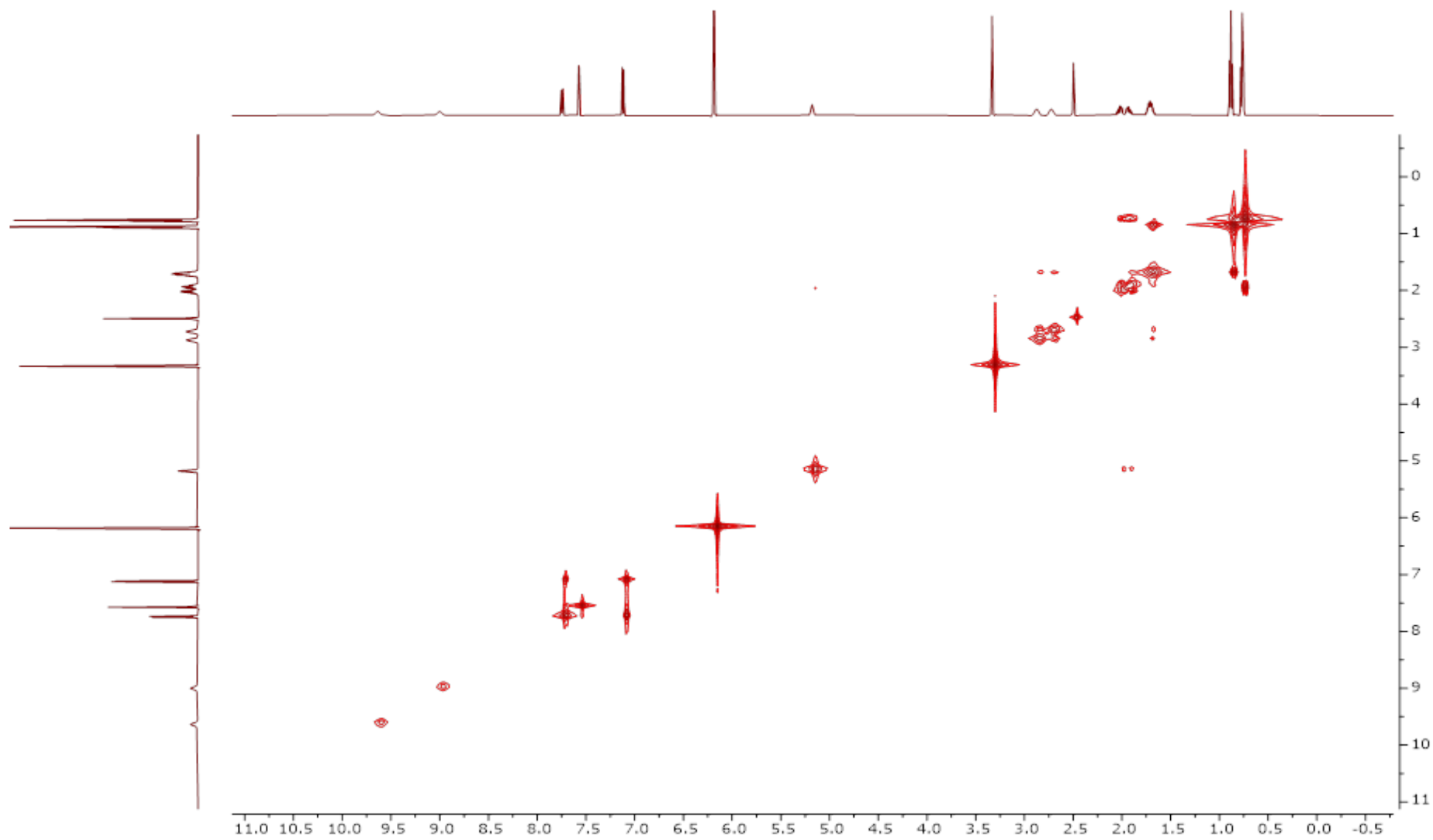


Figure S13: ^1H - ^1H COSY NMR spectrum of **9b** in DMSO-d_6 .

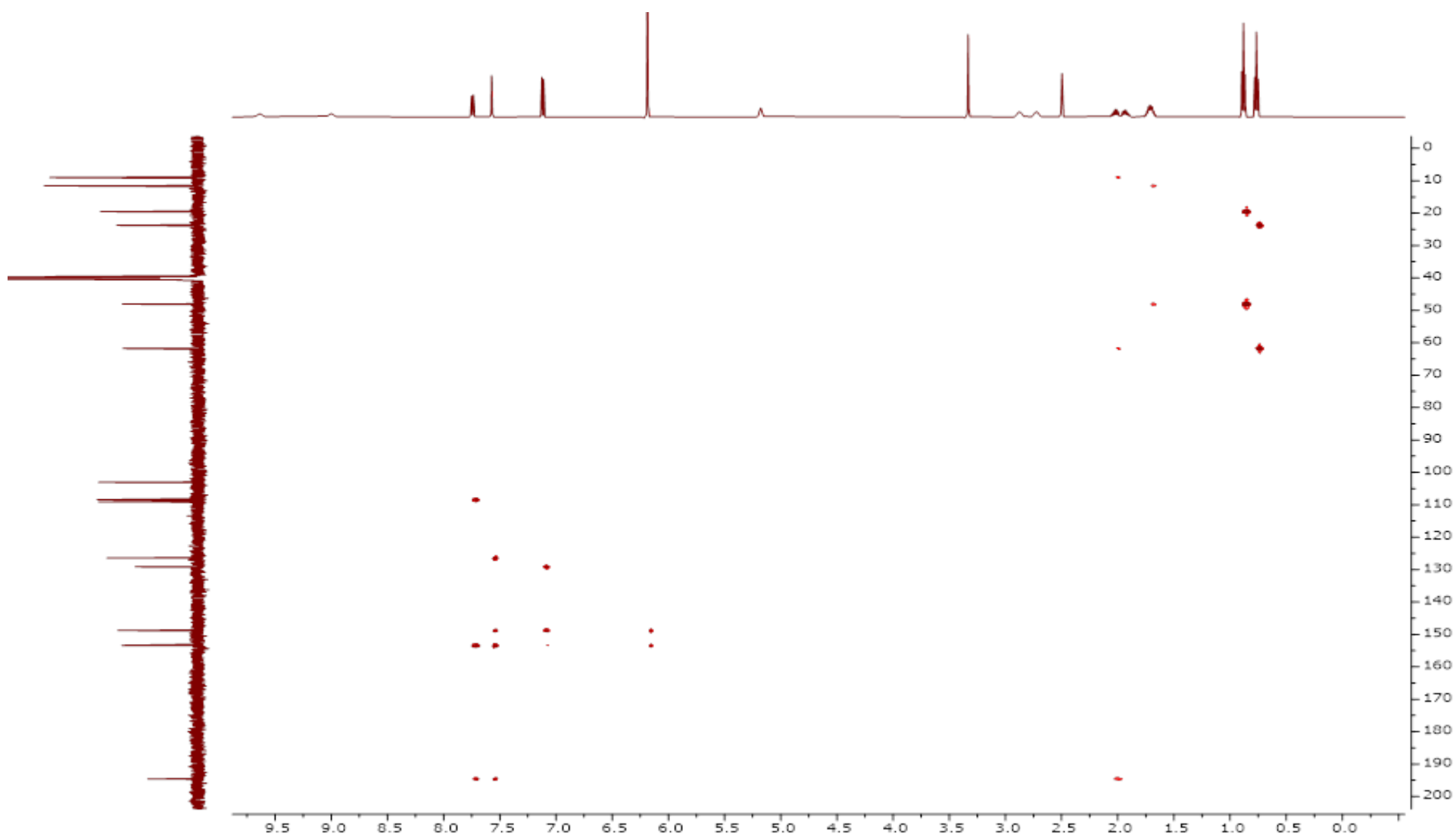


Figure S14: ^1H - $^{13}\text{C}\{^1\text{H}\}$ HMBC NMR spectrum of **9b** in DMSO-d_6 .

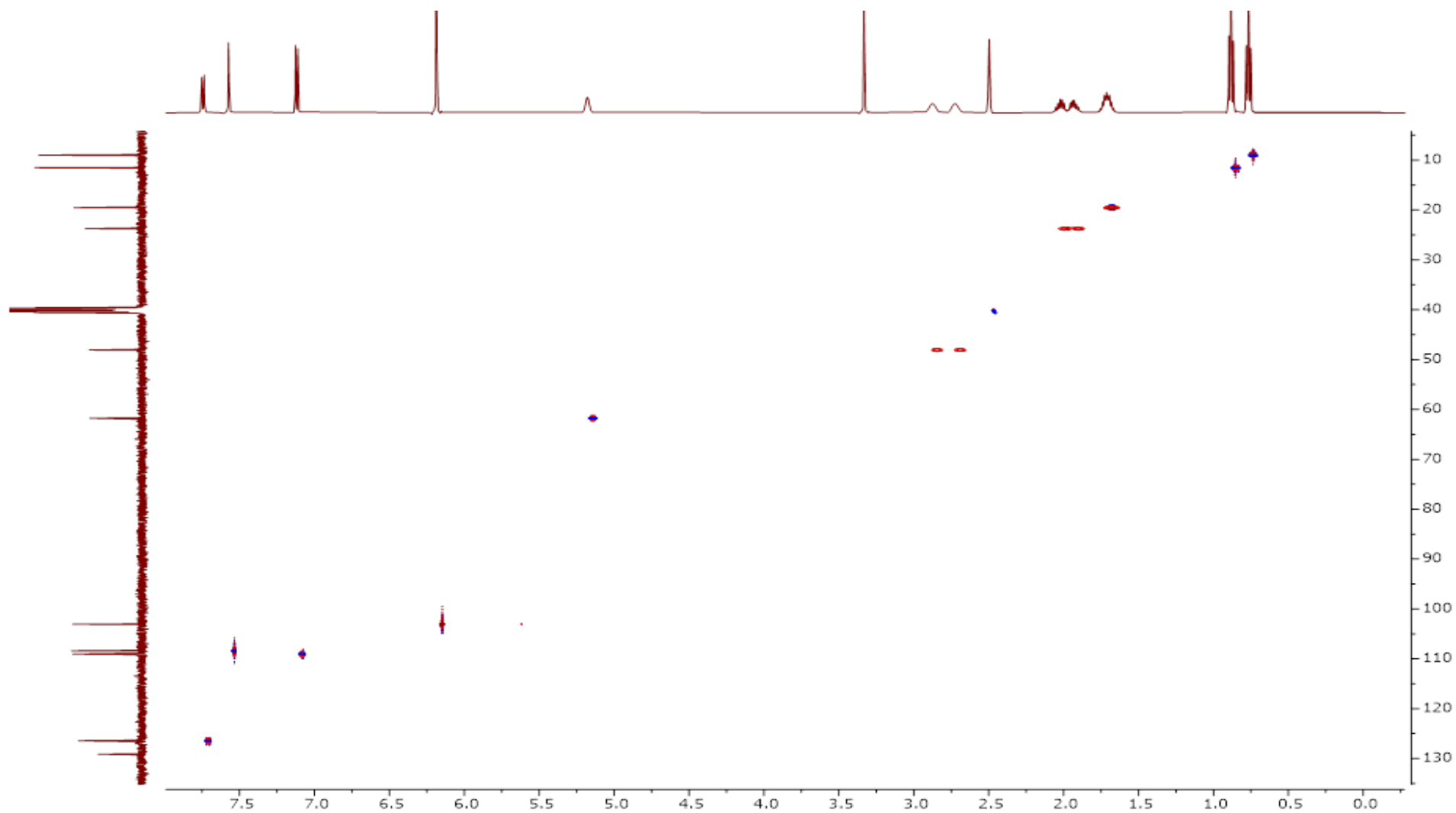


Figure S15: ^1H - $^{13}\text{C}\{^1\text{H}\}$ HSQC NMR spectrum of **9b** in DMSO-d_6 .

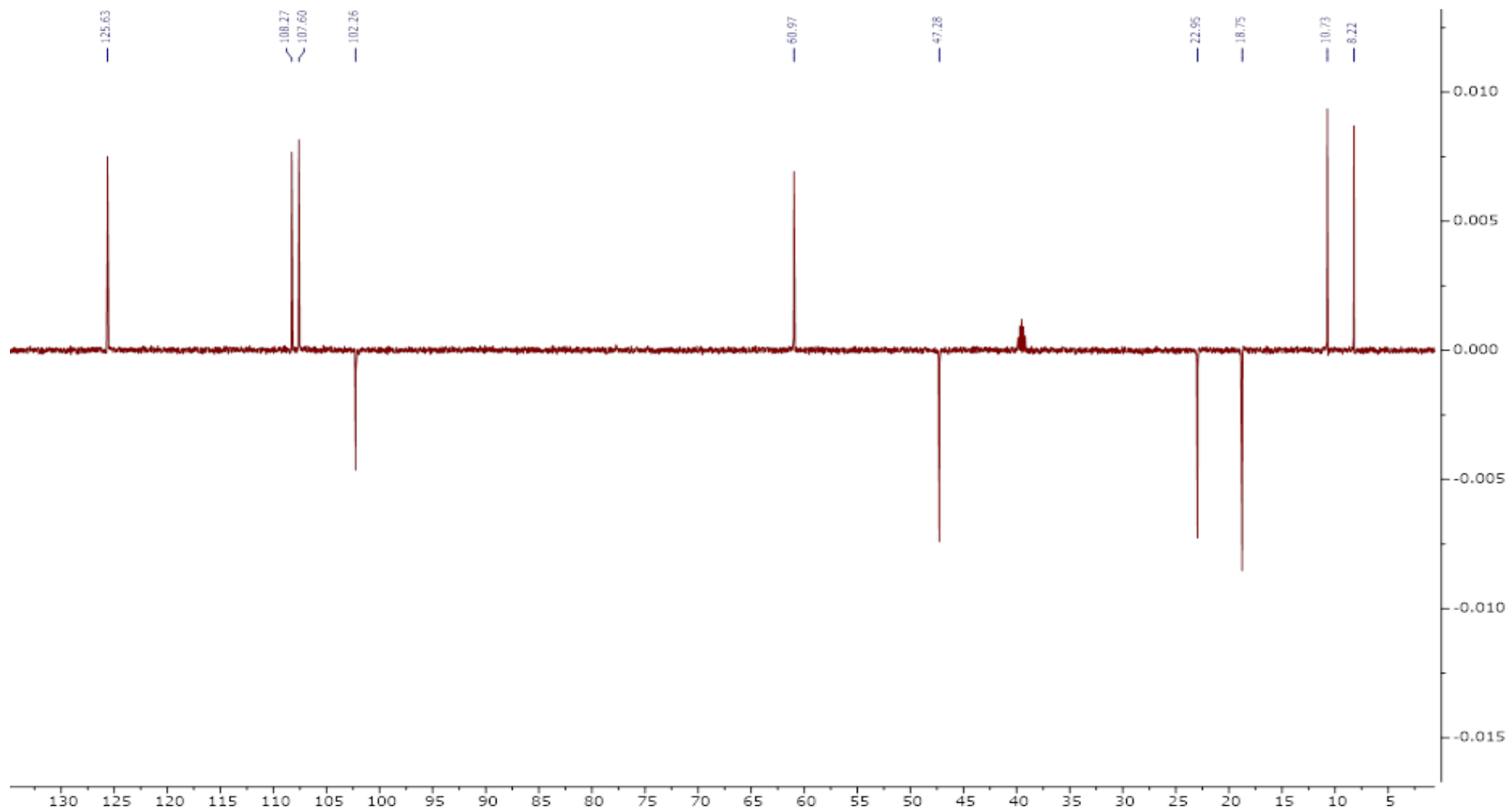


Figure S16: DEPT-135 NMR spectrum of **9b** in DMSO-d₆.

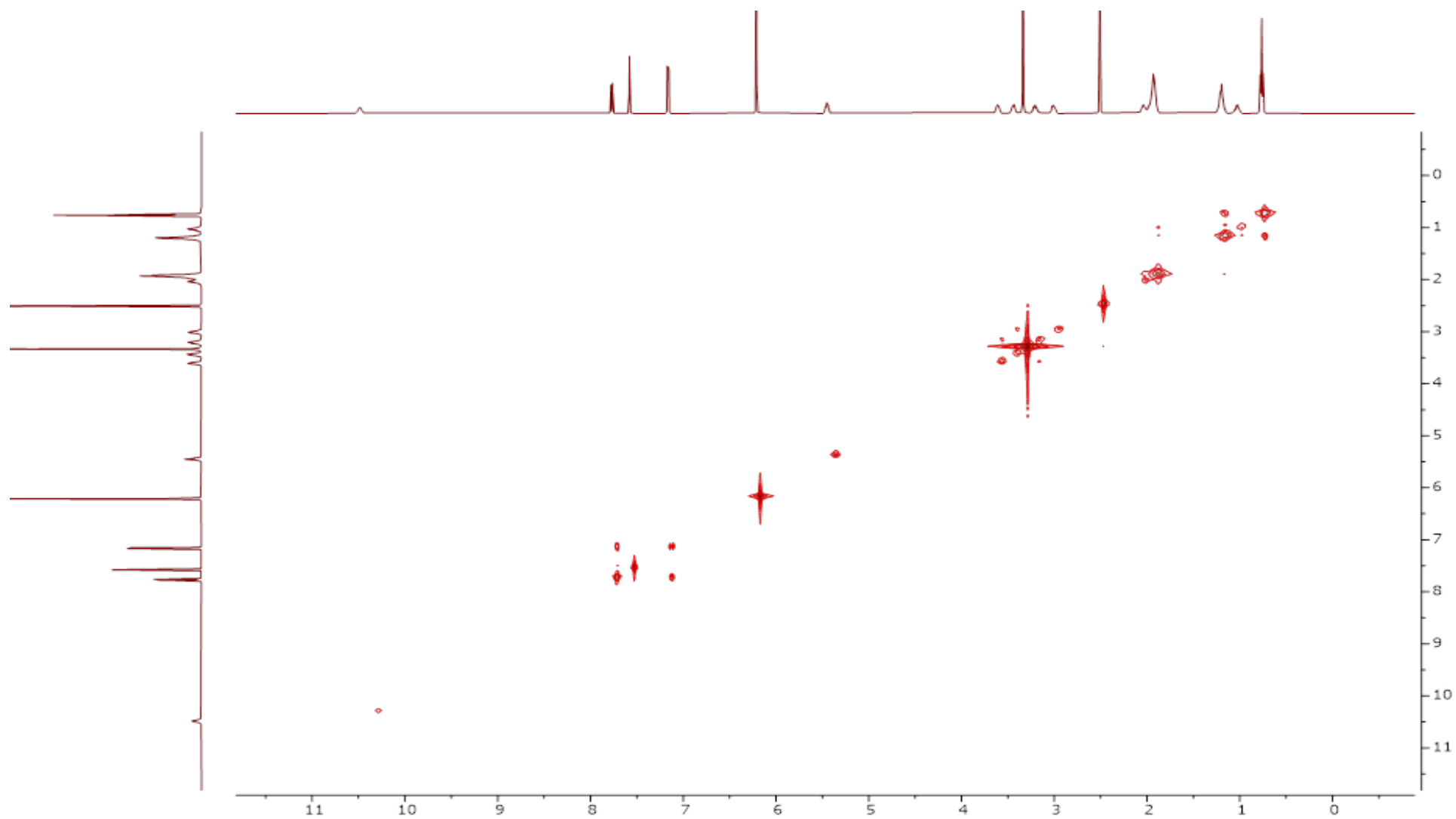


Figure S17: ^1H - ^1H COSY NMR spectrum of **10a** in DMSO-d_6 .

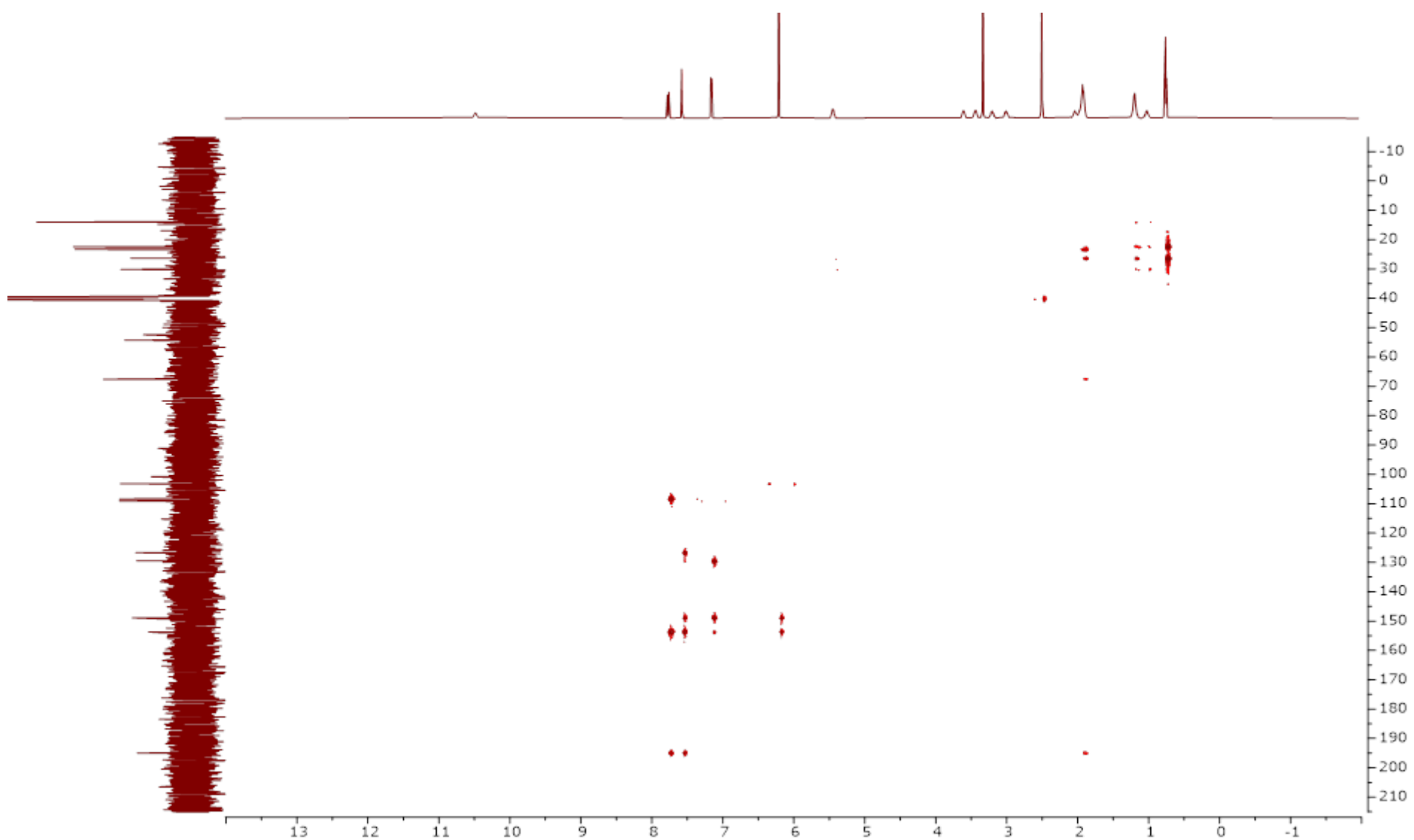


Figure S18: ^1H - $^{13}\text{C}\{^1\text{H}\}$ HMBC NMR spectrum of **10a** in DMSO-d_6 .

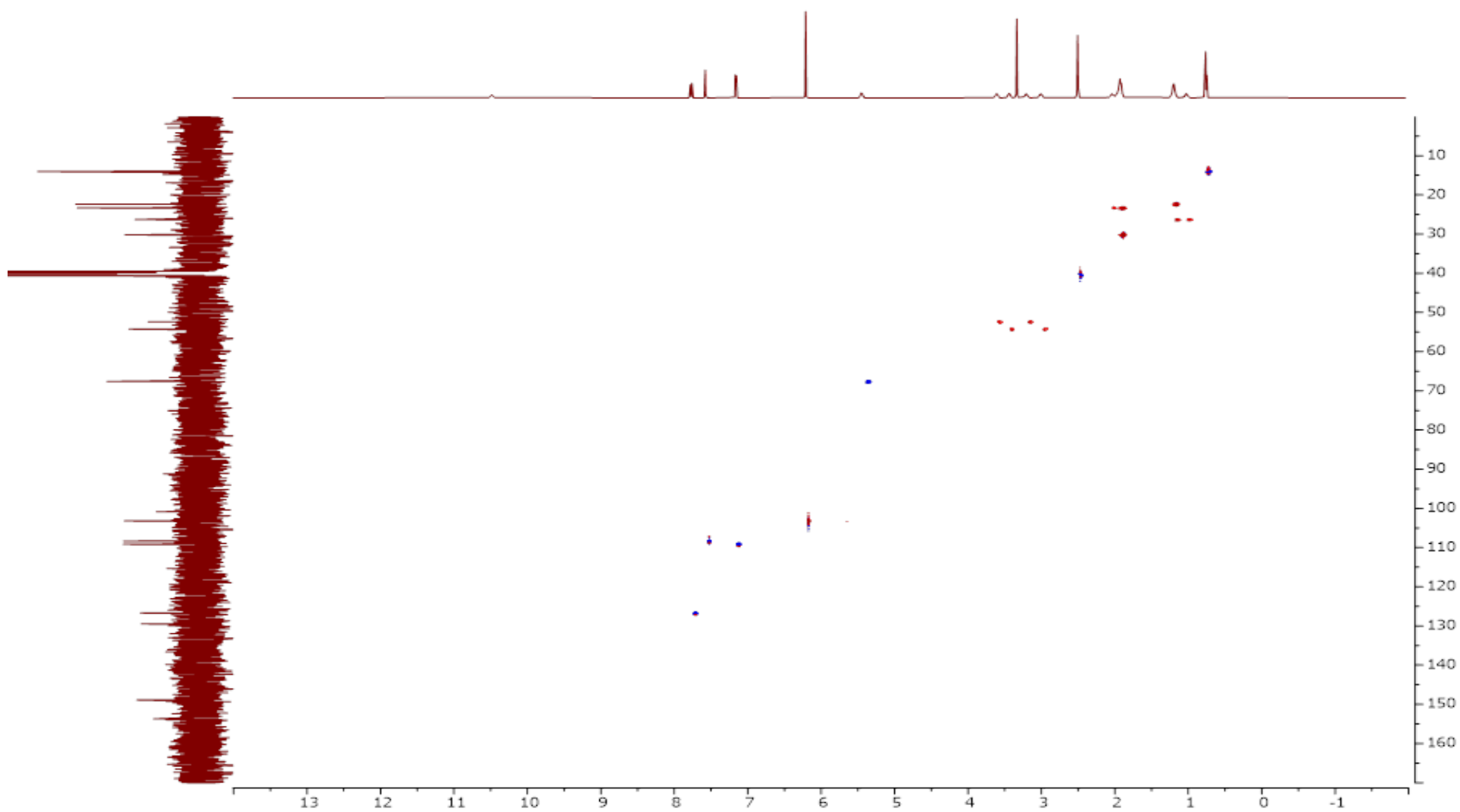


Figure S19: ^1H - $^{13}\text{C}\{^1\text{H}\}$ HSQC NMR spectrum of **10a** in DMSO-d_6 .

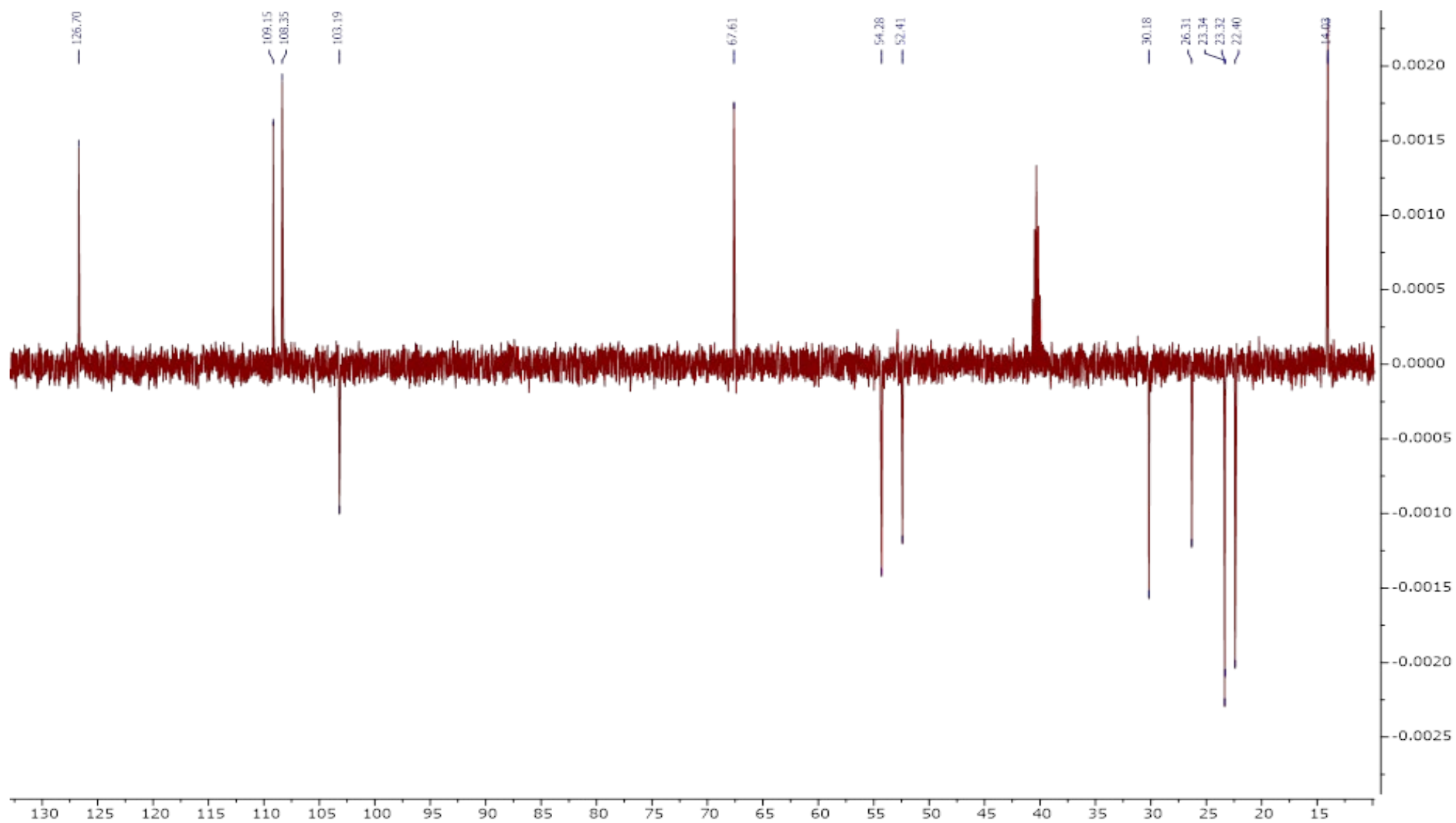


Figure S20: DEPT-135 NMR spectrum of **10a** in DMSO-d₆.

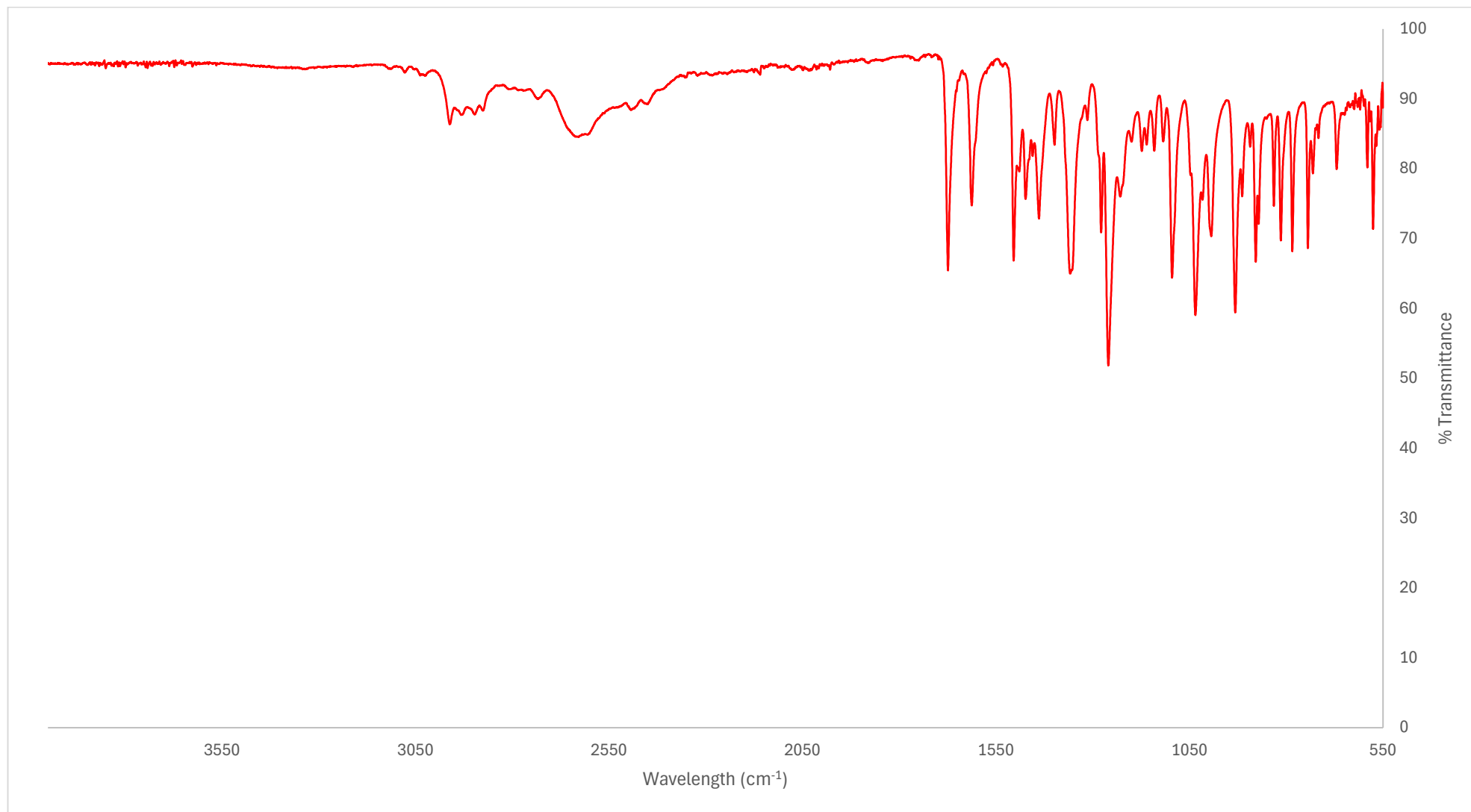


Figure S21: ATR FT-IR spectrum of dipentylone hydrochloride (**8b**)

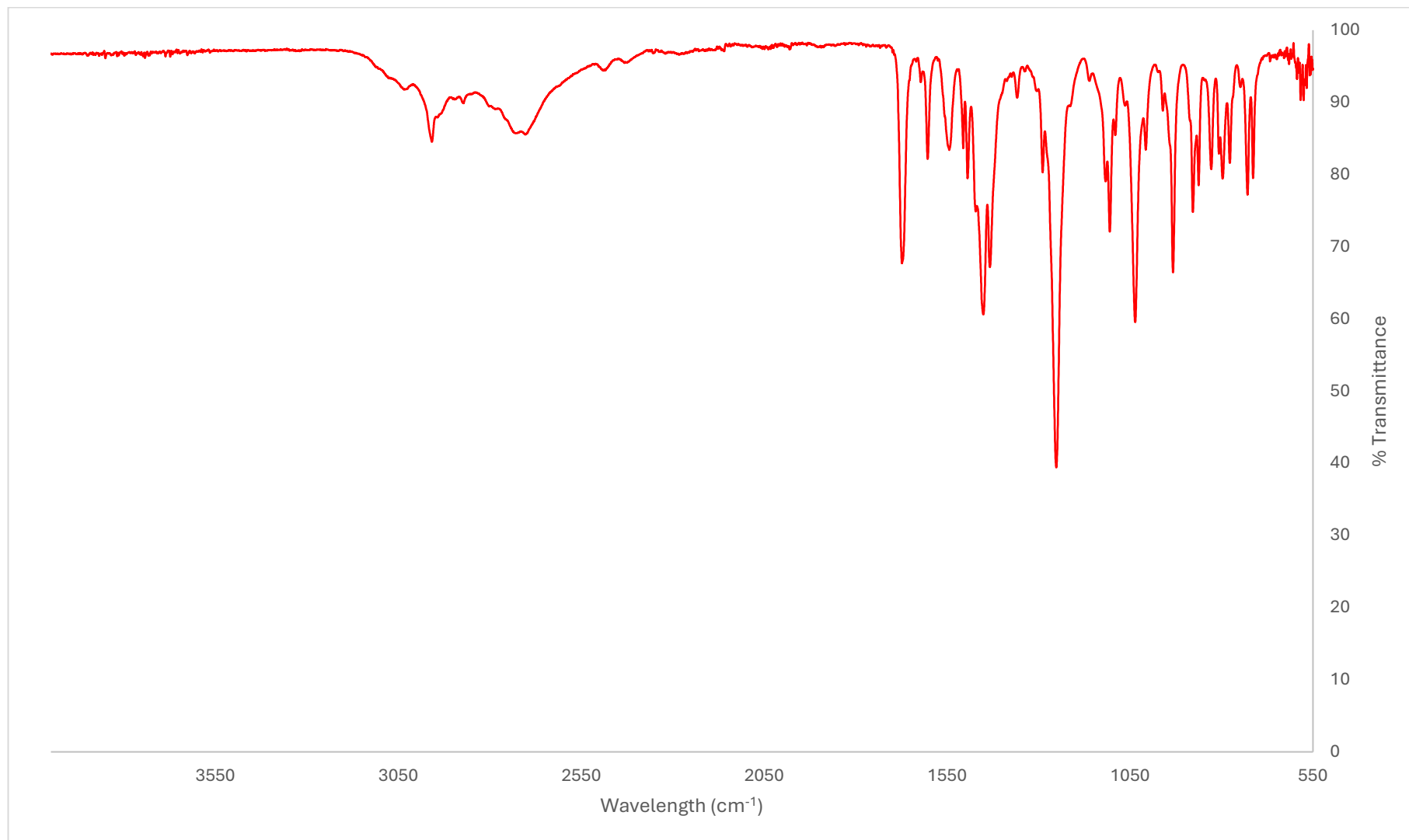


Figure S22: ATR FT-IR spectrum of N-ethylpentylone Hydrochloride (**8c**)

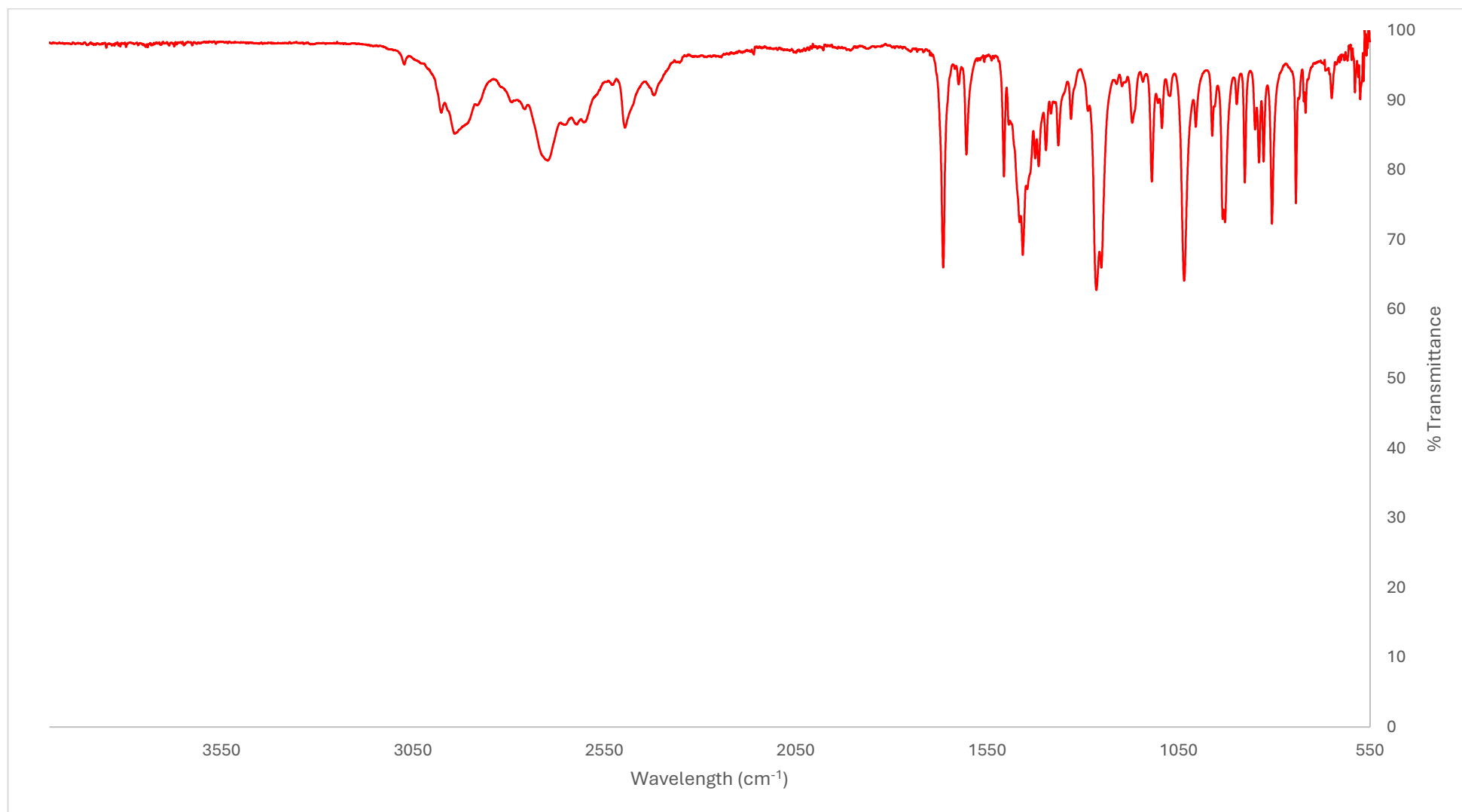


Figure S23: ATR FT-IR specrum of Butylone Hydrochloride retrieved from Excel (**9a**)

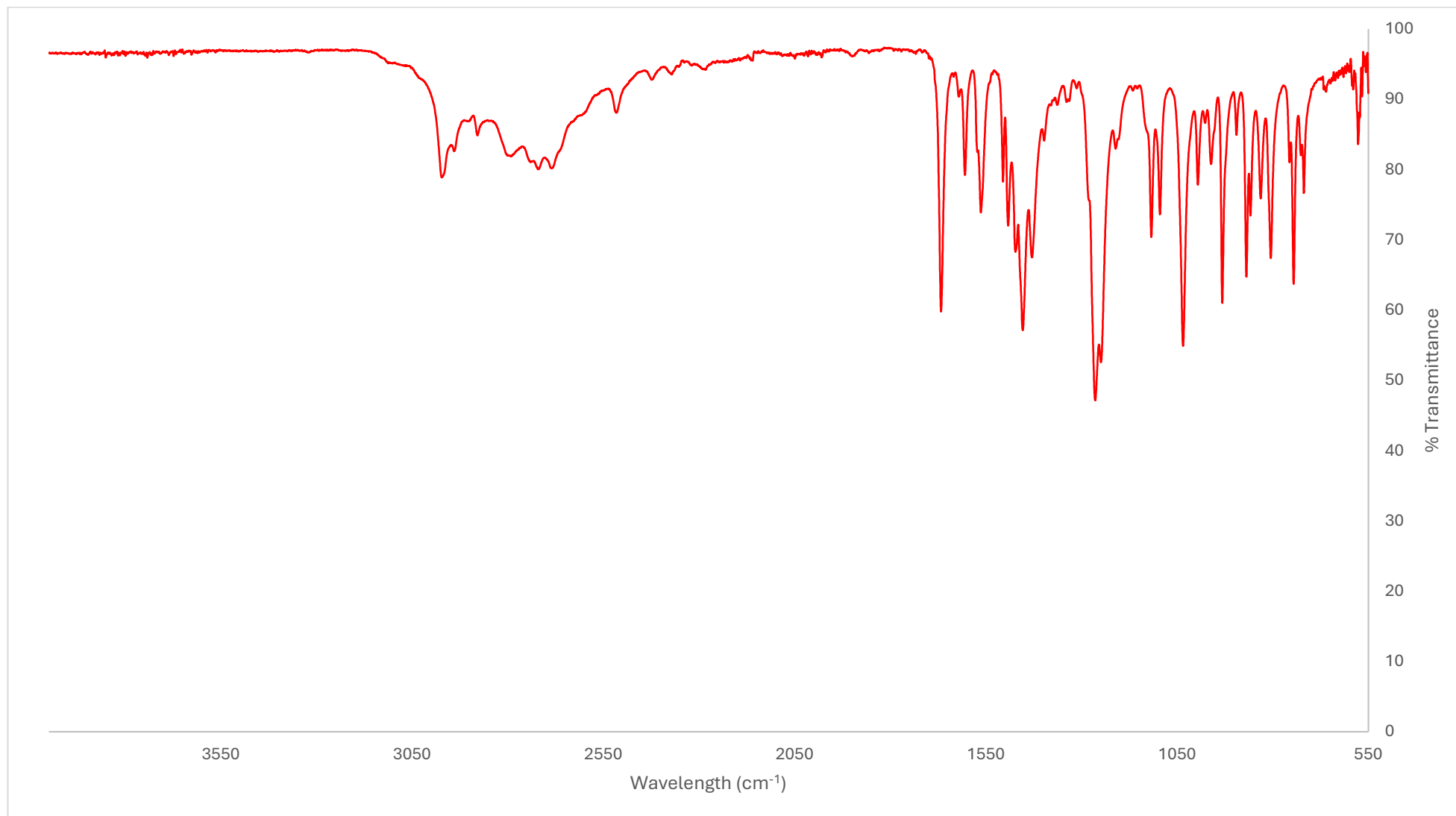


Figure S24: ATR FT-IR specrum of Putylone Hydrochloride retrieved from Excel (9b)

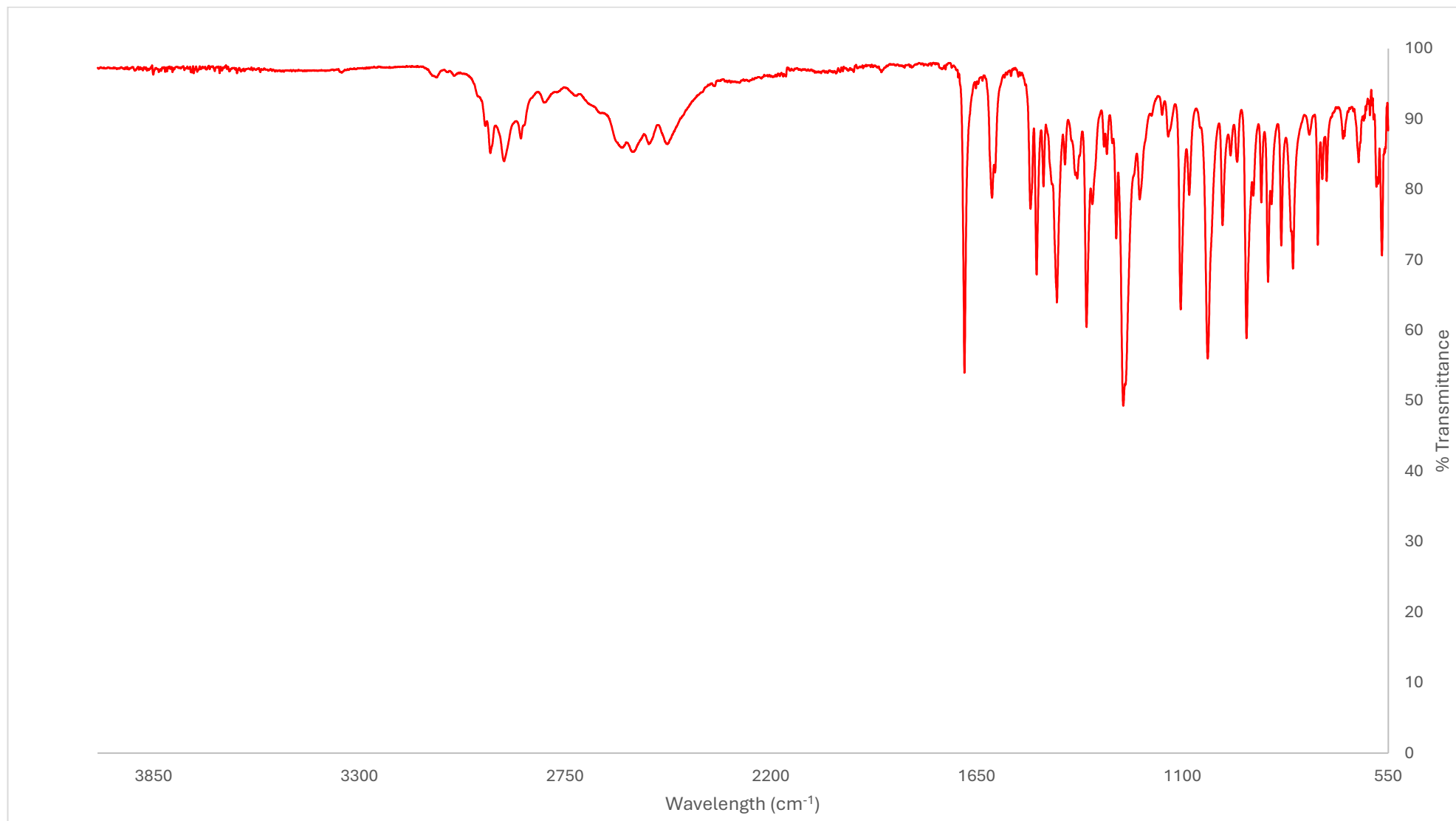


Figure S25: ATR FT-IR specrum of MDPHP Hydrochloride (**10a**)



Figure S26: Mass spectrum of dimethylpentylone hydrochloride (**8b**)

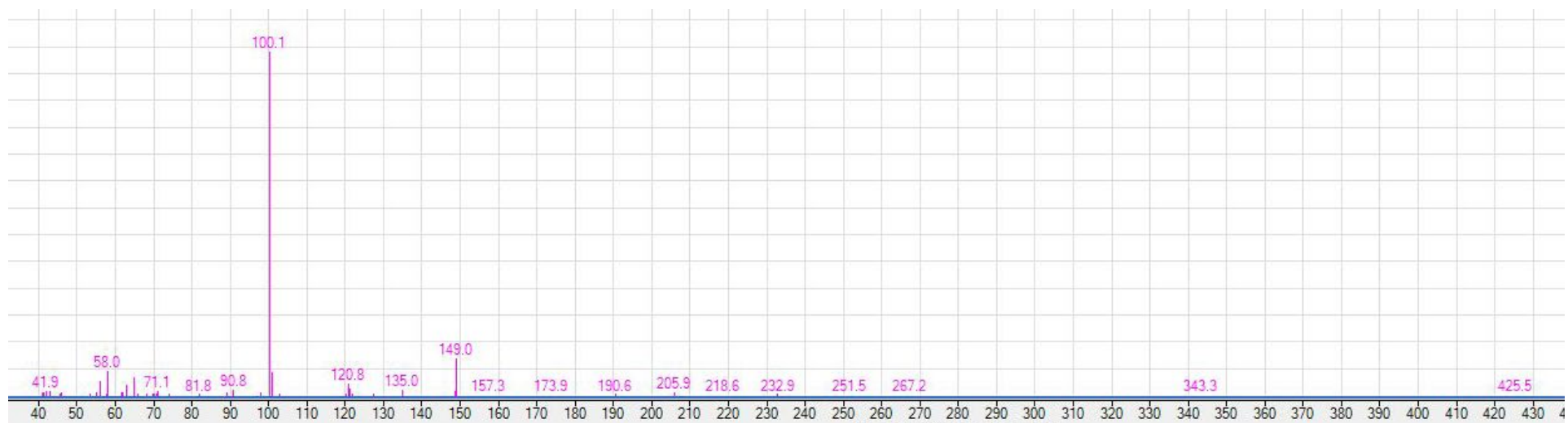


Figure S27: Mass spectrum of N-ethylpentylone hydrochloride (**8c**).

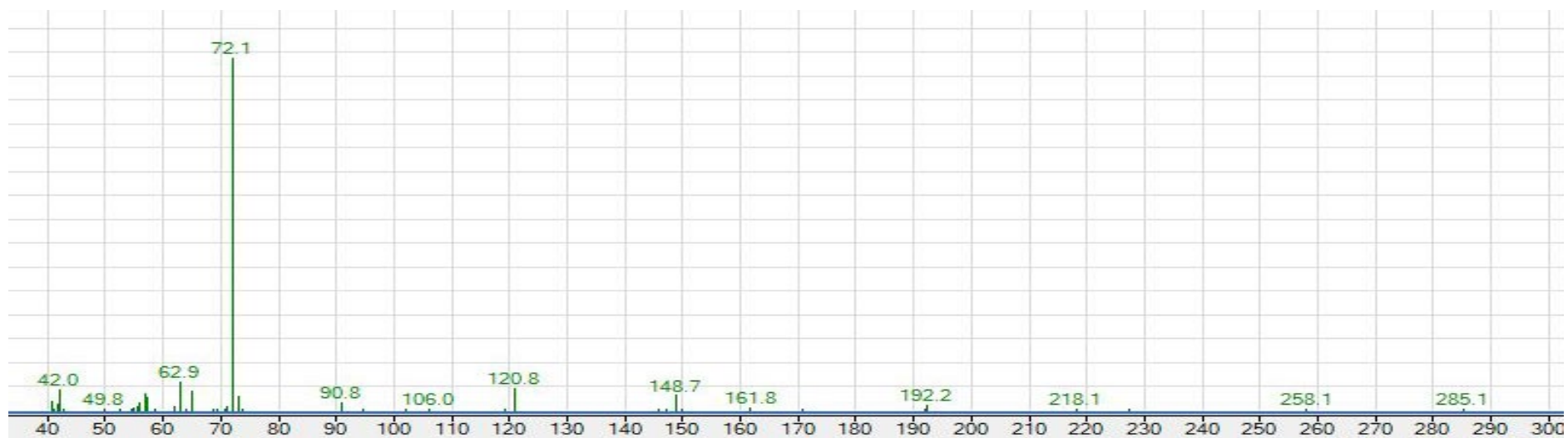


Figure S28: Mass spectrum of butylone hydrochloride (**9a**).

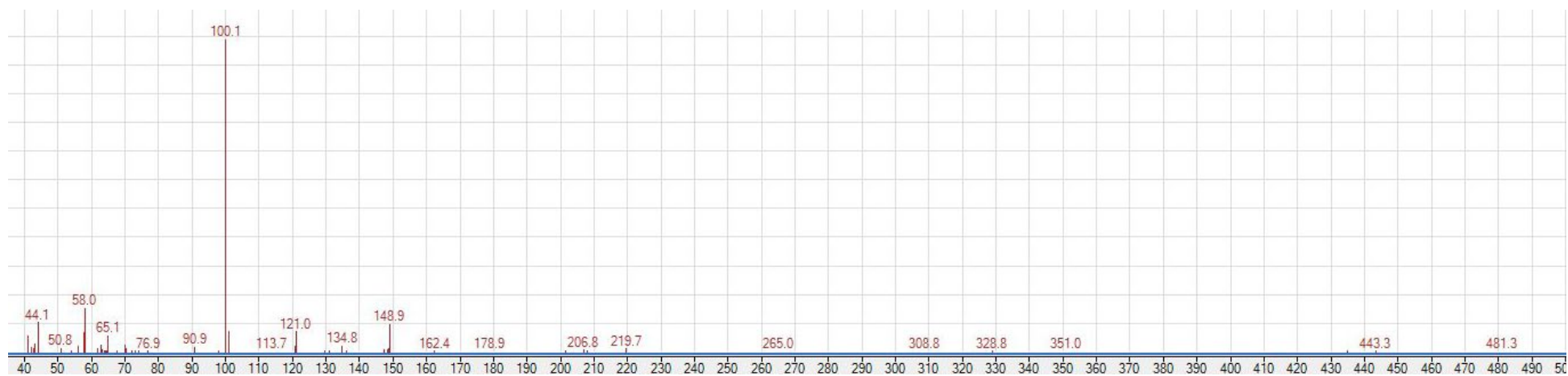


Figure S29: Mass spectrum of putylone hydrochloride (**9b**).

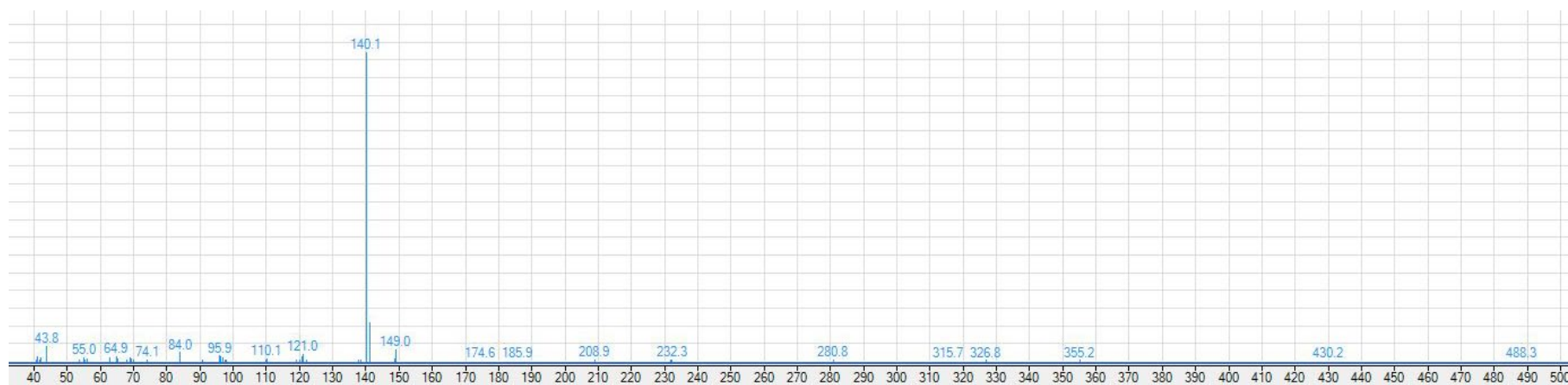


Figure S30: Mass spectrum of MDPHP hydrochloride (**10a**).